NASA-CR-195530

A MISSION TO MERCURY AND A MISSION TO THE MOONS OF MARS

FINAL REPORT

By the 1992-93 Senior Spacecraft Design Students
Penn State Department of Aerospace Engineering

Sponsored by the NASA/USRA Advanced Design Program

July 1993

EXECUTIVE SUMMARY

Introduction

Two Advanced Design Projects have been completed this academic year at Penn State — a mission to the planet Mercury and a mission to the moons of Mars (Phobos and Deimos). At the beginning of the fall semester the students were organized into six groups and given their choice of missions. Once a mission had been chosen, the students developed conceptual designs. These designs were then evaluated at the end of the fall semester and combined into two separate mission scenarios. To facilitate the work required for each mission, the class was reorganized in the spring semester by combining groups to form two mission teams. An integration team consisting of two members from each group was formed for each mission team so that communication and exchange of information would be easier among the groups.

The types of projects designed by the students evolved from numerous discussions with Penn State faculty and mission planners at the Lewis Research Center Advanced Projects Office. Robotic planetary missions throughout the solar system can be considered valuable precursors to human visits and test beds for innovative technology. For example, by studying the composition of the Martian moons, scientists may be able to determine if their resources may be used or synthesized for consumption during a first human visit.

Project Firefly: Mission to Mercury

Background

Mariner 10's observations of the planet Mercury started to answer many questions about the planet closest to the Sun. However, partial mapping of the planet and quick flybys left many questions unanswered. Since its mission in the early 1970's, many more questions have arisen. Are there prospects of using Mercury's resources to relieve Earth's dwindling

supply? Could Mercury support a laboratory for closer study of the Sun? Are there polar ice caps on Mercury? What is the make-up of the surface regolith?

Specifically, the scientific study of the planet by Project Firefly includes sending four landers to the surface to analyze seismic and tectonic activity, thermal conductivity of the soil, regolith composition, ice experiments, and mapping of the planet. This project also investigates the feasibility of propulsion via solar sail using a spiraling orbit to Mercury, composite systems to reduce thermal stresses, communication in an area of high solar activity, communication with an inflatable antenna, and thermal control challenges of keeping the spacecraft and its landers within an acceptable range while temperatures vary from -183°C to +467°C on the planet's surface.

Mission Objectives

Project Firefly is designed to send multiple landers to Mercury, conduct experiments, and map the planet. The primary objective is to study different regions of Mercury in an effort to understand their formation. Secondary objectives are to study the efficiency of a solar sail for interplanetary travel and to map, within a few decimeters, the entire planet.

Since different regions of Mercury show different evolutionary characteristics, it is important that as many of these regions as possible be studied. The differences in region formation may enlighten scientists as to the creation of the solar system. Also, Mercury may contain ice deposits from passing comets. Regolith analysis and seismic and tectonic studies will give insight into Mercury's evolution.

A secondary objective is to determine the feasibility of solar sail travel. Since the solar sail is relatively new in practice, Project Firefly will give insight into the practicality of interplanetary solar sail applications. The effects of sail angle, spacecraft trajectory and sail deployment will be helpful in understanding the physical constraints of the solar sail. Solar sails may prove to be a cost-effective means of future unmanned space transportation.

Another secondary objective is the total mapping of Mercury within a few decimeters. A laser altimeter will generate a three-dimensional map of each landing area with a resolution of 50 cm. After the landers are deployed, three-dimensional mapping of the entire planet will be attempted.

Mission Profile

The mission profile can be divided into two phases. The first phase includes those events occurring from Earth's surface to Mercury. The second phase includes actions taken in low Mercury orbit and on the planet. Figure 1 shows the scenario for Project Firefly.

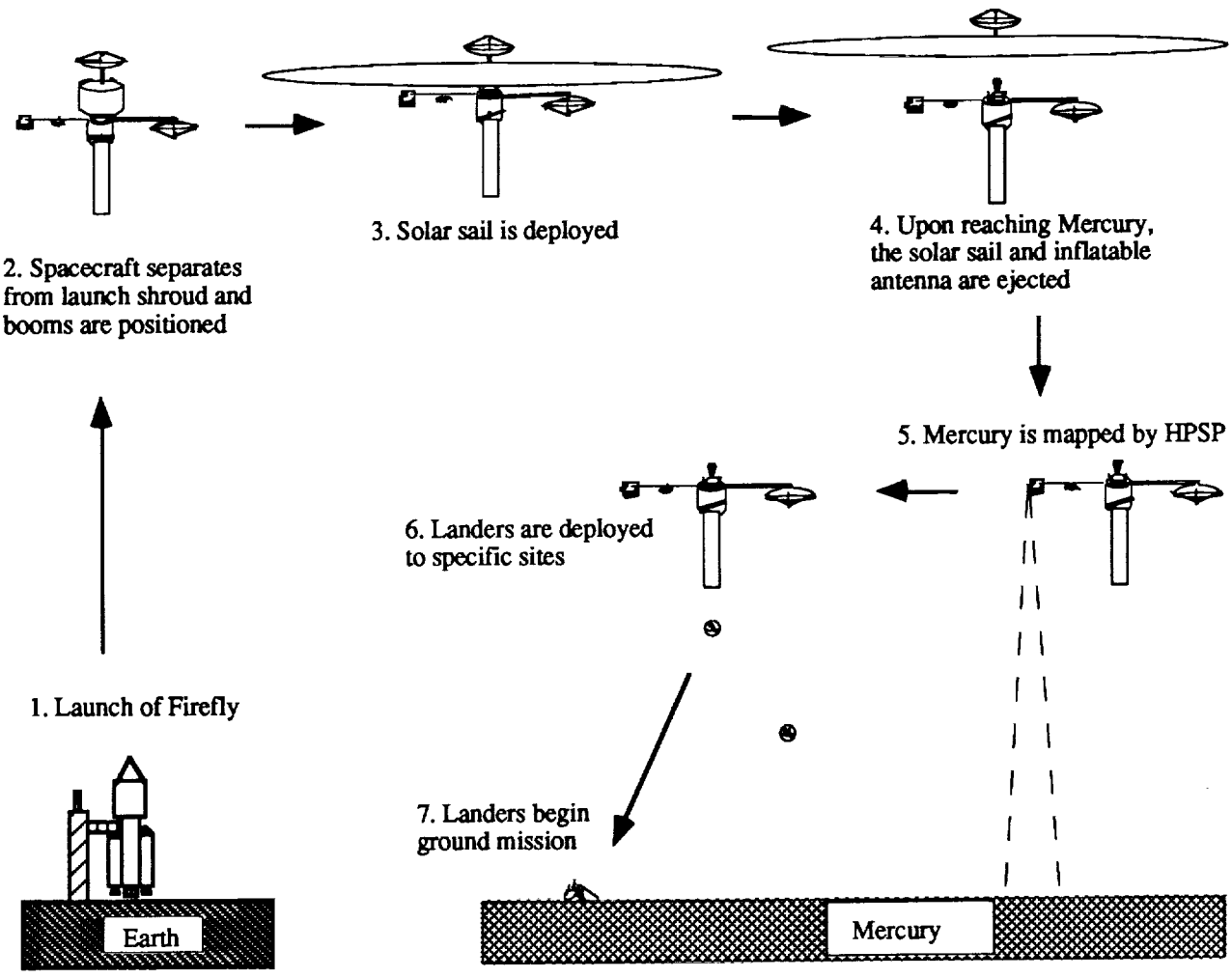

Figure 1. Project firefly Mission Scenario

Phase One — From Earth to Mercury: Due to the length and the large mass of the SPF-2000 spacecraft, many of the previously studied launch vehicles were eliminated. The only launch vehicle that would fit the specified spacecraft dimensions is the Titan IV. This vehicle will boost the craft from Earth to LEO where a systems check will be performed and the solar arrays and communication antennae deployed, as shown in Figures 2 and 3. The spacecraft will then use an RL-10A rocket motor for escape to an interplanetary transfer orbit. While on this hyperbolic escape orbit, the spacecraft will be spun and the solar sail deployed from a canister 4.84 m in diameter and 6 m long. Once the sail is completely unfurled, the spacecraft begins its spiral toward Mercury. This will take approximately 3.5 years. Once the spacecraft reaches Mercury's orbit, it will be turned 180 degrees, aligning itself for the eventual firing of the XLR-132A capture motor and insertion into a 500 km orbit above the surface of the planet.

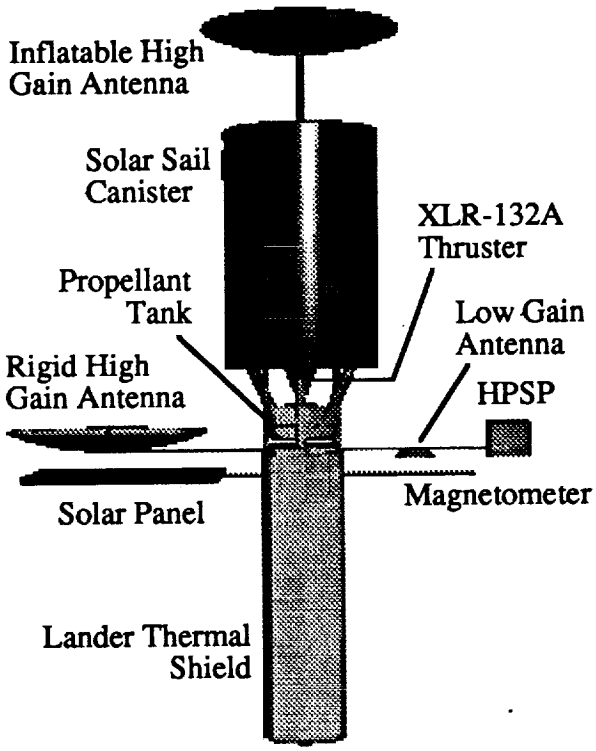

Figure 2. SPF-2000 Spacecraft

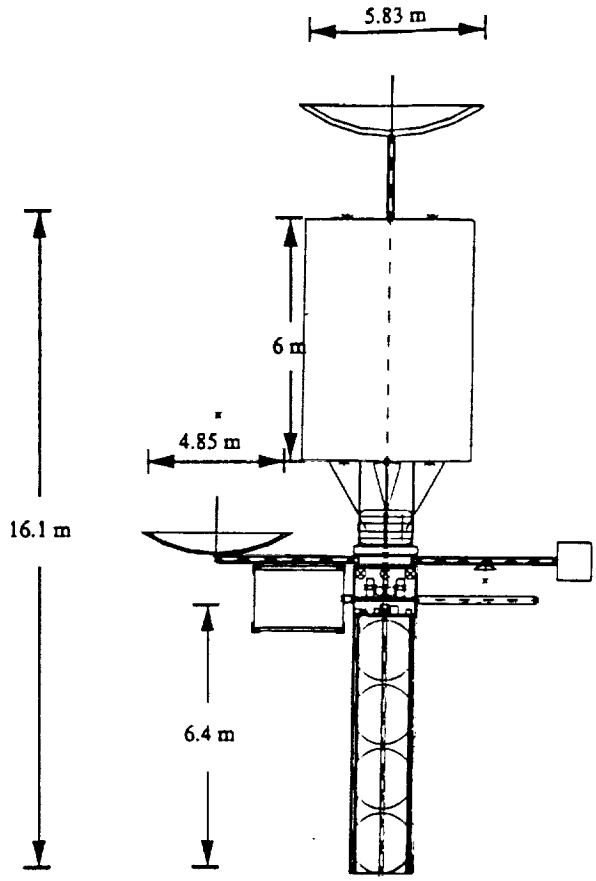

Figure 3. Side View Schematic of Spacecraft

Phase Two -- Mercury Orbit and Landings: After capture at Mercury, the spacecraft begins mapping the planet with its High Precision Scanning Platform (HPSP), as shown in Figure 4. After mapping is completed, the four predetermined areas are scanned for suitable landing sites. Suitable 20 km by 20 km regions in the Caloris Basin, Hilly and Lineated Terrain, the crater Bernini, and the Smooth Plains are determined by a ground support team. The main C&DH computer (the Rockwell RI-1750 A/B) then calculates the required trajectory for the landers to reach their sites. Once this is done, small attitude thrusters place the spacecraft in the necessary orientation and the first lander is ejected via explosive bolts. The spacecraft then adjusts to the next location and the second lander is released. The same procedure is

used for the third and fourth landers. (This mission is designed to place each lander on the surface near the dusk terminator so as to take advantage of the prime thermal conditions.) After the landers have been ejected, the orbiter will be used to store and relay information between Earth and each lander. It also continues to map the planet with cameras and a radar altimeter as well as determine the temperature changes over some significant portion of a local solar day. A magnetometer, extended from a boom on the orbiter, will be used to study the magnetosphere of the planet.

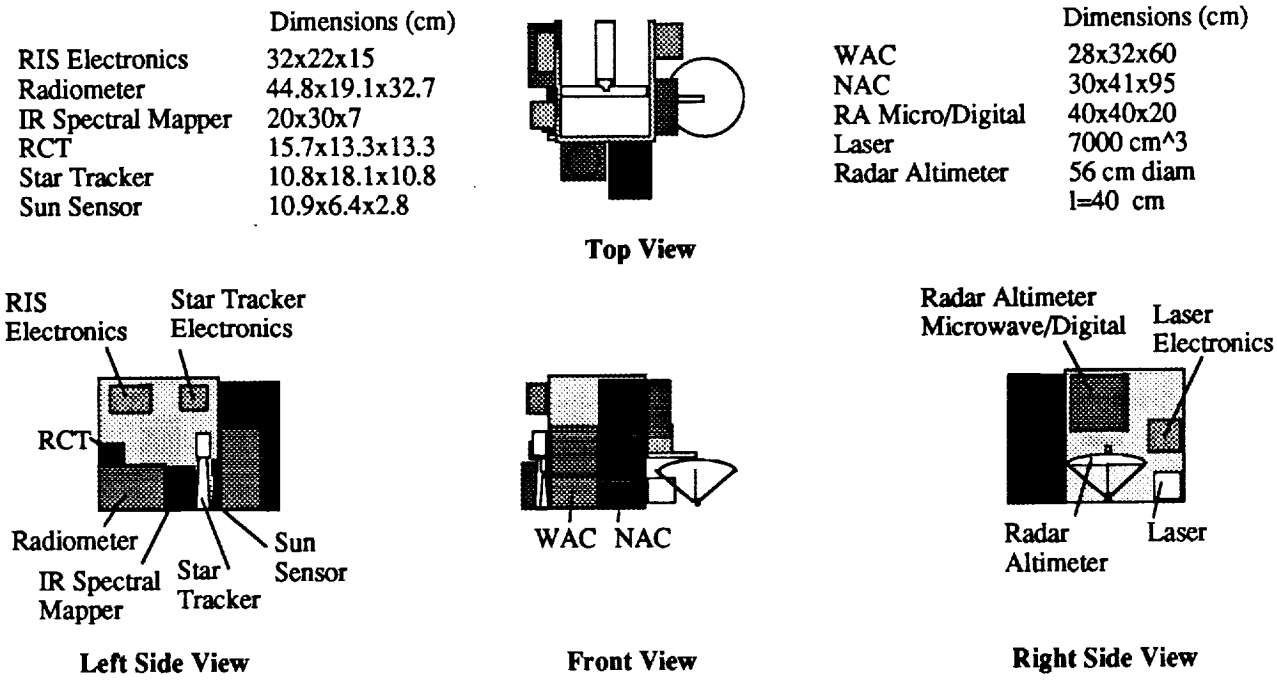

Figure 4. High Precision Scan Platform (HPSP) Configuration

Once a lander leaves the spacecraft configuration, S3K engines will fire to orient and land each lander. As the lander falls toward Mercury, a LEROS 20 thruster pack at the top will fire to aid in orientation. When the lander is close to the surface, the extendible

positioning system slowly opens the shell, as in Figure 5. The lander contacts the surface, adjusts to the local terrain, and begins testing. Regolith studies determine temperature conductivity, magnetic properties, and elemental composition. Cameras photograph the local landscape, while the seismometer monitors local tectonic and seismic activity. Each lander relays its information to the orbiter which, in turn, relays it back to Earth. Waste heat from the RTGs is used to keep the landers within their prescribed operational temperatures. Assuming a solar day of 88 Earth days, each lander will last for a maximum time of 136 Earth days. The lander is configured as shown in Figures 6 and 7.

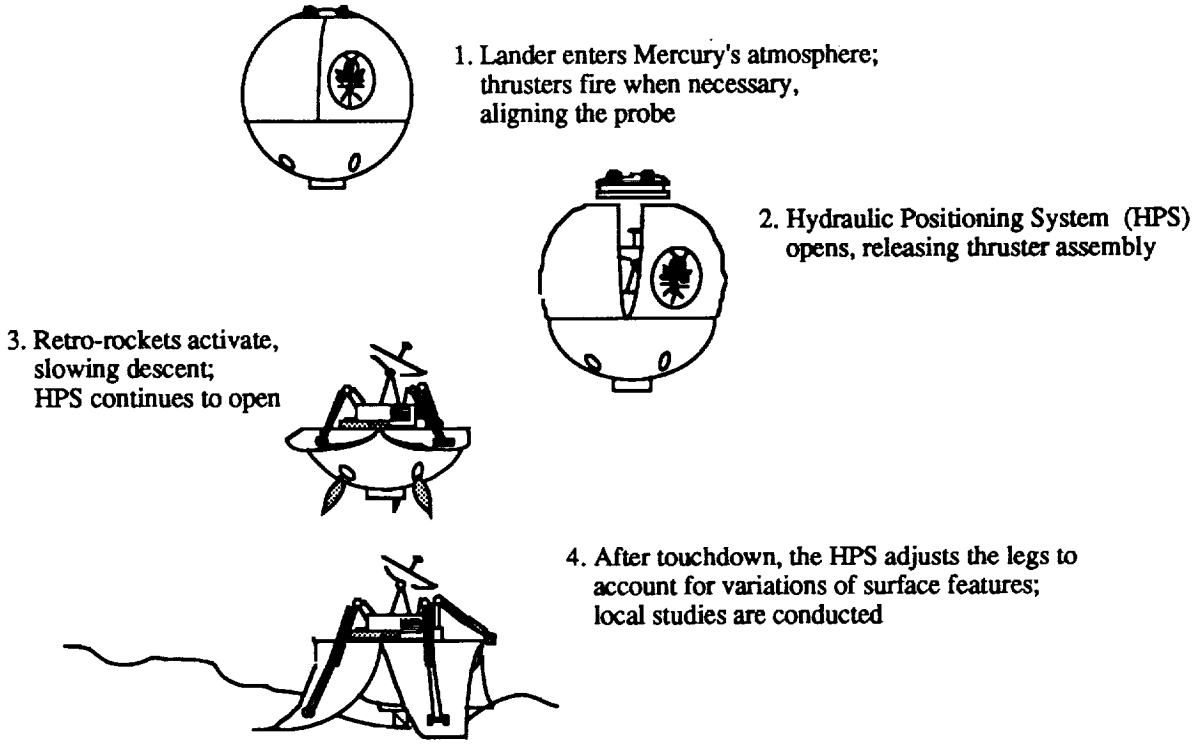

Figure 5. Landing Sequence

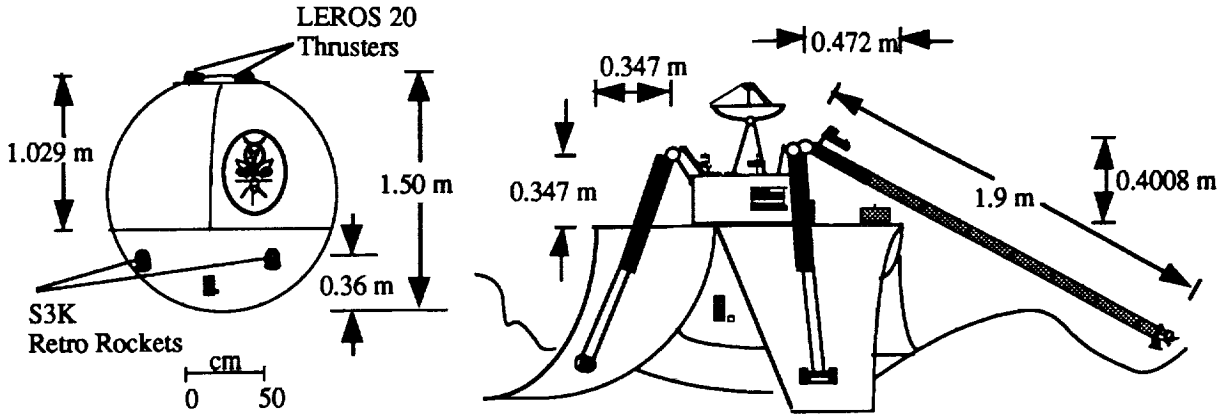

Figure 6. Lander Dimensions

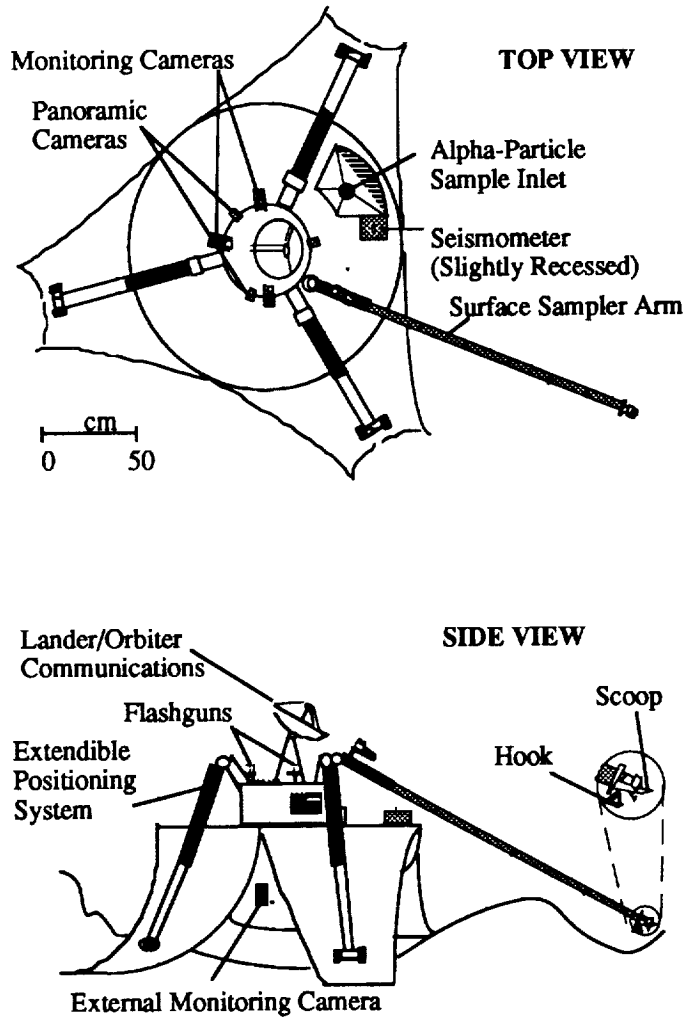

Figure 7. Lander Components

Summary of Mass, Power, and Cost

Using the "Cost Estimation Methods for Advanced Space Systems" by Kelly Cyr [1], the cost of each major component of the subsystems previously described was found. It should be noted that unless specified, the following costs are not *absolute* estimates for any of the systems. It is strictly a qualitative estimation based on weight, year of initial operation, and generation. Tables 1 and 2 list each subsystem and their respective masses, power requirements, and costs for the orbiter and landers. Subsystems with proven space worthiness, such as structures and scientific instruments, are assumed to be in an n^{th} generation at the time of launch. Other subsystems, such as propulsion, are designated as first generation models.

Table 1. Total Subsystem Mass, Power Requirements, and Cost (FY2010) for the Orbiter

Subsystem	Mass (kg)	Power (Watts)	Cost (M$)
Communications	120	165	118.3
C & DH	15	10	16.9
Power	50	0	3.3
Thermal Control	158	56	242.3
Structure	1408	0	852.9
Scientific Instruments	93	197	134.3
Propulsion	3792	0	1956.5
GNC	93	582	154.3
TOTAL	**5729**	**1177**	**3478.8**

Table 2. Total Subsystem Mass, Power Requirements, and Cost (FY 2010) for the Landers

Subsystem	Mass (kg)	Power (Watts)	Cost (M$)
Communications	15	65	14.4
C & DH	10	50	11.0
Power	36	0	25.5
Thermal Control	9	(Negligible)	37.0
Structure	30	0	68.2
Scientific Instruments	28	82	61.0
Propulsion & GNC	429	0	260.2
TOTAL	**557**	**197**	**$477.3**

Conclusion

Project Firefly will be ready for launch in early 2005. The spacecraft is an orbiter containing surface landers in tandem. Newly developed subsystem components such as inflatable antennas, a solar sail, and composite structural materials make Project Firefly unique. Multiple landers will provide redundancy in surface sampling while the increase in landing sites and study of those areas will give a better overall understanding of the planet's evolution. This understanding will prove to be valuable as insight into the makeup of Earth and the other planets in the Solar System. This project's cost comes to $5.388 billion in fiscal year 2005 dollars. The cost of this project, considering the first generation solar sail and other first generation components is reasonable. Many of the systems used in this project are proven systems, and reduce the risk of sending such a spacecraft to Mercury. This limited risk, accompanied with the wealth of scientific information it will gain, makes this a project worthy of consideration.

Project Arma: Mission to the Moons of Mars (Phobos and Deimos)

Background

Very little is known about the moons of Mars; Phobos and Deimos. Many previous missions to Mars have primarily focused on retrieving information about Mars with little information regarding the moons. Some of these missions include Viking, Mariner 9, and the recently launched Mars Observer. Of all the missions to the Mars system, only one has focused on Phobos. This mission was performed by the former Soviet Union which launched two satellites, Phobos-1 and Phobos-2, to study the moon. Unfortunately, contact with Phobos-1 was lost during interplanetary transfer, and contact with Phobos-2 was lost shortly after Mars capture. With Mars being a destination for future manned missions, propellant and other raw materials will be needed. If Phobos and Deimos have oxygen and hydrogen as expected, propellant for return trips to Earth can be extracted from the two moons [2]. Thus, a scientific mission to Phobos and Deimos (Project Arma) has been developed to analyze regolith and other moon properties, which may be of concern for future manned missions.

Mission Objective

The primary goal of Project Arma is to perform an in-situ analysis of each moon's regolith. Other goals of Project Arma include: (1) achieving a better understanding of the geology, geophysics, and climatology of the moons [3]; (2) shedding light on the origin and early history of the moons and the solar system [4]; (3) achieving a more accurate determination of their orbital characteristics; (4) obtaining a better understanding of the interactions between the moons and the solar wind [5]; and (5) studying the effects of one complete solar cycle in the absence of an atmosphere.

Mission Profile

Project Arma will be launched on a Proton rocket in the year 2010. The spacecraft consists of one orbiter, one lander per moon, and one penetrator. Upon arrival at the Mars system, an aerobraking maneuver will be implemented to slow the spacecraft and place it in an orbit about Mars. After capture into a Martian orbit, the orbiter will transfer to Deimos, map its surface, and perform other regolith analyses from orbit. When the orbiter finishes its mapping and regolith analysis of Deimos, the orbiter will release the first lander to the surface. The orbiter, second lander, and penetrator, will then transfer to an orbit about Phobos.

At Phobos, the orbiter will map and perform regolith analysis. Upon completion, the orbiter will release the second lander and the penetrator to Phobos' surface. The orbiter will then transfer to a final parking orbit between Phobos and Deimos. From the parking orbit, the orbiter will perform long term measurements of the Martian system and act as a communications link between the landing packages (landers and penetrator) and Earth. The mission scenario is depicted in Figure 8. Due to extensive mapping data, the limitations of the communications subsystem requires the landing packages to perform limited analyses until the orbiter completes mapping both moons. All parts of the spacecraft, except the penetrator, are designed to last a full solar cycle (11 Earth years).

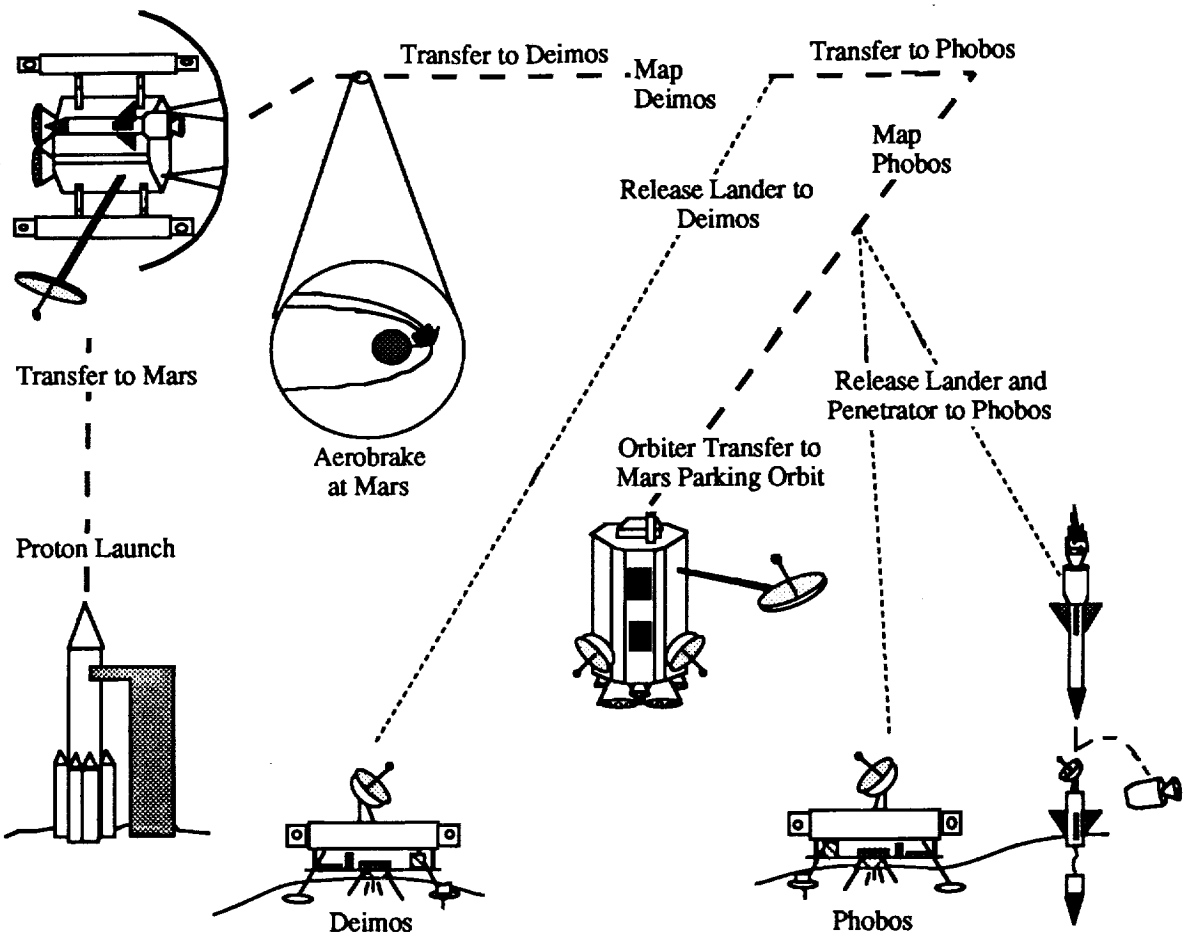

Figure 8. Project Arma Mission Scenario

Orbiter Function

The orbiter (see Figure 9) has three functions. The first function is to map and perform a regolith analysis on the moons, while in orbit about each. Mapping will consist of visual photography, radar sounding, gravity, magnetic field, temperature, and surface altitude measurements. The radar sounding will be used to determine the internal structure of each moon. During the mapping phase, a regolith analysis will also be conducted. The regolith analysis will determine surface history and surface composition of each moon. The scientific instruments are listed in Table 3.

The second function of the orbiter is to act as a communications link with Earth. The orbiter receives and transmits all information to and from the Martian system through a high-gain antenna. Low-gain antennas provide communications between the orbiter and the three landing packages (Deimos lander, Phobos lander and penetrator).

The third, less vital, function of the orbiter is to perform long term Martian system observations. The observations will be conducted from an orbit about Mars and will obtain information on solar wind interaction with Mars as well as magnetic, gravitational, and temperature measurements.

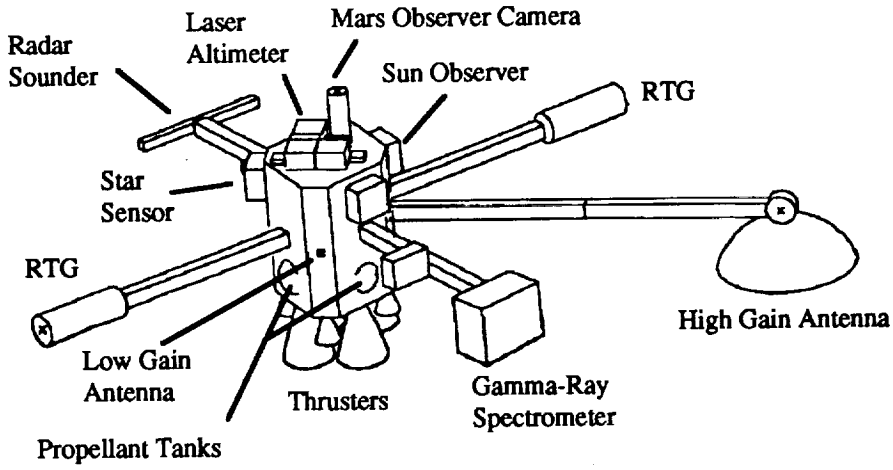

Figure 9. Arma Orbiter Configuration

Table 3. Orbiter Scientific Instruments

Instrument	Purpose
Laser Altimeter	Mapping a landing site
Near-Infrared Mapping	Calculating Temperature Profiles
Spectrometer Magnetometer	Determining moons' magnetic properties
Gamma Ray Spectrometer	Defining moons' elemental composition
Mars Observer Camera	Visual photography and mapping
Radar Sounder	Determining moons' internal structure
Retarding Potential Analyzer	Determining moons' magnetic properties
Mass Spectrometer	Analyzing regolith composition
DION	Investigating moons' surface history

Lander Function

The two landers have three identical functions. The first is to perform an in-situ regolith analysis, via an X-Ray Florescence Spectrometer. The second function is to record temperatures, seismic activity, and radiation levels for a full solar cycle. These measurements will aid in understanding the effects of the Sun's cyclic activity on all celestial objects. The third function is to obtain visual pictures of the moons' surfaces. The only difference between the landers is that the Phobos lander will also photograph Mars, using a wide angle camera. The scientific instruments are listed in Table 4 and the lander configuration is in Figure 10.

Table 4. Lander Scientific Instruments

Instrument	Purpose
Radiation Experiment	Determining radiation
Temperature Probe	Obtaining temperature variations
Panoramic Camera	Surface visuals
Seismometer	Determining ground wave characteristics
X-Ray Fluorescence Spectrometer	Analyzing regolith composition
Wide Angle Camera (Phobos)	Surface visuals of Mars

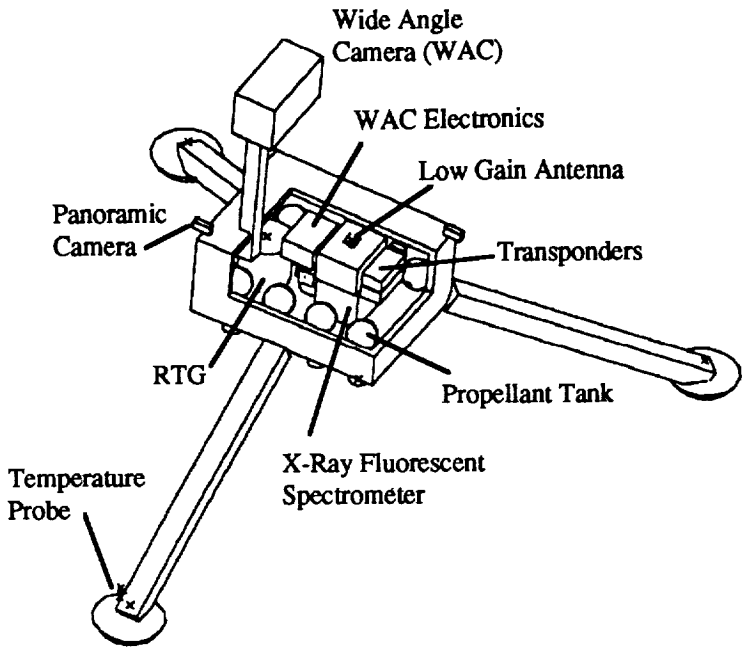

Figure 10. Arma Lander Configuration

Penetrator Function

The penetrator consists of a surface and subsurface section. To insure the safety of the penetrator's subsystems, the communication components and other electronics will be allowed to remain on top of Phobos' surface, yet remain connected to the embedded tip of the penetrator, by means of an extensible cord. This configuration will protect the subsystems from the energy of the impact.

The penetrator has two functions. The first function is to perform a regolith analysis below the surface of Phobos by an X-Ray Fluorescence Spectrometer. This analysis is important since scientists speculate that the surface dust is contaminated by meteor impacts, and will therefore not indicate the moon's true composition. By comparing the penetrator's regolith analysis to the orbiter's and lander's analysis, the homogeneity of the moon's surface and internal composition can be verified.

The second function of the penetrator, is to act as a experimental prototype. Using penetrators is of current interest for future Mars missions, since NASA has yet to successfully obtain a core sample from a celestial body. Thus, the operational data obtained from this penetrator will aid in the future technological development of such devices.

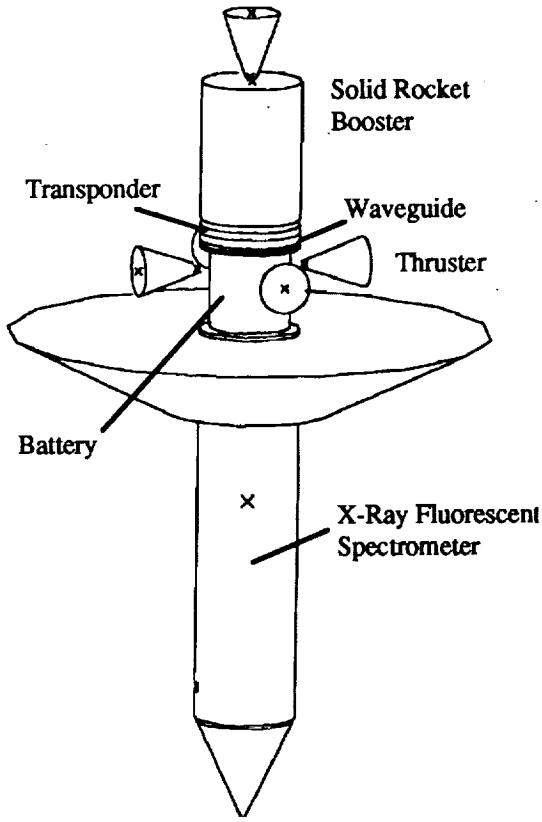

Figure 11. Phobos Lander Penetrator

Design Overview

The mass, power, and cost of individual subsystems for the orbiter, landers, and penetrator have been calculated and are tabulated in Tables 5, 6 and 7, respectively. Many of the subsystem costs were not available, thus a cost estimation program developed by Kelly

Cyr [1] has been utilized. The inputs of the cost estimation program were: total wet mass (5141.9 kg), launch year (2010), and the type of spacecraft (exploration). Using this cost estimation package, a total cost of approximately $1.48 billion in 1993 dollars has been obtained and in the launch year of 2010, the cost is projected to be $2.41 billion.

The total spacecraft wet mass is 4285.0 kg, including the orbiter, two landers, and penetrator. With a generous 20% added for items such as the aerobrake heat shield and mass contingencies, the total wet mass is 5141.9 kg. This total mass is well below the Proton launch vehicle limit of 6200 kg.

The mass and power estimates for the orbiter are listed in Table 5. The orbiter's total wet mass is 3539.9 kg. The aerobraking maneuver will yield a considerable mass savings by reducing the propellant needed, by as much as 25%, to achieve Mars capture orbit. The total power is estimated to be 601.4 Watts, while the peak power consumption is estimated to be 596.9 Watts, and 657 Watts with a 10% design margin. The power discrepancy exists because instruments used to study Mars will not be operational until the orbiter is placed into its final parking orbit.

Table 5. Orbiter Mass and Power Estimates

Subsystem	Mass (kg)	Power (W)
Propulsion	2892.5	60.0
Communications	24.9	75.0
C & DH	73.2	29.0
Power	86.6	—
Structure	145.4	—
GNC	174.0	221.0
Scientific Instruments	115.7	189.4
Thermal	27.7	—
TOTAL	**3539.9**	**601.4**

The total wet masses for the Deimos and Phobos landers are 256.6 kg and 280.2 kg, respectively. The total power requirements for the Deimos and Phobos landers are 72.6 Watts and 88.9 Watts, respectively. With the exception of the cameras, all instruments will record data at 30 second intervals. Also, the wide angle camera will only be used at Phobos and will be used for long term observation of Mars. Project Arma's penetrator has a total wet mass of 208.3 kg, and a total power requirement of 37.4 Watts. Table 6 lists the mass and power, estimates for the landers and Phobos penetrator.

Table 6. Lander and Penetrator Mass and Power Estimates

Subsystem	Lander		Penetrator	
	Mass (kg)	Power (W)	Mass (kg)	Power (W)
Propulsion	116.0	20.0	137.0	6.0
Communications	8.5	15.0	6.8	15.0
C & DH	35.0	9.6	2.5	6.6
Power	26.3	—	0.3	—
Structure	46.1	—	30.8	—
GNC	5.0	—	5.0	—
Scientific Instruments	43.0	44.3	20.0	8.0
Thermal	8.8	—	6.4	1.8
TOTAL for Deimos Lander	**256.6**	**88.9**		
TOTAL for Phobos Lander	**280.2**	**72.6**		
TOTAL for Penetrator			**208.3**	**37.4**

Conclusion

A mission to study the Martian moons (Phobos and Deimos) was been proposed. Project Arma will send a lander to each moon, with the Phobos lander containing a surface penetrator. An orbiter will map each surface and act as a communications relay to Earth.

Among the technology demonstrations are the use of an aerobrake maneuver and the Phobos penetrator. Furthermore, by using a Russian Proton launch vehicle, international space relations could be greatly enhanced and strengthened. Scientific study of the moons could provide scientists with valuable insight into the formation of the solar system, as well as, possible raw materials for use in rocket propellants. The success of Project Arma could be a positive first step to a manned mission to the Martian system.

References

1. Cyr, Kelly, "Cost Estimation Methods for Advanced Space Systems," NASA Johnson Space Center, 1988.
2. Mulqueen, J., "Manned Mission Transfer from Mars Parking Orbit t Phobos and Deimos," Manned Mars Mission Working Group Papers, Vol. 1, NASA Marshall Spaceflight Center, Huntsville, AL, May 1986.
3. Blume, W., Dodd, S., and Whetsel, C., "Mars Observer Mission Plan," *Journal of Spacecraft and Rockets*, Vol. 28, No. 5, October 1991.
4. Glasstone, S., *The Book of Mars*, NASA Office of Technology Utilization, 1986, p. 72.
5. Zaitsev, Y., "The Success of Phobos-2," *Spaceflight*, November 1989, pp. 375-777.

Volume I

Project Firefly: Mission to Mercury

The Pennsylvania State University

Department of Aerospace Engineering

MISSION TO MERCURY

(Project Firefly)

by

Doug Buzzard, David Chart, Kimberly Clemons, Mark Filetti, John Florek, Michael Fludovich, Kevin Gallagher, Jeffrey Gray, Francis Hsia, Shane Kessler, Michael Koiro, Joseph Krug, Gene Lee, Jeffrey Nichols, Eric Perritt, Mark Ryan, Rick Sleutaris, Rebecca Spath, George Truman

July 1993

Table of Contents

List of Figures

List of Tables

1.0 Introduction

Mariner 10's observations of the planet Mercury started to answer many questions about the planet closest to the Sun. However, partial mapping of the planet and quick flybys left many questions unanswered. Since its mission in the early 1970's, many more questions have arisen. Are there prospects of using Mercury's resources to relieve Earth's dwindling supply? Could Mercury support a laboratory for closer study of the Sun? Are there polar ice caps on Mercury? What is the make-up of the surface regolith?

Specifically, the scientific study of the planet by Project Firefly includes sending four landers to the surface to analyze seismic and tectonic activity, thermal conductivity of the soil, regolith composition, ice experiments, and mapping of the planet. This project also investigates the feasibility of propulsion via solar sail using a spiraling orbit to Mercury, composite systems to reduce thermal stresses, communication in an area of high solar activity, communication with an inflatable antenna, and thermal control challenges of keeping the spacecraft and its landers within an acceptable range while temperatures vary from -183°C to +467°C on the planet's surface.

Project Firefly is designed to send multiple landers to Mercury, conduct experiments, and map the planet. The primary objective is to study different regions of Mercury in an effort to understand their formation. Secondary objectives are to study the efficiency of a solar sail for interplanetary travel and to map, within a few decimeters, the entire planet.

Since different regions of Mercury show different evolutionary characteristics, it is important that as many of these regions as possible be studied. The differences in region formation may enlighten scientists as to the creation of the solar system. Also, Mercury may contain ice deposits from passing comets. Regolith analysis and seismic and tectonic studies will give insight into Mercury's evolution.

A secondary objective is to determine the feasibility of solar sail travel. Since the solar sail is relatively new in practice, Project Firefly will give insight into the practicality of

interplanetary solar sail applications. The effects of sail angle, spacecraft trajectory and sail deployment will be helpful in understanding the physical constraints of the solar sail. Solar sails may prove to be a cost-effective means of future unmanned space transportation.

Another secondary objective is the total mapping of Mercury within a few decimeters. A laser altimeter will generate a three-dimensional map of each landing area with a resolution of 50 cm. After the landers are deployed, three-dimensional mapping of the entire planet will be attempted. Figure 1.1 illustrates a scenario for Project Firefly from launch to the landing of the probes on the surface of Mercury.

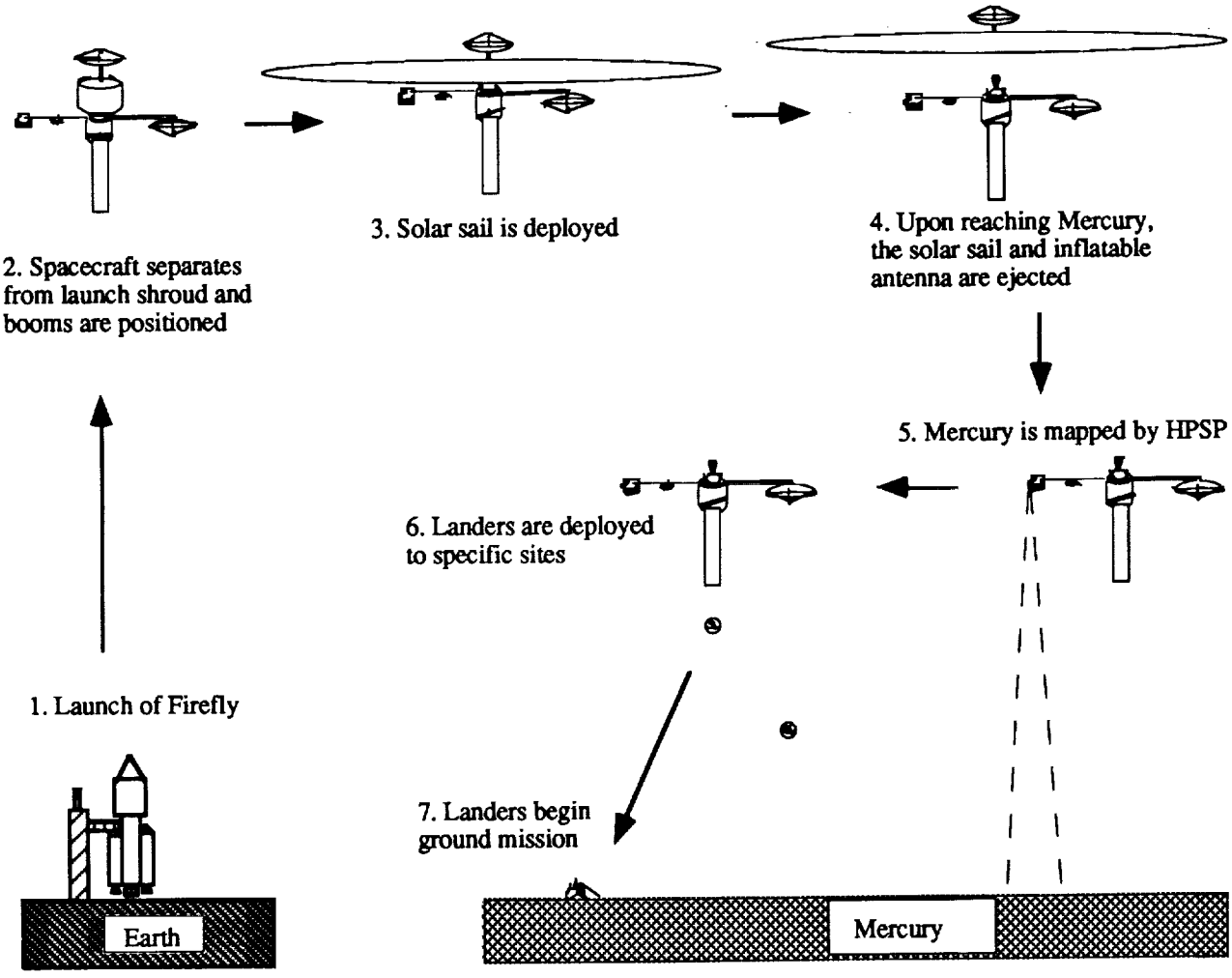

Figure 1.1. Project Firefly Mission Scenario

2.0 Spacecraft Structures

2.1 Requirements for Spacecraft Configuration

For the design of the Mercury exploration spacecraft, a number of constraints are placed upon the structural design by several of the major subsystems. For the scientific instruments, the constraints are as follows: the landers must be deployed from the spacecraft; the infrared mapper and remote imaging system must have a clear view of the planet; the magnetometer must be mounted on a boom so that it does not receive electronic interference from other subsystems; and the high precision scan platform (HPSP) must be despun.

The propulsion subsystem also places several limitations on the craft. A booster used for Earth orbit escape, a thruster and propellant tank used for Mercury insertion, and a solar sail container must be attached to the craft. The solar sail must be located on the spacecraft where it can be deployed, ejected, and spun for rigidity.

The guidance, navigation, and control subsystem requires that thrusters spin and stabilize the spacecraft. To minimize required stabilization, propellant, propellant symmetry is desired. Finally, the sun sensor, star tracker, and steerable horizon sensor must be despun.

The power subsystem requires on rotatable boom for the solar array, and batteries within the main body of the spacecraft.

The communications subsystem requires one inflatable high-gain antenna behind the solar sail, one high-gain antenna on a despun boom, and one low-gain antenna also on a despun boom. The thermal control subsystem requires louvers on a fairing around the landers.

2.2 Spacecraft Configuration

The spacecraft configuration is shown in Figure 2.1. Four landers oriented along the center axis, and surrounded by a louver fairing are attached to the front of the orbiter. The landers are aligned in this way to keep the center of mass along the central axis as each lander

is deployed. The landers and fairing are supported by three beams parallel to the center axis. The landers are attached to each other by explosive bolts which eject the landers when required. The main body of the orbiter houses the reaction wheels and inertia guidance system; the C&DH module, computer, and recorder; as well as the batteries. Two booms extend from the main body, one for the magnetometer and the other for the rotatable solar array. The rigid high-gain antenna boom and scientific instruments/GNC platform boom are located on the despun platform attached behind the despun platform. The solar sail canister is connected to the back of the thruster. Finally, the inflatable antenna attaches to the aft end of the sail container. Upon arrival at Mercury, the sail is ejected using explosive bolts.

The booms are extended in low Earth orbit (LEO) with pyrotechnic latches and springs. Figure 2.2 shows the spacecraft before the booms are extended and Figure 2.3 shows the spacecraft with the solar sail and booms extended. Due to the large size of the solar sail, the entire sail is not shown in Figure 2.3. Figure 2.4 shows the orbiter portion of the spacecraft with the landers and sail removed. For simplicity, the lander fairing is not shown in this figure. Figures 2.5 - 2.7 are schematic diagrams of the spacecraft at LEO. Figure 2.8 illustrates the mass distribution of the spacecraft. The boom lengths were coordinated with their tip masses to balance the mass distribution of the spacecraft.

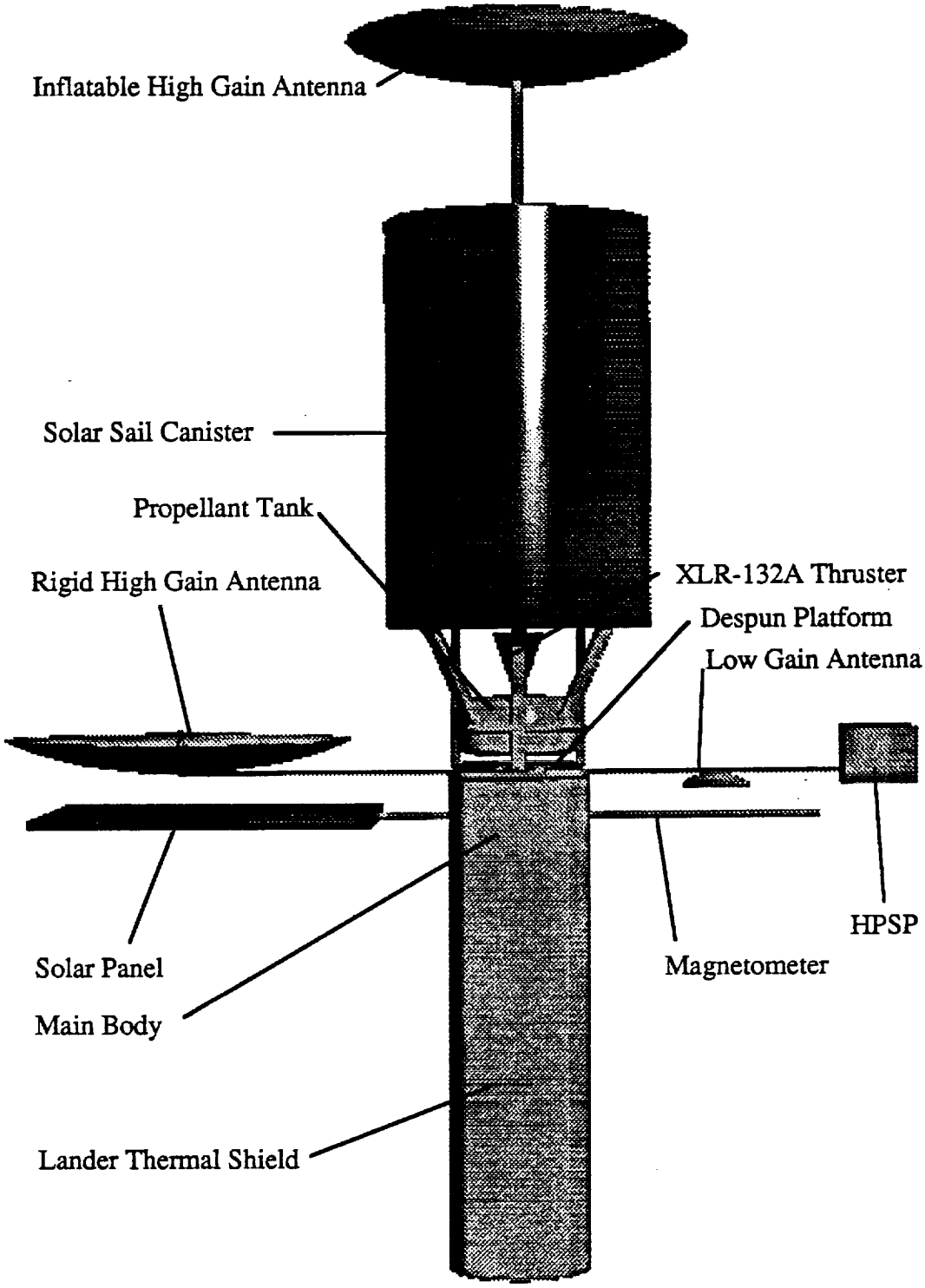

Figure 2.1. Side View of Spacecraft

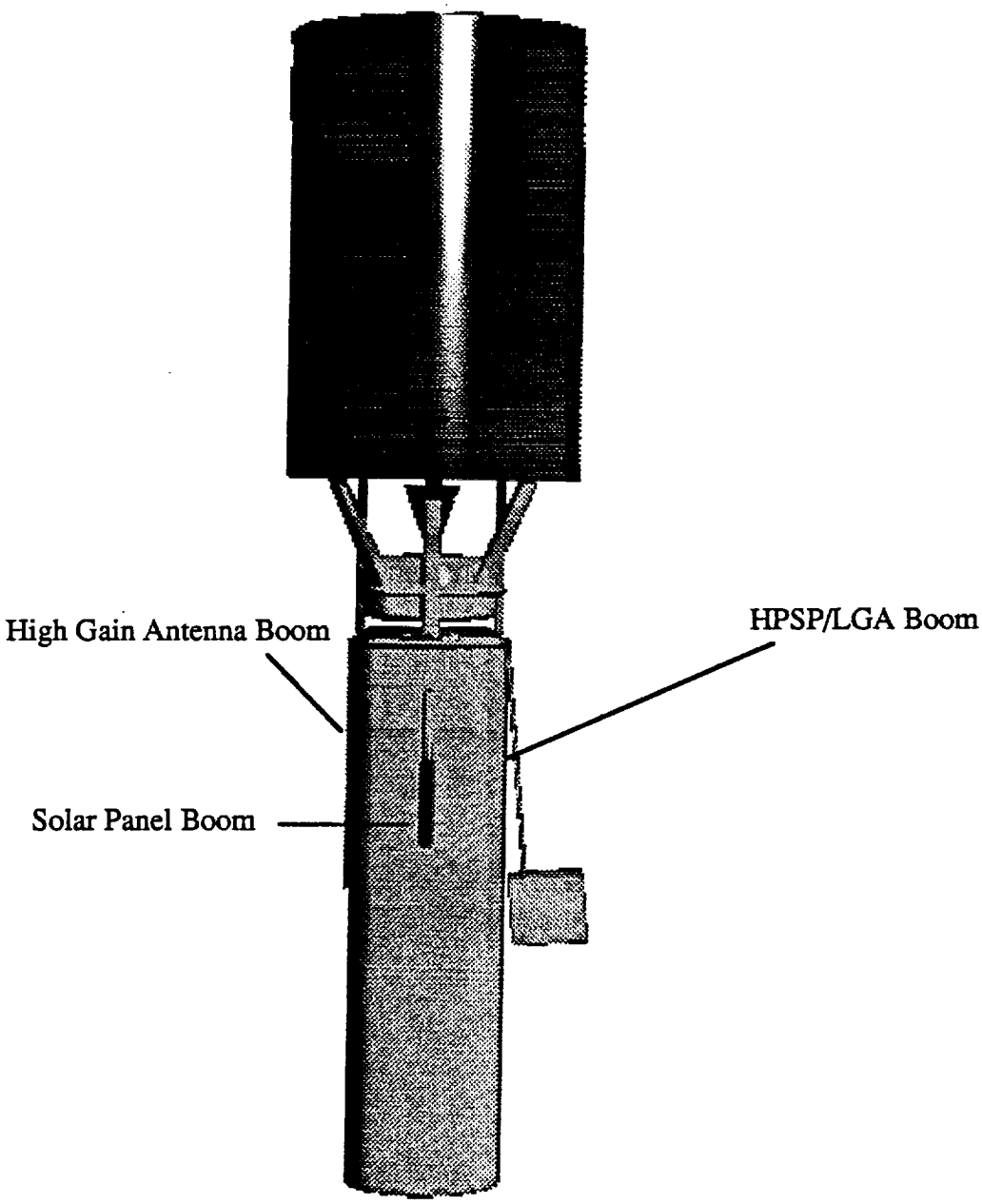

Figure 2.2. Spacecraft Configuration in Payload Fairing

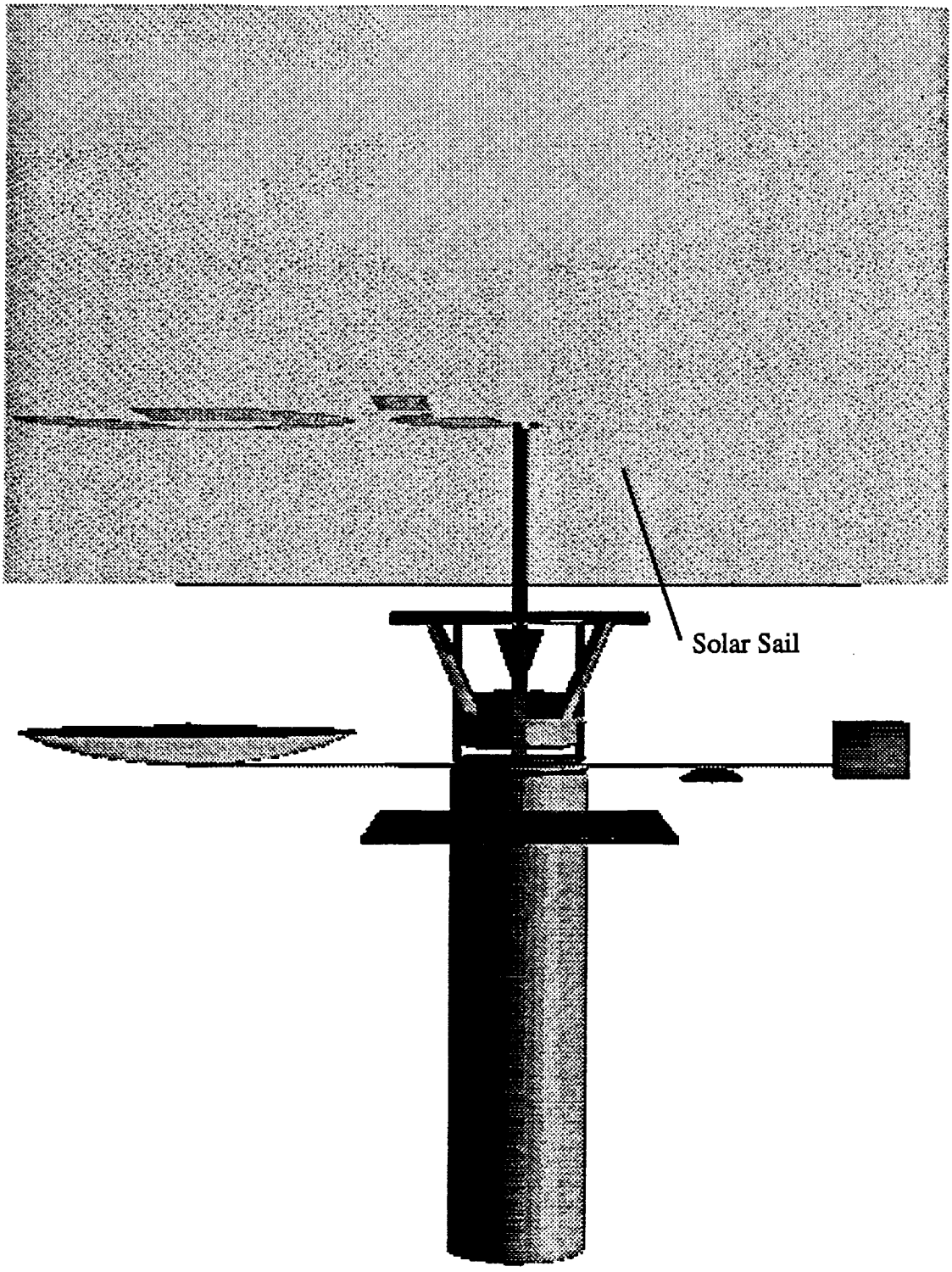

Figure 2.3. Spacecraft Configuration during Mercury Transfer

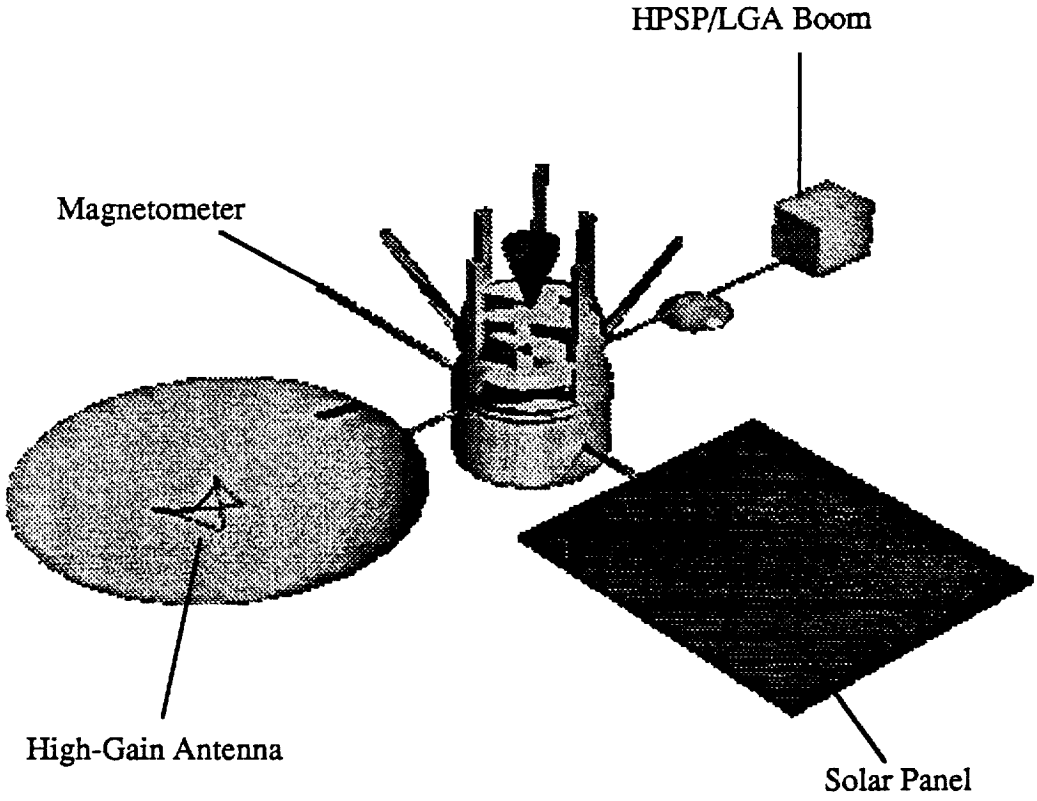

Figure 2.4. Orbiter Configuration

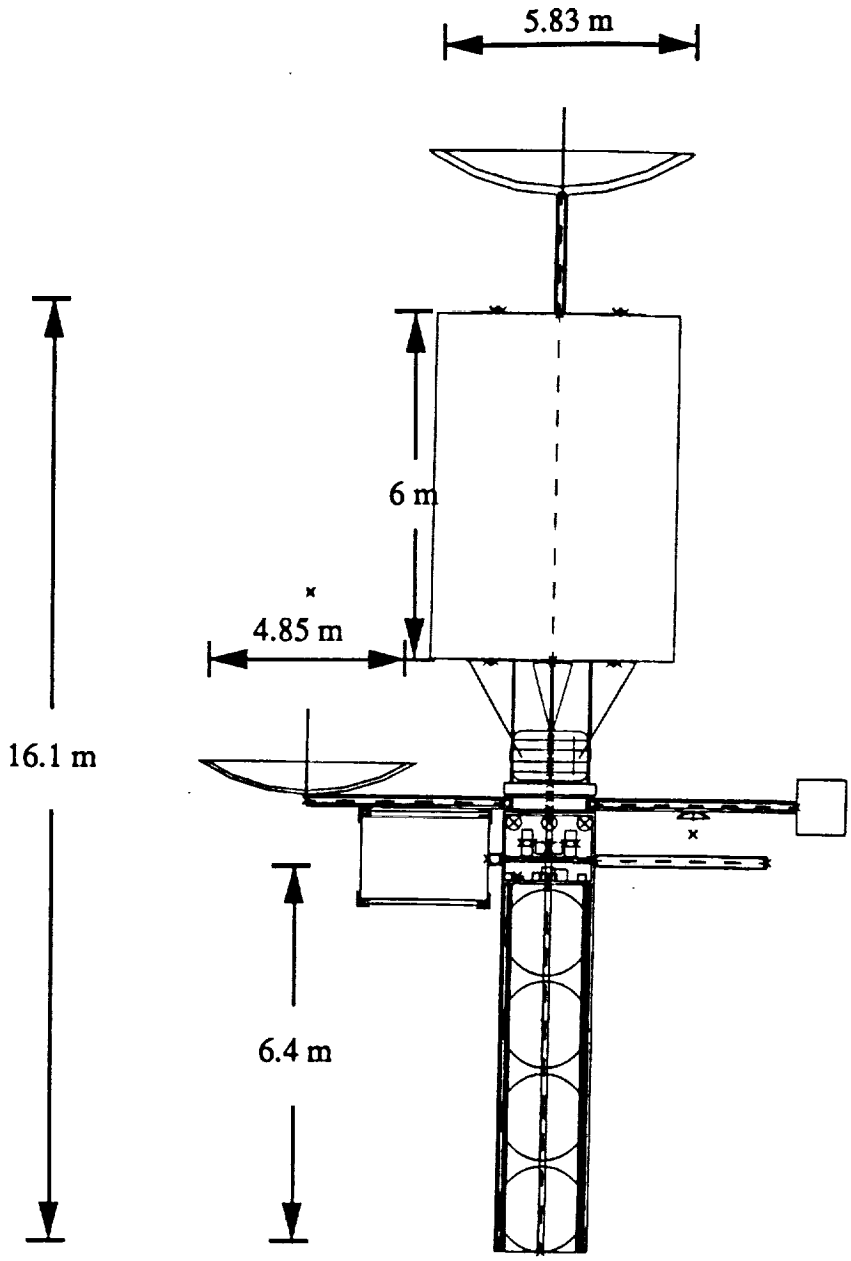

Figure 2.5. Side View Schematic of Spacecraft

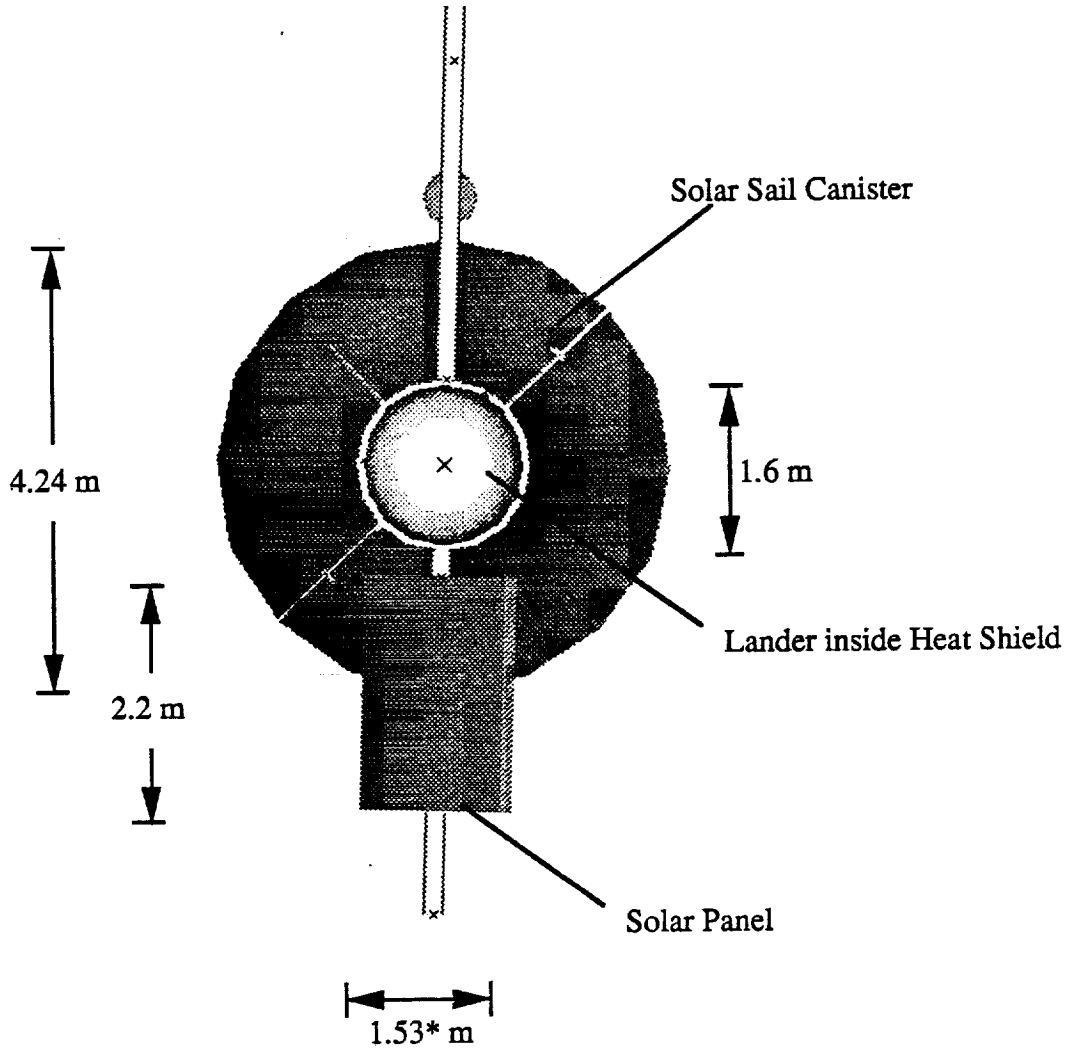

* Note: Solar array is oriented at a 50° angle.

Figure 2.6. Bottom View Schematic of Spacecraft

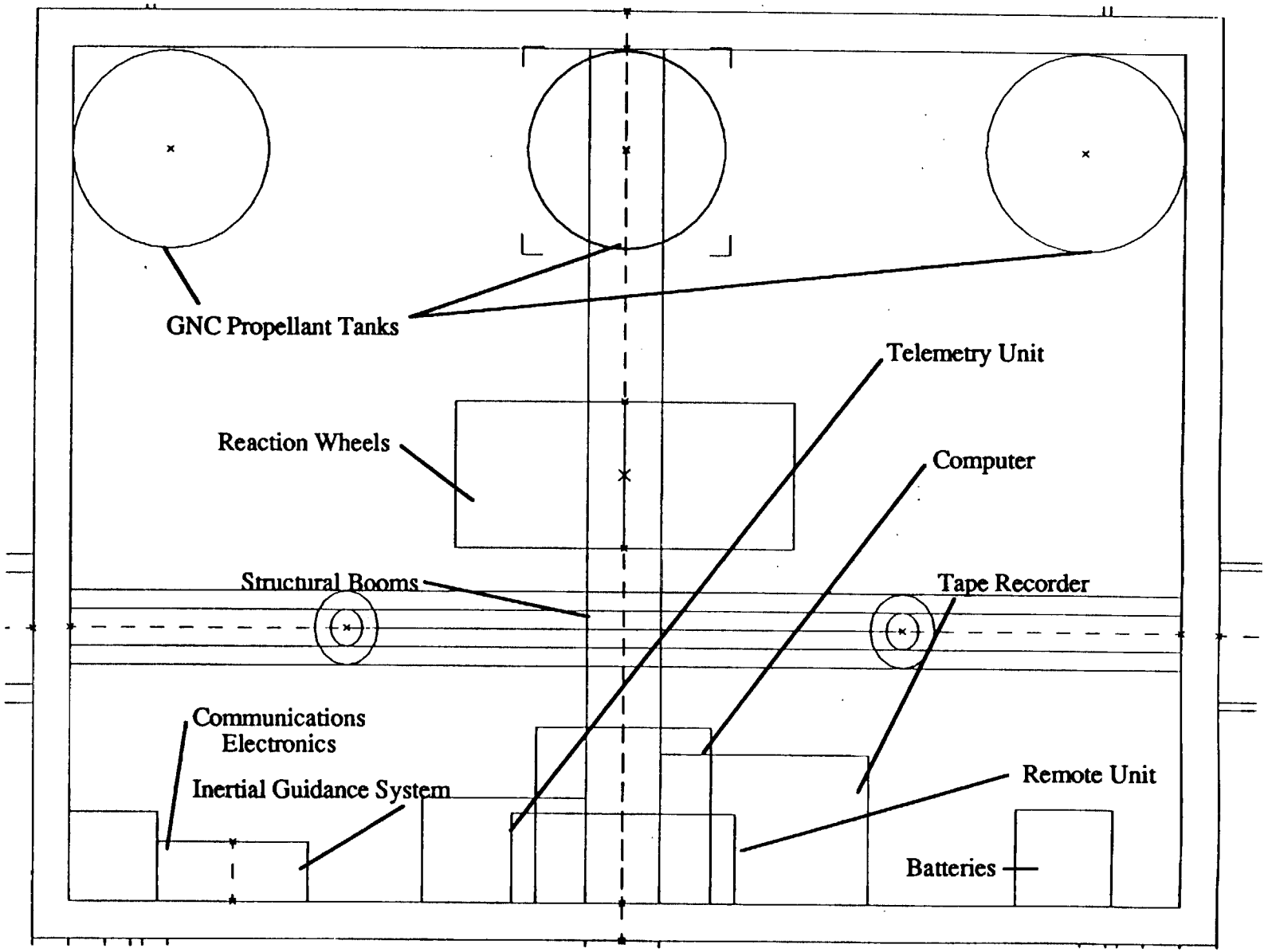

Figure 2.7. Internal Configuration of Main Body

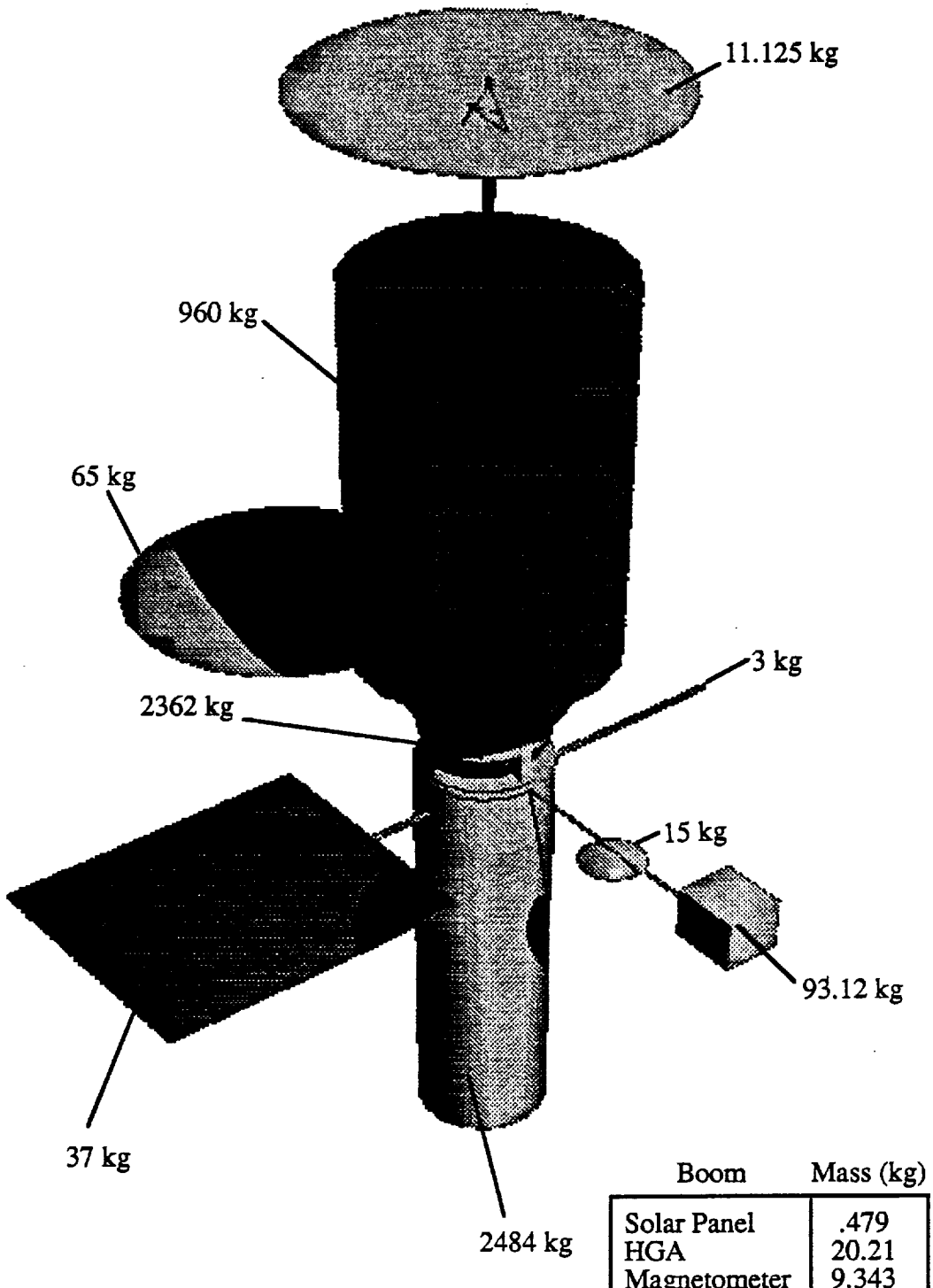

Boom	Mass (kg)
Solar Panel	.479
HGA	20.21
Magnetometer	9.343
HPSP / LGA	18.284

Figure 2.8. Mass Distributions of Spacecraft

2.3 Spacecraft Boom Analysis

An analysis of the four booms is done to optimize size and mass. Several dimensions of the booms were tested and the results are summarized in Appendix A. The inside diameter of the solar array boom is determined by the size of the heat pipe located between the array and the craft. Based on the calculated loads, the moments at the root are determined and compared to the moment of the opposite boom. The length of opposite booms are varied to achieve equality of the moments. The lengths, masses, stresses, deflections, and materials are listed in Table 2.1.

Table 2.1. Summary of Spacecraft Boom Analysis

Boom	Material	Mass (kg)	OD Radius (m)	Stress (MPa)	Deflection (cm)	Length (m)
Communication	Graphite Epoxy	20.201	0.0377	35.18	7.288	3.452
Solar Array	Al 6061-T6	0.479	0.025	2.74	0.034	0.25
Magnetometer	Al 6061-T6	9.343	0.0227	2.65	5.07	3.1
Sci. Instruments	Graphite Epoxy	18.284	0.0377	10	10.813	3.5

2.4 Requirements for Lander Configuration

The design parameters of the landers are governed by several subsystems. The scientific instruments subsystem requires a camera on the bottom of the lander, a camera on the surface sampler arm, and camera mounted in clear view of the surface. The alpha particle x-ray instruments must be kept away from any thrusters and the surface sampler arm must have access to the seismometer.

GNC and propulsion requires the placement of thrusters such that a controlled descent and landing can occur. For the power subsystem, RTGs must be insulated from sensitive instruments. The communications subsystem requires a low-gain antenna on board, and the

C&DH subsystem needs a recorder and computer. Thermal control requires the RTGs to be insulated from the lander. Additionally, heat pipes with thermal switches will help maintain the landers temperature within operational limits.

2.5 Lander Configuration

The final lander design consists of a 1.5 m diameter spherical probe with internal instruments. There are four thrusters on the bottom of the probe for descent and landing purposes. A camera is in the middle of the thruster configuration. The propellant tank and RTG are above the descent thrusters. The instruments (the facsimile cameras, the alpha ray particle sampler, the sampler arm, and the seismometer) are on a platform above the propellant tank. The extendible arms that open the top of the lander and form the legs of the probe are located on the platform. The low-gain antenna is positioned on one side of the platform as well. In the center, there is one tube supporting the upper GNC thrusters. The tube contains propellant lines for the thrusters located at the top of the lander.

2.6 Selection of Materials

2.6.1 Material Requirements

Strong, reliable materials are a necessity for this mission. Strength and rigidity are required for both the main body and the booms of the spacecraft. These booms must be able to withstand the large cantilever moments produced by the tip masses when impulsive burns are conducted. Good fatigue resistance is also desired because the transfer time to Mercury is several years, and repeated pressure cycling on the spacecraft may weaken the supports.

Because the landers house some of the most important instruments, a strong, reliable material should be used. Initially, the high temperatures on the planet's surface raised concern as to material selection. A material that expanded very little when heated and retained its material properties at such high temperatures would be needed. However, the

mission scenario later specified that the landers were to be deployed on the dark side of the planet. The temperature on this side of the planet is estimated to be -187 °C at its coldest point. Given this mission scenario, the material would have to withstand cold temperatures rather than hot.

2.6.2 Material Consideration

Several materials have been considered for selection in the various aspects of the mission. They are listed with their properties in Table 2.2. A cost comparison is discussed below.

Table 2.2. Spacecraft Materials

Material	Density (g/ccm)	Ultimate Tensile Strength (MPa)	Specific Strength ($x10^3$ Nm/kg)	Young's Modulus (GPa)	Specific Modulus ($x10^3$ Nm/kg)	Thermal Expansion ($x10^{-6}$ /K)
Steel	7.6	1309	172	200	26.3	11
Titanium	4.43	1034	233	110	24.8	8.8
Aluminum	2.8	523	187	71	25.4	28.9
Graphite/Epoxy	1.49 - 1.69	620 - 1340	367 - 893	82 - 289	55 - 171	-1 - 0
Boron/Epoxy	2.01	717 - 1337	357 - 665	115 - 206	57.2 - 102.5	4.2 - 4.6
Aramid/Epoxy	1.38	1378	999	75	54.9	-4.0
Glass/Epoxy	1.8	1062	590	39	21.4	8.6
Boron/Aluminum	2.6	1491	573	214	82.3	4

Data taken from:

— Wertz, J.R. and Larson, W.J., Space Mission Analysis and Design, Klewer Academic Publishers, 1991, p. 394.

— Agarwal, B.D. and Brontman, L.J., Analysis and Performance of Fiber Composites, Wiley Publishing, 1990, p. 437.

2.6.3 Material Selection

When selecting materials for the spacecraft, the main body was the foremost concern. A trade study was conducted to compare the materials in Table 2.3 and select the suitable

one. Material cost, risk, performance, and ease of manufacture (merit) were compared. Each material was rated in the four categories of a scale of 1 (low) to 5 (high). Weighting factors were assigned to each variable in terms of its importance on a scale of 1 (least important) to 10 (most important). The following performance equation incorporates cost (C), risk (R), ease of manufacture (E), and performance (P),

$$J = 6C + 8R - 3E - 10P \tag{2.1}$$

The trade study results are listed in Table 2.3. The material with the lowest corresponding trade value (J) is the optimum choice for this set of parameters.

Table 2.3. Material Trade Study

Material	Cost (C)	Risk (R)	Ease (E)	Perf. (P)	J
Steel	2	3	5	2	-5
Titanium	3	3	4	3	0
Aluminum	*2*	*3*	*5*	*4*	*-19*
Graphite/Epoxy	5	2	3	5	-13
Boron/Epoxy	4	2	2	4	-6
Aramid/Epoxy	4	2	3	4	-9
Glass/Epoxy	3	2	3	4	-15

As indicated, aluminum was chosen as the primary material for the spacecraft. Aluminum is lightweight and has a reliable record in space applications. High performance materials are not required for this application, so a lower cost material will suffice. Thermal concerns are not a problem on the orbiter because the thermal control of the craft will keep the temperature between -15 and 40 °C. This is within the normal operating temperature of all the materials

listed in Table 2.2. Specifically, the main body, despun platform, and the lander shroud will be made of aluminum.

The only two components of the orbiter that will not be made of aluminum are the propellant tank and the solar sail. The propellant tank will be made of graphite/epoxy composite. This decision is based on two reasons. First, epoxy resin is a corrosion resistant material; whereas aluminum, as with most metals, does not react favorably to corrosive materials. Since hydrazine and nitrogen tetroxide are the propellants of the Earth escape rocket, their corrosive properties must be taken into account. Second, graphite/epoxy is stronger and stiffer than aluminum. These properties are required of a pressure vessel such as a propellant tank. Mylar was chosen for the solar sail because it is a low density material.

The landers will be made of two materials. Because the base of each lander will be in contact with the cold surface of Mercury, a thermally insensitive material is desirable. A layer of aramid/epoxy composite will cover the bottom of each lander, acting as a thermal shield. Aramid/epoxy is less brittle than other composites. This also will be helpful in absorbing the landing impact. Since the material is expensive, it will not be used on the entire skin, but only where required. The lander's thermal control will keep the temperature of most of the lander between -15 and 40 °C, as in the orbiter. Also, the rest of the lander will not be under any severe structural loads, the remainder of the lander's structure will be aluminum. As mentioned earlier, its reliability, low cost, and low density are the reasons it will be used.

2.6.4 Material Cost

The material cost is listed in Table 2.4. These values are just material costs, and do not take into consideration the manufacturing costs of high performance composites. The total cost of the spacecraft's materials will be approximated as ten times the material cost [3].

Table 2.4. Approximate Material Cost

Material	Young's Modulus (GPa)	Cost ($/lb)
Aluminum	71	4
Aramid/Epoxy (Kevlar)	113	25
Graphite/Epoxy	414	610
Graphite/Epoxy	311	220
Graphite/Epoxy	166-228	43
Graphite/Epoxy	146	17

In the case of graphite/epoxy, the cost is dictated by the material's performance. Therefore, the stiffnesses of the four most common graphite/epoxy composites are listed with their respective prices. A more detailed choice of graphite/epoxy composite for the propellant tank was not done for this report.

2.7 Summary of Structural Design

The spacecraft consists of several major components. The main body contains delicate orbiter instruments. Four landers encased in a louver fairing are attached to the front end of the main body. A thruster and propellant tank are located at the opposite end of the main body. A solar sail and its canister are attached near the thruster by explosive bolts. Communication antennas, the HPSP, a magnetometer, and a solar array are all attached to the main body by booms.

Most of the spacecraft is made of aluminum because of its reliability in space applications, low density, and low cost. In areas where greater performance is required, composites are used. The components made of composites include the propellant tank, two booms, and the bottom skin of the landers.

3.0 Power Subsystem

3.1 Power Requirements

The power system is designed for one purpose, to provide the electrical power required by the spacecraft. The system must also be highly reliable in order for the mission to be accomplished. These are the only limiting requirements on the system. The power demanded by the spacecraft components is the overall design parameter for the power system. Mass, cost, and reliability are also important parameters which were considered in the design.

3.2 Orbiter Power System

The primary missions of the orbiter, transport and data relay, are highly dependent upon the power subsystem. Because of the proximity of Mercury to the Sun, the first source of power investigated was solar arrays. Other options such as radioisotope thermoelectric generators (RTGs) and solar dynamics were researched and evaluated. However, as Table 3.1 shows, these options were not as feasible as the solar arrays.

$$J = K_1(cost) + K_2(complexity) - K_3(heritage) - K_4(performance) \qquad (3.1)$$

K_1=5, K_2=4, K_3=3, K_4=5
1=Best, 5=Worst

Table 3.1. Trade Study for Power Source

Option	Cost / Watt	Complexity	Heritage	Performance	J
Silicon	3	3	5	3.5	-5.5
GaAr	3.3	3.3	4	5	-10
$InPO_4$	3.7	3.7	3	4.5	-4.5
RTG	5	1	4	1	12
Solar Dynamic	2	5	1	2	17

In Table 3.1, solar cells were separated into three categories according to the type of photovoltaic cell employed. The type of cells evaluated were silicon (Si), gallium arsenide (GaAr), and indium phosphate ($InPO_4$). It is evident from the trade study that solar arrays are the best source of power for the system; however, the choice of which photovoltaic cell to use for the power source was not easy to determine. Silicon seemed the most economical choice with a greater heritage than either GaAr or $InPO_4$. However, silicon's performance efficiency and rate of radiation degradation as compared to the other two eliminated this as a possible option. Because of the intensity of the solar radiation at Mercury, the rate of degradation was a high factor in the evaluation. Silicon has a degradation rate of 2.5% per year as compared to 1.25% and 0.25% for GaAr and $InPO_4$, respectively. Based on this factor alone, $InPO_4$ would be the best option for the array, but the higher cost and complexity, along with a shorter heritage, outweighs the fact that it degrades the slowest due to radiation. Therefore, GaAr was chosen as the cell material because it has a higher resistance to radiation damage that Si, greater heritage than $InPO_4$, and a higher conversion efficiency then either of these.

Once the power source was chosen, a power budget was compiled. The completed power budget, broken into individual subsystem power requirements, is shown in Table 3.2.

Table 3.2. Orbiter Power Budget

Subsystem	Maximum Power Req'd (W)
Thermal Control	56
Scientific Instruments	197
Propulsion	—
GNC	582
Communications	165
C&DH	177
TOTAL	1177
TOTAL w/ 10% Margin	**1295**

The solar array area was calculated by examining the three independent power requirements that the subsystem must meet and sizing the arrays based on the limiting case. The first condition requires 600 W of power to be supplied at LEO to allow for instrument standby and GNC operations. The second condition is to provide a minimum of 600 W during transit to Mercury. Finally, the power subsystem must provide a peak power of 1295 W while orbiting Mercury. Calculations in Appendix B show that providing 600 W at LEO is the limiting case and dictates a solar array area of 4.4 m^2. This size array allows for an angle of incidence of up to 14° at Earth, and 50° at Mercury. This large range of angles at mercury provides a variety of benefits. First, a large angle increases the longevity of the cell lifetime by reducing the direct radiation intensity of the array surface. Also, should a component draw too much power or cell damage occur, the array could provide up to 900 W of additional power by taking the angle of incidence to 0°. While this would harm the cells in time by dramatically increasing the radiation degradation, it is an option that does exist. The 4.4 m^2 solar array will be mounted on a single boom that will actively track the Sun and adjust the angle of incidence according to power needed and radiation accepted. This area results in a mass of the solar arrays of approximately 36 kg, not including the boom. The total array cost is $3.3M (FY1993).

Because of the extreme temperatures and radiation that the solar cells will encounter at Mercury, non-textured cover slides, coating, and back-surface reflectors will be installed on the solar arrays. The combination of these components will decrease the cell operating temperature and decrease reflective losses of the solar cells.

Three types of batteries were examined to provide power to the orbiter during Earth and Mercury eclipse periods. They were NiCd (Nickel Cadmium), NiH (Nickel Hydrogen) with individual pressure vessel design (ipv), and NiH with common pressure vessel (cpv) design. The trade study comparing these options is shown in Table 3.3.

$$J = K_1(cost) - K_2(heritage) - K_3(performance) \qquad (3.2)$$

K_1=4, K_2=3, K_3=5
1=Worst, 5=Best

Table 3.3. Trade Study for Power Storage Options

Option	Cost	Heritage	Performance	J
NiCd	2	5	1.5	-14.5
NiH (ipv)	3	3.5	4	-18.5
NiH (cpv)	5	2.5	5	-12.5

A NiH battery with individual pressure vessel design was chosen over NiCd due to its higher depth of discharge and specific energy density, and over NiH with a common pressure vessel design due to a greater heritage. As shown in Appendix C, the batteries were sized to meet both Earth and Mercury requirements. At Earth, they must provide 600 W of power during the 85 minute Earth eclipse periods, and they must provide a maximum of 1295 W of power during the 35 minute Mercury eclipse periods. The power needed at Earth was the limiting case, therefore the batteries will have an approximate mass of 26 kg and occupy a space on the orbiter of 2130 cm^3.

The distribution of the power received from the arrays is also critical to the system operation; regulation and control of the power voltage must be considered. The power bus that distributes the power to the various components must be regulated directly or indirectly. The bus voltage was chosen to be 28 VDC because it is "off-the-shelf" technology that has been proven many times [4]. From here the power is distributed to well over 100 different components. This will be done through a series of power converters along the main bus line in order to regulate the power to each component and change the baseline voltage from 28 V to the operating voltage of the individual components.

Distribution from the bus will result in a series of switches and fault protection devices used in series and parallel. Mechanical switches will be used because the solid state switches have not been space-qualified at this point. The fault protection devices will be connected to the onboard computer which will make the system autonomous because the spacecraft will be far from Earth. The computer will locate and isolate the fault before damage to the system or electric component it supplies can occur. After this is accomplished, the computer will reroute the power around the fault to ensure that the component can function. Therefore, the system must be highly redundant in nature to assure the success of the mission; for this reason the bus itself will be doubly or even triply redundant. Further development of this system is required before the spacecraft can be sent on its mission to Mercury [5].

The solar array will be regulated by a peak power tracking (PPT) system. This system monitors the power drawn by the spacecraft and adjusts the array angle to compensate for the power level. The PPT also functions while the secondary batteries are charging. When the batteries are charged, it adjusts the array for the power required by the various spacecraft components. This method is less efficient than the Direct Energy Transfer (DET) method because it uses 7-10% of the total power. However, the DET uses shunt resistors to dissipate excess power from the solar arrays; this causes more thermal loading on the spacecraft. Because of the mission's proximity to the Sun, this increased thermal loading is an undesirable side effect. On the other hand, the PPT will increase the array angle if a low power demand is made, thereby helping to lengthen the lifetime and preserve the solar cells [6].

The mass of the distribution system will be approximately 20% of the power system mass. This mass will include the harnesses, wiring, converters, switches, busses, and all the rest of the components that control the distribution of power to the systems. The estimate of this mass is 7.2 kg.

Primary batteries, most likely lithium cells, will be used to provide for equipment standby power during launch and until solar array has been deployed.

3.3 Lander Power System

The four landers destined for Mercury will utilize the same power system in order to alleviate design costs. The source of power for these landers was a great concern for thermal control reasons. A list of options could not be made until the landing sites of the landers was determined. After it was determined that the landers would land at night on Mercury, a list of three options was developed. The options were RTGs, fuel cells, and primary batteries. Table 3.4 shows the trade study between these options.

$$J = K_1(cost) - K_2(efficiency) - K_3(performance) + K_4(mass) - K_5(heat) \quad (3.3)$$

K_1=2, K_2=1, K_3=5, K_4=3, K_5=4
1=Best, 5=Worst

Table 3.4. Lander Power Source Trade Study

Option	Cost	Efficiency	Performance (@ 90 °K)	Mass	Waste Heat	J
RTG	5	3	5	2	5	-32
Primary battery	2	2	2	4	1	0
Fuel cell	3	2	3	4	3	-11

The nighttime climate on Mercury is extremely cold, 90 K or -183 °C. In this extreme temperature, primary batteries have a very low efficiency and a shortened lifetime. This places an extra burden on the thermal control system. In addition to this, the batteries are bulky and have a large mass. Fuel cells, like batteries, also are bulky and have a large

amount of mass. While they do give off some waste heat, the fuel cells also have a low efficiency and give off unnecessary water. This leaves RTGs as the best option. RTGs have two disadvantages, they are very expensive and produce a large amount of waste heat. However, in the climate of the dark side of Mercury, this waste heat is seen as beneficial for the thermal control of the lander. There was concern over the waste heat that will be produced in transit to Mercury. However, this has been solved by "starting" the RTGs at Mercury instead of at Earth. This would be accomplished by separating the mass into several smaller parts and then amassing it upon arrival at Mercury. Also, the RTGs have no moving parts and would last well after the lander has melted on the day side of Mercury.

Table 3.5 shows the power budget for one lander. The total power requirement is 218 W. The RTG was sized using the modular RTG, or MOD-RTG, with each module, or slice, supplying about 18 W of power. Therefore, 13 slices will be required to obtain the total power requirement. These slices will in turn produce 2800 W of waste heat that will be used by the thermal control system to heat the scientific instruments and other vital electrical components on the lander. With this number of slices, the RTG mass and cost was calculated to be 30 kg at $3.7M (FY1993). Also, the RTG will stand 26 inches high and have a square cross-section of 18 inches with the heat transfer fins attached [7].

Table 3.5. Lander Power Budget

Subsystem	Maximum Power Req'd (W)
Thermal Control	18
Scientific Instruments	55
Propulsion	—
GNC	10
Communications	65
C&DH	50
TOTAL	198
TOTAL w/ 10% Margin	**218**

Like the orbiter distribution system, the lander will have a 28 VDC bus that is at least doubly redundant. The system will operate very much like that of the orbiter. However, since the source of power is an RTG, the PPT is not required in the system. A variation of a DET system will be used to control the bus voltage during lander operation. The excess power will be dissipated through shunt resistors as extra heat with the rest of the RTG waste heat. The mass of this distribution system will be approximately 6 kg.

3.4 Power Design Summary

The power subsystem was designed in two components, the orbiter power system and the lander power system. The orbiter will utilize a solar array with a maximum projected surface area of 4.4 m^2. A peak power tracker will control the array and regulate the power obtained by the arrays. Secondary batteries will be used during the eclipse periods of the array. A doubly or triply redundant distribution system was designed for very high system reliability. The total mass of the orbiter system is 74.4 kg at a cost of about $4M (FY1993).

The second power system is for the landers. All four landers will use the same power source, a MOD-RTG. The RTG produces 218 W of power and 2800 W of waste heat. A variation of the direct energy transfer control system is used to regulate the power supplied to the bus through the use of shunt resistors. The distribution system is patterned much like the orbiter's in the other aspects. The system has a mass of 35.9 kg at a cost of $4M (FY1993).

4.0 Propulsion Subsystem

4.1 Requirements

The propulsion subsystem of the SPF-2000 can be broken down into the primary and secondary systems. The primary system is the solar sail which will be used to propel the spacecraft from LEO to Mercury orbit. The secondary system consists of the components used to escape Earth's gravity, to insert into Mercury's orbit, and to land the probes safely on the surface of the planet.

4.2 The Solar Sail

The primary source of propulsion for this mission is the solar sail. The solar sail consists of a 0.1 mm layer of Mylar, which includes a layer of aluminum for reflection of the Sun and thick rip-stop doubles. These rip-stops help prevent tear propagation, creep, and elongation [8]. Figure 4.1 shows an enlarged view of the cross section of a solar sail sheet.

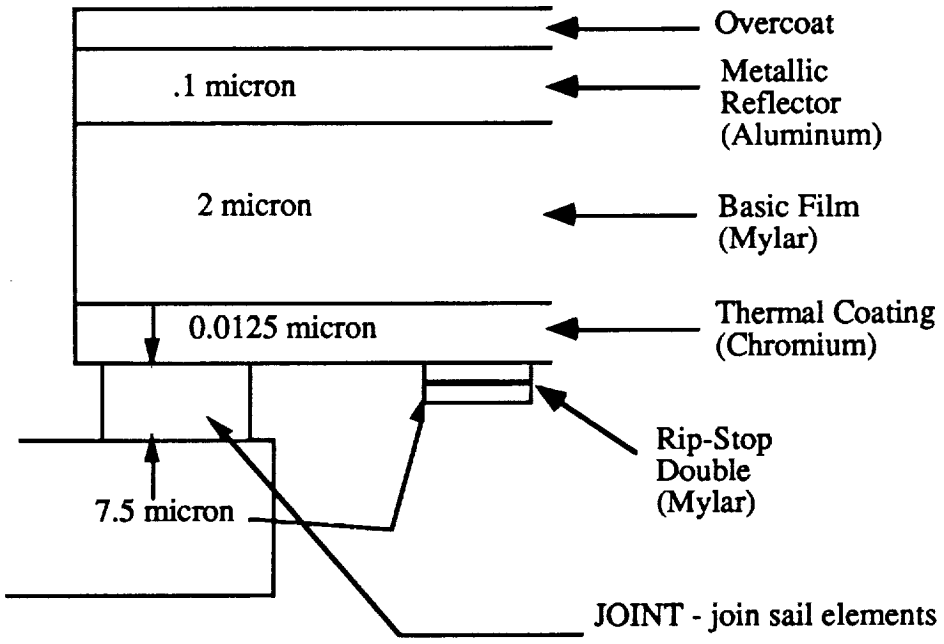

Figure 4.1. An Enlarged View of the Cross Section of a Solar Sail Sheet [Adapted from Friedman, Louis, *Star Sailing, Solar Sails, and Interplanetary Travel*, 1989, p. 30]

4.2.1 Determining the Area of the Solar Sail

The area of a solar sail required to produce a specified thrust depends on the mass of the spacecraft and the characteristic acceleration, a_c, which is a function of the desired transit time. Given the a_c and the mass of the spacecraft, the average force needed to get from Earth to Mercury can be determined using Newton's equation.

$$F = m \bullet a_c \tag{4.1}$$

The necessary power to achieve this force can then be found from Equation 4.2.

$$F = 2P/c \tag{4.2}$$

where c is the speed of light, (2.99E8 m/s), and P is the power needed to achieve the average force. Since the resultant force comes from both the incoming and reflected light, P must be multiplied by 2.

Equation 4.3 shows the relationship between the required power, the solar flux per unit area, S, and the area of the sail, A.

$$P = SA \tag{4.3}$$

The solar flux during travel is related to the solar flux at Earth by Equation 4.4,

$$S=S_0(D_0/D)^2 \tag{4.4}$$

where D is the distance of the spacecraft from the Sun, D_0 is the distance of Earth from the Sun, (1 AU. or 1.5×10^{12} m), and S_0 is the solar light flux at Earth, (1.4 kW/m^2). By setting S equal to S_0 (1.4 kW/m^2) at Earth, and using Equations 4.1 to 4.3, the maximum area for the solar sail can be approximated [9]. If the SPF-2000 has a mass of approximately 5000 kg

(including the sail), and a characteristic acceleration of 0.6 mm/s^2 is desired, an approximate sail area of 0.32 km^2 is required. This sail area will be achieved using a circular sail with a radius of 319 m. One important item to take into account is that unless the spacecraft is traveling directly away from the Sun, the sail will be oriented at some angle, θ, with respect to the Sun. This will result in an area that reflects light being less than the total area of the sail. The equation then used to find the varying force on the sail as the spacecraft approaches Mercury then becomes,

$$F = 2\ S\ A/c\ \sin^2\theta \tag{4.5}$$

4.2.2 Determining the Time of Transit and Trajectory with the Solar Sail

In order to predict the time of transit of the solar sail, a program was developed [by Dr. Roger Thompson, Aerospace Engineering Department, Penn State University] that calculates the trajectory of the spacecraft using Encke's Method (see Appendix D). Encke's method integrates the difference between the primary acceleration and all perturbing accelerations. At a given initial time, or epoch, an osculating orbit is calculated using the given conditions. This osculating orbit is a conical orbit about some principal gravitational source. In this case, the gravitational source is the Sun. At epoch, the osculating and true orbits are in contact. When the true orbit deviates too far from the osculating orbit (as a result of perturbing accelerations), a new epoch and starting point are chosen and the integration continues from this point. A new osculating orbit is then found from the true radius and velocity vectors, neglecting perturbations. This process is known as rectification [10].

With the angle of the sail set at 60 degrees with respect to the solar flux, the sail gets the maximum force possible at all times during the mission. With the 0.32 km^2 sail, this force at Earth is 2.24 x 10^{-3} kN. At Mercury, it is 5.78 x 10^{-3} kN. The initial velocity of the spacecraft is equal to 29.262 km/s (which is the sum of the velocity of the Earth around the

Sun and the escape velocity), and the initial radius is the heliocentric radius of Earth, 1.49×10^8 kilometers. With these conditions, the time of transit to Mercury was found to be approximately days 1314 days (3.6 years). The final velocity of the spacecraft as it approaches Mercury is 46.9 km/s and the orbital parameters with respect to the Sun can be seen in Table 4.1.

Table 4.1. Orbital Parameters as the SPF-2000 Approaches Mercury

r	Distance Between the Spacecraft and the Sun	6.023×10^7 km
v	Velocity of the Spacecraft as it Approaches Mercury	46.9 km/s
E	Specific Mechanical Energy	-1177.171 km^2/s
e	Eccentricity of the Orbit	0.05399
a	Semi-major Axis	5.607×10^7 km
h	Specific Angular Momentum	2.795×10^9 km^2/s

As can be seen from the eccentricity and the value of the semi-major axis, the final orbit is almost circular. It is important to note that in calculating these values, Mercury, Venus, and Earth are assumed to be in circular coplanar orbits. Once the spacecraft has reached Mercury's heliocentric orbit, the sail will be discarded and an XLR-132A motor will be used for insertion into a 500 km orbit around the planet.

4.3 Probe Propulsion Rocket Motor

The primary propulsion system on the probe will consist of four rocket motors. These motors will provide the ΔV necessary for the probe to descend from a 500 km orbit to the surface of Mercury. The motors will then be used as braking devices to land the probes safely. The descent will take place with roughly three to four engine firings. The first burn, fired opposite to the orbiter's motion, causes the probe's velocity to decay rapidly and begins the landing sequence. The second firing will reduce the craft's velocity slightly and enable it

to make any trajectory corrections. The final burn, performed near the surface, will allow the probes to land softly and smoothly.

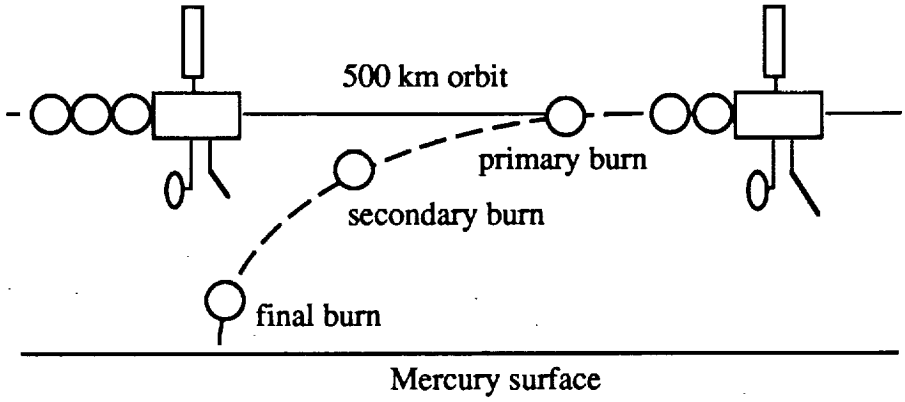

Figure 4.2. Probe Landing Scenario

To select the proper motor for the mission, the total ΔV's with respect to the orbiter's altitude were found and the amount of thrust that the motor must provide was determined. The time of descent was also calculated, and the minimum burn time for the motor was determined. The ΔV needed for the primary burn is simply the ΔV needed for the probe to perform the descent. This change in velocity can be found using Equations (4.6) through (4.8).

$$V_c = \sqrt{\frac{\mu}{r_c}} \tag{4.6}$$

$$\frac{1}{2}V^2 - \frac{\mu}{r} = -\frac{\mu}{2a} \tag{4.7}$$

$$\Delta V = |V_c - V| \tag{4.8}$$

By varying the altitude of the orbiter above the surface of Mercury, a series of orbits was examined to determine where the least possible ΔV will occur. As expected, the smallest ΔV occurs in the lowest orbit.

The sum of the ΔV's required for the second and the third burns is equal to the total ΔV required to bring the probe to a complete stop. Equation (4.7) can be used to solve for the velocity at touchdown by setting the variable "r" equal to the radius of Mercury instead of the orbit radius. The chosen thruster must not only work to counter the free fall motion, but also be able to give the probe sufficient time to make any navigational adjustments before touchdown.

To solve for the time of descent, Kepler's time equation was used. The calculated results of the ΔV and the descent time are shown in Table 4.2. Table 4.3 lists the properties for the various motors being considered.

$$E - eE\sin E = \sqrt{\frac{\mu}{a^3}}(t - T_o) \tag{4.9}$$

Table 4.2. ΔV and Time of Descent for Various Altitudes Above Mercury

Parameter	500 km Altitude	400 km Altitude	300 km Altitude
Semi-major axis length	2079 km	2029 km	2004 km
e, Eccentricity	0.41349	0.399	0.391
E, Eccentric anomaly	5.368	5.5	5.57
Time of descent	213.5 s	177.8 s	159.7 s
ΔV needed for descent	0.6453 km/s	0.63 km/s	0.622 km/s
ΔV needed for braking	2.75 km/s	2.7 km/s	2.677 km/s
Total ΔV needed	3.396 km/s	3.333 km/s	3.3 km/s

Table 4.3. Rocket Motor Properties [Wilson, Andrew, *Interavia Space Directory*, 1991-1992 Jane's Information Group, Alexandria, VA, 1991, pp. 254-357]

Parameter	S3K	Marquardt R-40A	Star 13/13B	KTDU-35
Isp (sec)	352	281	285	281
Thrust (N)	3500	3870	3800	4090
Dry Mass (kg)	14.5	10.25	9.1	—
Length (mm)	1030	1039	980	—
Propellant Type	MON3 & MMH	N_2O_4 & MMH	Nitric Acid	—
Mp (kg) *	1.8231 m_o	2.8621 m_o	2.7779 m_o	2.8621 m_o
Burn Time (sec)	91.283	103.462	103.725	97.896
Number needed	4	4	4	4

* m_o is the dry mass of probes (203 kg)

Equations (4.10) through (4.12) were used to determine the propellant mass needed to obtain the desired thrust. It should be noted that the mass of the probe, which is 203 kg dry, is the driving factor in the mass of the propellant.

$$m_{ps} = m_f(e^{\Delta Vs/I_{sp}g} - 1) \tag{4.10}$$

$$m_{po} = (m_f + m_{ps})(e^{\Delta V/Ispg} - 1) \tag{4.11}$$

$$burn\ time,\ t = m_{po}gI_{sp}/Thrust \tag{4.12}$$

where m_{po} is the amount of propellant used to initially decay the orbit, m_{ps} is the mass of the propellant used to surface the probe, and m_f is the final mass of the orbiter.

A trade study was done to determine which motor would be the best for this mission. The key factors considered in this study are the mass, performance, and reliability of each motor. All three factors were very important, but the mass of each motor is slightly more significant than the other two since it directly affects the cost of the spacecraft. This parameter takes into account the motor's dry mass, propellant mass, and the mass of the structure (nuts, bolts, etc.). Since half of the probe's total mass will consist of the propulsion

system, and since the reduction of the mass of the spacecraft is a major concern, this parameter was weighted the highest at 3.5. The performance of the motor takes into consideration the motor thrust, Isp, and burn time. The probes are useless if they cannot land safely on Mercury. Thus a factor of 3 was chosen for this parameter. Finally, the reliability of the motor took into account the number of missions on which the motor had been used and when its first launch occurred. Some of the motors chosen were launched only recently and some have only been tested staticly. A more reliable motor reduces the risk of the mission, thus a value of 3 was also given to this parameter. Equation (4.13) shows the equation used to determine the performance indices for each motor. Table 4.4 shows the weighting factors, k, for each parameter and the performance indices, J , for the motors considered. As a result of the trade study, the S3K motor was chosen as the probe's main engine.

$$J = k1(performance) + k2(mass) + k3(reliability) \tag{4.13}$$

Table 4.4. Trade Study for Probe Motors

Motor	Performance	Mass	Reliability	J
S3K	1.5	1.5	2.5	17.25
R-40	2	3	1.5	21
Star 13/13B	2	2.5	2	20.75
KTDU-35	2	3	1	19.5

4.4 Probe Propulsion - Attitude Thrusters

The main purpose of the attitude thrusters is to correct the probe orientation so it can land upright on the planet. To determine the amount of thrust that must be provided, the situation shown in Figure 4.3 should be considered.

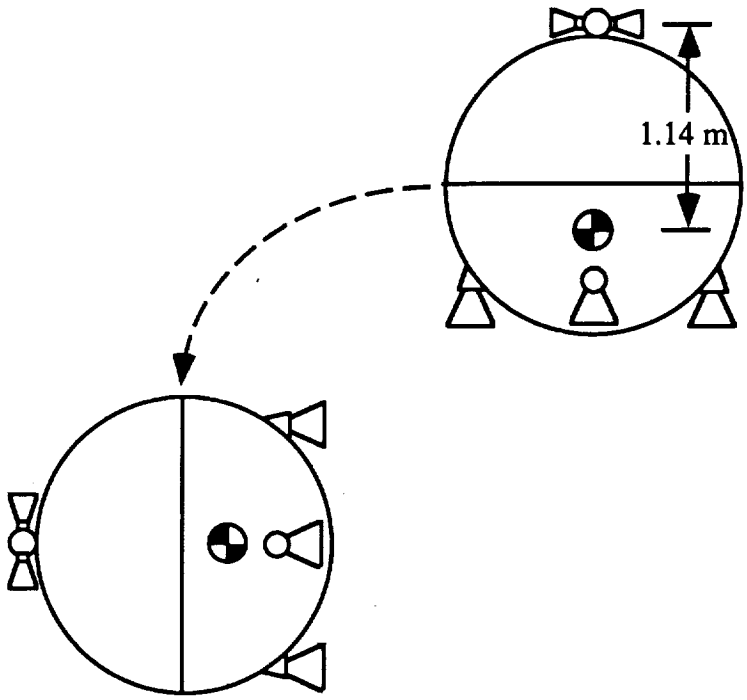

Figure 4.3. Probe Adjustment Scenario

The probe has fired the initial burn and it is now descending into the transfer orbit. At first the probe is stable and is falling at the proper orientation. But during the descent, some disturbance causes the probe to rotate slowly out of its position. The attitude thruster must fire to stop this rotation and continue to burn until the probe moves back into the upright position. The attitude thruster should then fire again to end the recovery rotation. Equations (4.14) and (4.15) were used to estimate the thrust needed to recover the probe at a spin acceleration, α, of 1.0 rad/s^2. If the probe can recover from this spin rate, it should be able to recover in an actual situation. Note that the moment of inertia, I, of the probe is 46.46 kg m^2.

$$Torque,\ T = I^{*}\alpha \qquad (4.14)$$

$$Moment = F * L = Thrust * 1.14\ m \tag{4.15}$$

For this value of α, the required thrust is 40.75N. Properties of the thrusters considered can be seen in Table 4.5.

Table 4.5. Properties of Various Thrusters [Wilson, Andrew, *Interavia Space Directory*, 1991-1992, Jane's Information Group, Alexandria, VA, 1991, pp. 281-282]

Parameter	CHT 20.0	Leros 20	MRE-5/GRO	MRE-15
Isp (sec)	235	295	240	225
Thrust (N)	20	22.2	24.5 x 2	89
Dry Mass (kg)	0.36	0.45	1.13	1.13
Length (mm)	195.74	—	210	269
Propellant Type	CHTs	MON & MMH	—	N_2O_4 & MMH
Number needed	8	8	4	4

Once again a trade study was done using Equation (4.13) to choose a suitable thruster. The parameters and their weighting factors were the same as those used in choosing the probe's main engine. Table 4.6 shows the results of this study.

Table 4.6. Thruster Trade Study

Thruster	Performance	Mass	Reliability	J
CHT 20.0	4	4	4	38
Leros 20	1.5	2	3.5	21.75
MRE-5/GRO	4	3.5	2	30.5
MRE-15	4.5	1	4.5	32.25

From Table 4.6 it can be seen that the Leros 20 would be the best choice for this mission. An added benefit to this thruster is that it uses the same type of propellant as the S3K engine. This will save unnecessary tankage mass since all propellant can be drawn from one tank.

4.5 Probe Propellant

Both the rockets and the attitude thrusters chosen for the probes use the same type of bipropellant. The fuel to be used is monomethylhydrazine (CH_3NHNH_2) or MMH. MMH has been used extensively as a fuel in spacecraft rocket engines, particularly in small attitude control thrusters. It has superior heat transfer properties and better shock resistance to blast waves than pure hydrazine. It also has a larger liquid temperature range. The tankage materials used to store pure hydrazine are also used to hold MMH. Yet MMH is soluble in many hydrocarbons in which hydrazine is not.

One of the disadvantages when using MMH is that it is very toxic. Atmospheric concentrations of all hydrazines should be kept below 0.1 ppm when people are exposed for long periods of time. Monomethylhydrazine decomposes at 491 K, while hydrazine explodes at 369 K when subject to pressure shocks of identical intensity [12].

The oxidizer for the probe is MON3. MON is a mixture of NO and N_2O_4. Different grades have between 2 and 30% NO content. The combination of MMH and MON is very common for a bipropellant. MON is a high-density, yellow-brown liquid. Although it is the most common storable oxidizer used in the United States today, its liquid temperature range is narrow and it is easily frozen or vaporized. It is only mildly corrosive when pure, but forms strong acids when moist or allowed to mix with water. But if it is stored in a sealed containers made of compatible material, it can be stored indefinitely [13].

4.6 Mercury Capture

The patched conic technique was used to approximate the propulsion requirements for capture into a Mercury orbit. A schematic of the capture scenario is presented in Figure 4.4.

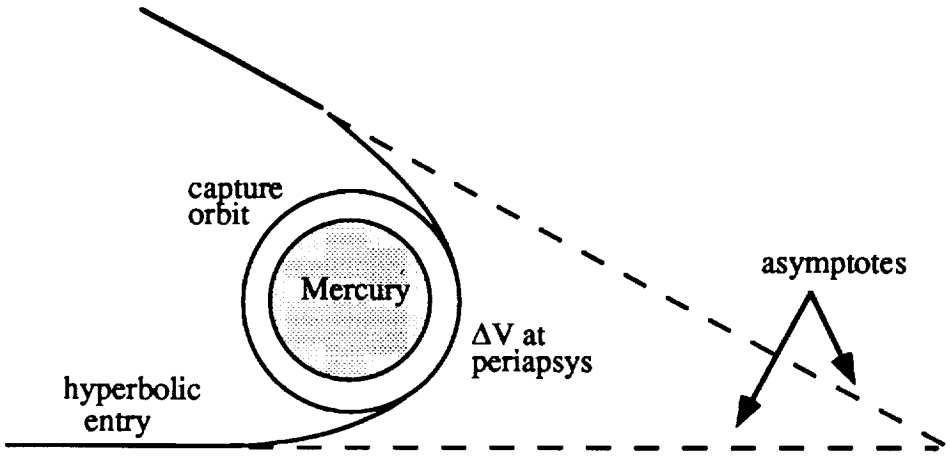

Figure 4.4. Schematic of Capture Scenario

In order to use the least amount of propellant possible, a near zero approach velocity, relative to the planet ($V_\infty \approx 0.5$ km/s) is used. Equation (4.14) is used to determine the required impulse burn for capture into a 500 km high orbit above Mercury,

$$\Delta V = \sqrt{V_\infty^2 + \frac{2\mu_{Mr}}{r_p}} - \sqrt{\frac{\mu_{Mr}}{r_p}} \tag{4.14}$$

where r_p is the sum of the orbit radius, 500 km, and the radius of the planet, 2439 km, and μ_{Mr} is 22320 km^3/s^2. In this case, ΔV is 2.1415 km/s. The mass of the propellant required can be expressed in terms of the final mass after the burn and the specific impulse (I_{sp}) of the rocket motor used. The burn time can also be expressed in terms of the propellant used, I_{sp}, and thrust of the motor. Equations (4.15) and (4.16) define these relationships.

$$m_p = m_{final}(e^{\Delta V/Isp g} - 1) \tag{4.15}$$

$$burn\ time,\ t = (m_p g I_{sp})/Thrust \tag{4.16}$$

Table 4.7 lists the specifications for the various motors being considered. Because the propellants must be carried for an extended period of time during transit to Mercury, only motors with storable propellants are considered here.

Table 4.7. Properties of Motors being considered.

Parameter	R-40B[1] (2 in parallel)	XLR-132A[2]	Transtar[3]
Manufacturer	Marquardt	Rocketdyne	Aerojet
Development Status	qualified	adv. development	ready for qualification
Isp (sec)	312	340	328
Thrust (kN)	2 x 4	16.65	16.65
Dry Mass (kg)	2 x 11.36	57.27	75.0
Propellant type	N_2O_4/UDMH	N_2O_4/MMH	N_2O_4/MMH
Propellant mixture ratio	1.65:1	2.0:1	1.8:1
Burn time (sec)	734.90	3266.86	3310.02
Mp (kg)	1920.86	1813.4	1856.3

[1]Marquardt Company, 12-40B Specifications, September 1985.
[2]Aerojet Tech Systems, XLR-132A Specifications, August 1991.
[3]Aerojet Tech Systems, Transtar Specifications, January 1989.

The trade study done to determine the best possible motor takes into consideration four key factors: the propellant mass, the dry mass, the burn time, and the developmental status of the motor. Equation (4.17) was used to calculate the performance indices:

$$J = k1(\text{propellant mass}) + k2(\text{dry mass}) + k3(\text{burn time}) + k4(\text{development status}) \quad (4.17)$$

The weighting factors, k1 through k4, ranged between 1 and 5, with 5 defining the most critical parameter. These values can be found in Table 4.8.

Table 4.8. Weighting Factors for Choosing the Mercury-Capture Rocket Motor

Parameter	Weighting Factor	Value
Propellant Mass	k1	5.0
Dry Mass	k2	4.0
Burn Time	k3	3.0
Developmental Status	k4	2.0

The first parameter, propellant mass, was the most important concern because of the large masses involved. Thus its weighting factor had the highest value. The motor dry mass, although critical, was considered less important than the propellant mass. The burn time weighting factor was given a medium value because low burn times generally require less stabilization and course correction. The developmental status received the lowest of all values because all of the rockets being considered are being manufactured to date.

Each parameter was then rated on a scale of 0 to 3, with 3 defining the worst case. The results of this trade study can be seen in Table 4.9. From the trade study, it can be seen that one XLR-132A engine is the best choice as the Mercury-capture motor.

Table 4.9. Results of Trade Study for Chemical Rocket Motor for Mercury Capture

Motor	k1	k2	k3	k4	J
R-40B	3	1	3	1	30
XLR-132A	1	2	1	3	22
Transtar	2	3	1	2	29

4.7 Escape from Low Earth Orbit

The escape trajectory and magnitude, like the Mercury capture, uses the patched conic method. A schematic of the escape scenario is presented in Figure 4.5.

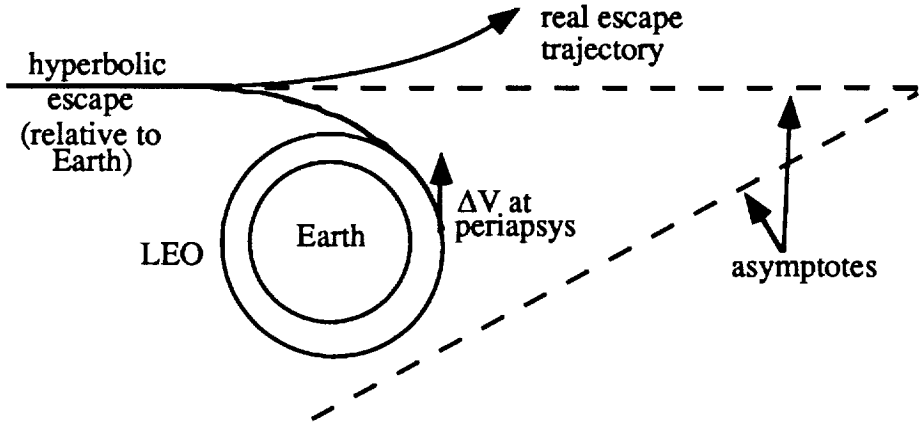

Figure 4.5. Schematic of the Low Earth Orbit Escape Scenario

The ΔV required is again given by Equation (4.18).

$$\Delta V = \sqrt{V_\infty^2 + \frac{2\mu_E}{r_p}} - \sqrt{\frac{\mu_E}{r_p}} \tag{4.18}$$

Where r_p is the sum of the orbit radius, 200 km, and the radius of Earth, 6378 km and μ_E is 3.986×10^5 km^3/s^2.

A wide range of escape velocities exists depending on the capability of the launch system, performance of the solar sail, and desired transit time to Mercury [13]. In order to estimate the performance for the rocket motors available, two escape velocities were assumed, giving some definite upper and lower bounds to the calculations. The two escape velocities chosen:

1.) high escape $V_\infty = 5$ km/s ($\Delta V = 4.307$ km/s)

2.) med.-low escape $V_\infty = 2$ km/s ($\Delta V = 3.4046$ km/s)

Their respective propellant masses can be found using Equations (4.19) and (4.20).

$$m_p = m_{escape}(e^{439.46/Isp} - 1) \tag{4.19}$$

$$m_p = m_{escape}(e^{347.41/Isp} - 1) \tag{4.20}$$

The burn time equations are of the same form as those used to determine the burn time necessary for Mercury capture.

Table 4.10 lists the relevant specifications for the motors considered. The propellant masses and burn times are in terms of the final mass that is sent on the escape trajectory, m_{escape}.

Table 4.10. Specifications of Chemical Rocket Motors for Escape from LEO [Interavia Space Directory, 1991-1992, Jane's Information Group, Alexandria, VA, pp. 339, 348, 358 & 249.]

Parameter	RL-10A	Proton	Tsyklon	Ariane
Manufacturer	Pratt & Whitney	Soviet Union	Soviet Union	France
Development	qualified	qualified	qualified	qualified
Isp (sec)	446	352	331	444.6
Thrust (kN)	73.4	85	78	62.3
Dry Mass (kg)	138.35	303	158	155
Propellant type	LO_2/LH_2	N_2O_2/UDMH	N_2O_2/UDMH	N_2O_2/UDMH
Propellant mixture ratio	5.0:1	2.6:1	1.9:1	5.14:1
Mp				
(5 km/s escape)	1.6787 m_{esc}	2.485 m_{esc}	0.7723 m_{esc}	1.687 m_{esc}
(2 km/s escape)	1.1792 m_{esc}	1.6831 m_{esc}	1.8564 m_{esc}	1.185 m_{esc}
Burn time				
(5 km/s escape)	0.099 m_{esc}	0.1008 m_{esc}	0.1153 m_{esc}	0.118 m_{esc}
(2 km/s escape)	0.0702 m_{esc}	0.0683 m_{esc}	0.0772 m_{esc}	0.083 m_{esc}

The trade study done to determine the best option utilizes the same performance index equation as the Mercury capture study done in Section 4.6 (see Equation (4.17)), along with the same k factors (see Table 4.8). Since the values for either escape scale, high or medium-low, are the same for each motor, only the 2 km/s escape is considered. The results of this study are found in Table 4.11. From this study it can be seen that the best engine for this part of the mission is the RL-10A motor.

Table 4.11. Results of Chemical Propulsion Motor Trade Study for Escape from LEO

Motor	k1	k2	k3	k4	J
RL-10A	1	1	2	1	17
Proton	2	3	1	1	27
Tsyklon	3	2	3	1	34
Ariane NM-7B	1	2	4	1	27

Using the mass of propellant for Earth escape, 9147.67 kg, and the mass of the propellant for Mercury capture, 2774.48 kg plus the mass of the XLR-132A motor (57.27 kg) and RL-10A motor (138.35 kg), the initial mass of the spacecraft is 17043.77 kg. This mass also takes into account the mass of the orbiter, 1692 kg, the total mass of the landers (with propellant), 2274 kg, and the mass of the solar sail, 960 kg. Results of combining the XLR-132A motor and the RL-10A can be seen in Appendix E.

5.0 Guidance, Navigation, and Control

5.1 General Requirements

The total guidance, navigation, and control for the mission has four subdivisions. The first part, the main spacecraft assembly (orbiter and probes), examines control from LEO to Mercury orbit. Part two discusses the GNC for the solar sail during transit to Mercury, while the third part addresses GNC requirements of the orbiter (in Mercury orbit). The final division analyzes GNC for the four surface probes. For the transit to Mercury, the craft is spin stabilized. At Mercury, the orbiter and probes are three-axis stabilized.

5.2 GNC for LEO to Mercury Orbit

GNC for the main spacecraft during transit to Mercury is primarily responsible for slow turning of the craft with the sail, proper navigation of the entire craft (main spacecraft and sail), and deployment of the solar sail (discussed in the sail GNC section). The main spacecraft must be slowly turned about an axis perpendicular to the orbit plane so that it remains aligned with the turning of the sail. Slow turning can be accomplished by the thrusters mounted at the front and back of the craft or by the reaction wheels located in the center body. Thrusters apply a very short pulse with every rotation to change the direction of the angular momentum vector. Because the entire craft is spinning, the star trackers and sun sensors used for navigation will be mounted on the despun scientific instrument boom. This despun system and its damping device is based on the despun platform of the HS-376 satellite [11]. The star trackers and sun sensors along with a Honeywell ring laser gyro are responsible for relaying attitude and navigation information to the main computer [17]. An integral part of navigation will be the ability of the main spacecraft to deliver proper guidance information to the control vanes of the sail.

The GNC for the main spacecraft has four secondary concerns. First, before spin-up, the craft must be oriented properly with respect to the Sun. Second, separation pulses are

needed when the spacecraft separates from the Earth escape booster and when the craft separates from the sail before Mercury capture. A final concern is the dissipation of energy from the flexible booms, the solar sail, and the despun boom section. Losses that will require some small corrections with momentum wheels and thrusters are accounted for by an addition of a 10% margin to the total GNC thruster propellant budget for the main spacecraft.

The attitude control system for the main spacecraft consists of 24 MRE-5 thrusters, mounted in pairs, and 4 Honeywell HR15M reaction wheels (see Appendix F for specifications). Four thruster pairs are mounted 90° from each other on a ring near the capture motor. Four more are arranged in an identical configuration between the first and second probes. They were placed off the main body to avoid plume damage to the solar array and to provide a larger moment arm. The last four pairs are positioned so that they can spin and despin the craft. Their axial location is at the center of mass of the craft after the sail has been discarded so that the craft can be despun with minimum wobbling.

The MRE-5 thrusters were chosen for three reasons. First, their monopropellant design is simple and since they use the same propellant as the capture motor, excess tankage mass is avoided. Second, their thrust range is sufficient to perform the required craft slewing maneuvers described below and in the orbiter GNC section. Third, their recent development will ensure that the technology is current at the time of implementation. The four HRM15 momentum wheels are mounted so that their spin axes are at right angles to each other. The fourth unit is mounted at a skewed angle so that it can apply a moment in either the x, y, or z planes. Although the HR15M reaction wheels were chosen primarily because of their momentum range, they also are radiation hard and their control interface is digital instead of analog (like many other Honeywell reaction wheels).

The amount of torque required to turn the craft slowly can be estimated by considering the maximum turning rate required by the sail. The rate of change of the angle (which is roughly the angular velocity of the craft in its orbit) is highest near Mercury. For a

spinning spacecraft, the moment required to steadily change the direction of the angular momentum vector can be calculated using Equation (5.1).

$$\Delta H = 2H_o \Delta\theta \rightarrow M_{req'd} = 2H_o\dot{\theta} \tag{5.1}$$

Given a spin rate of 0.2 rad/s, a moment of inertia about the spin axis of 2724 kg·m^2, and dθ/dt of 9.2x10^{-7}, the moment required, 5.08x10^{-4} N·m, can easily be supplied by the reaction wheels.

5.3 Solar Sail GNC

The guidance, navigation, and control subsystem for the circular solar sail must satisfy four requirements. First, the sail must be deployed tangle free at the proper rotation rate (to keep it sufficiently stiff) and with the correct orientation for placement into the desired trajectory. Second, the entire sail structure needs to be slowly turned around an axis perpendicular to the orbit plane in order to maintain a constant angle with respect to the solar pressure. Third, the sail requires constant monitoring for severe vibrations and tears. Finally, the craft must have a mechanism to discard the sail prior to injection into Mercury orbit.

The circular sail was chosen because it had the best performance with the least size and complexity [18]. One of the initial drawbacks of the circular sail design was the lack of a practical deployment technique. However, a method devised by Cambridge Consultants Limited in 1990 offers a promising means of deploying a circular solar sail [19]. The method, adapted for this project, is detailed below. After escape from LEO, the spacecraft must be spun so that the deployed sail is also spinning. The required propellant for this spin is given by Equation (5.2):

$$M_p = I_{SS}\,\omega_S / (L_{ts}g\,I_{sp}) \tag{5.2}$$

where I_{ss} is the moment of inertia about the spin axis, ω_s is the angular velocity of the craft, and L_{ts} is the thruster lever arm length [20]. In addition to the 4 MRE-5 thruster pairs positioned for spinning and despinning the main spacecraft, 4 MRE-15 thrusters are mounted on the ends of the solar sail protective canister (see Figure 5.1).

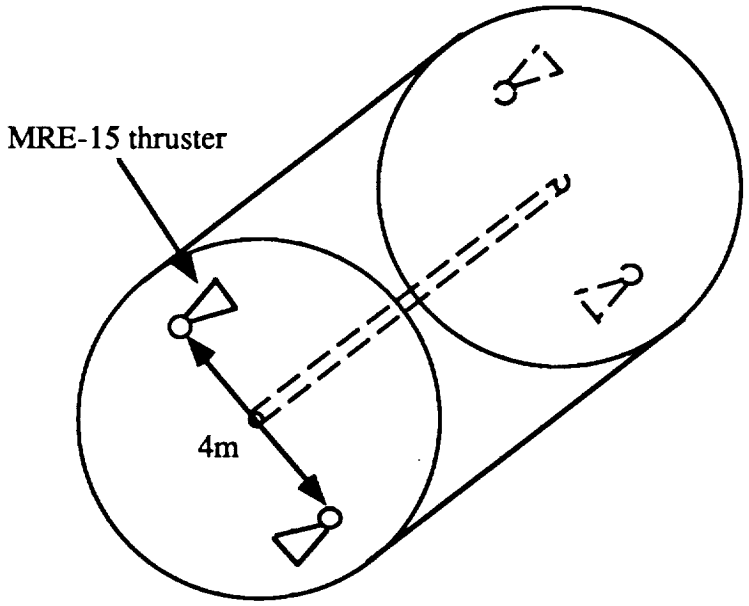

Figure 5.1. Spin thruster placement on the solar sail canister

The thrusters are mounted slightly in from the outer radius to reduce the chances of plume damage to the sail during deployment. If I_{ss} is the moment of inertia about the y-axis of the craft, the initial spin-up to 0.2 rad/s will consume only about 0.7 kg of propellant. The angular velocity of 0.2 rad/s is the ω required to maintain stiffness in the deployed sail [21]. Following the initial spin-up, the sail is deployed in the manner shown in Figures 5.2a through 5.2d.

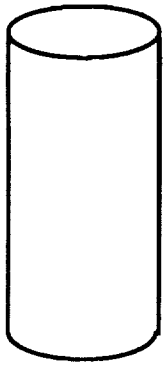

Figure 5.2a. Solar sail in canister

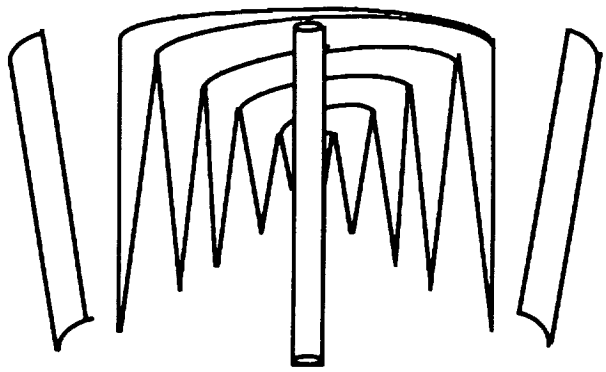

Figure 5.2b. Solar sail at beginning of deployment

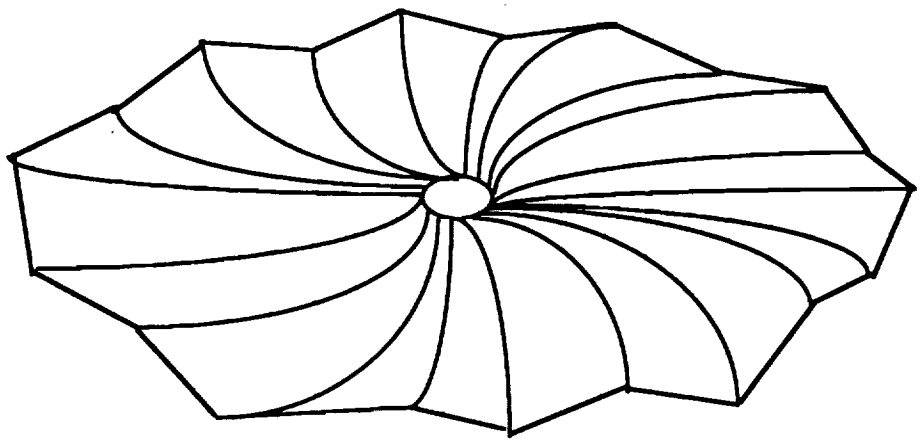

Figure 5.2c. Solar sail near full deployment

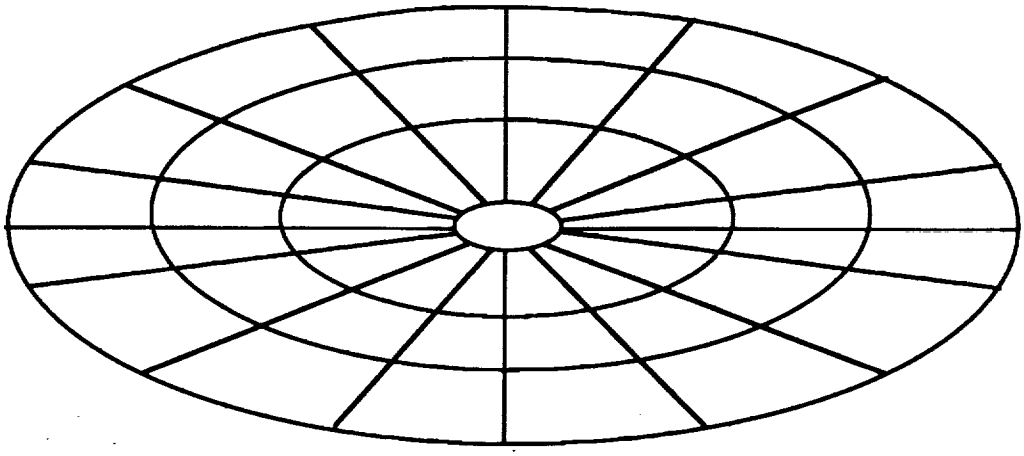

Figure 5.2d. Solar sail fully deployed

From the initially closed, spinning canister (Figure 5.2a), the protective shroud is released and the spiral-packed sail elements begin to unfurl because of centrifugal forces on the sail and the controlling vanes (not shown). In order to keep the sail expanding and spinning at a constant 0.2 rad/s, a steady torque must be applied by the MRE-15 thrusters. The equations for the amount of torque required are given below. Assuming rotation occurs in one direction only:

$$M = \frac{d}{dt}H = \frac{d}{dt}(I\omega) = \frac{dI}{dt}\omega \quad \text{for } \omega \text{ constant} \tag{5.3a}$$

if $I = 1/2\ m_{sail}\, r^2 + (\#\ of\ control\ vanes,\ n_{cv})\ m_{cv}\, r^2$

$$M = \omega\left(m_{sail} r \frac{dr}{dt} + n_{cv} m_{cv} r \frac{dr}{dt}\right) \tag{5.3b}$$

To find the time of deployment , the moment is integrated over a time as follows:

$$\int_0^t M\,dt = \int_{R_o}^{R_f} \frac{dI}{dt}\,dt \rightarrow M\Delta t = \omega\left[\left(\frac{m_{sail}}{2} + m_{cv}\right)\left(R_f^2 - R_o^2\right)\right] \tag{5.4}$$

Given a sail radius of 319 meters (R_f), the packages sail radius, R_0 = 2.5 m, sail mass of 960 kg, ω of 0.2 rad/s, 16 control vanes, and a total applied moment from the four thrusters of 640 N·m, the sail requires 4 hours and 16 minutes to deploy. This long time period ensures that any large forces that might cause a tear or strain in the sail are avoided. The corresponding propellant mass for this steady burn is 558 kg of hydrazine. To account for any off-axis wobbling and for, more importantly, dissipation due to the flexible nature of the sail, a 10% margin is added to the deployment propellant.

Because of its importance in deployment, the packaging structure of the sail is included in the GNC subsystem. One can visualize the packing procedure by running the deployment cycle backwards (Figures 5.2d through 5.2a). While every reinforcement wire location is alternately raised and lowered, the center cylinder draws the sail in by slow rotation. Each sail element (i.e. a piece bounded by the composite reinforcement) wraps in a spiral shape around the center cylinder (see Figure 5.3). Figure 5.4 shows a side view of the packaged sail in its cylinder with some of the free space taken up by the control vanes.

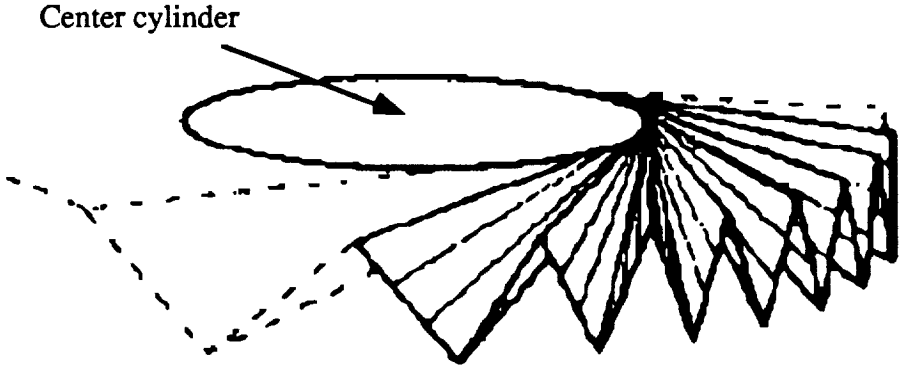

Figure 5.3. Packing of the sail near the central cylinder [Groves, G.V., "Sailing to Mars on Sunlight," *Spaceflight Magazine*, The British Interplanetary Society, Vol. 32, No. 6, June 1990, p. 188.]

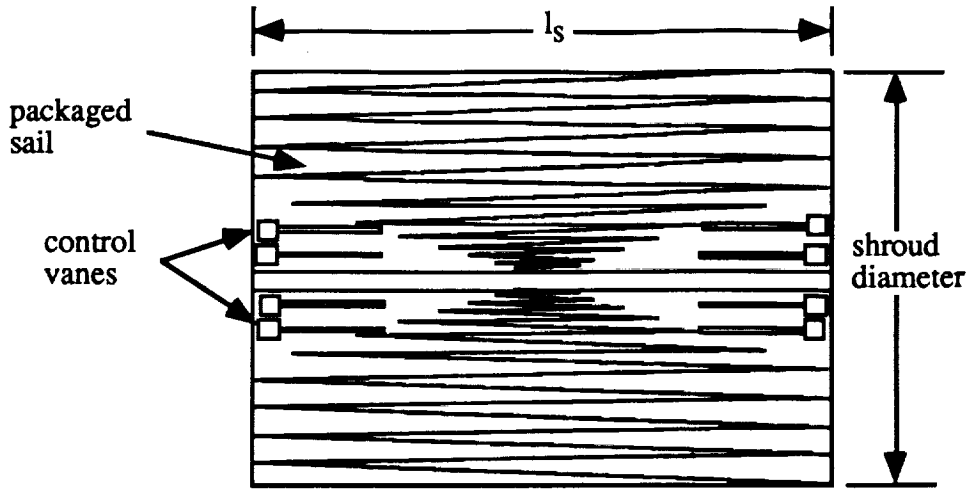

Figure 5.4. Side view of packaged sail.

Because each sail element is much larger at the outer radius, the packed sail requires more area further away from the center cylinder.

The calculations for the volume that the packed sail occupies use a nominal sail thickness of 0.15 mm. This value, much higher than the actual sail thickness, considers the thickness of the reinforcement wires. By fixing a length of six meters for the protective shroud, the number of sail elements is calculated as a function of sail size using the following equation:

$$\# \, elements = E = 2\pi R_{sail}/l_s = 334 \tag{5.5}$$

Where R_{sail} is the radius of the deployed sail and l_s is length of the protective shroud. The area that the packed sail occupies is then evaluated using the number of sail elements and their thickness and length. The equation is as follows:

$$A = EtR_{sail} = 15.98m^2 \tag{5.6}$$

where t is the sail thickness. There will be a high degree of "bunching" near the center cylinder so the total area probably needs a 15% margin. With the current sail area of $0.32km^2$, the packaged diameter is 4.84 m.

After deployment, the sail must be slowly turned around an axis perpendicular to the orbit plane in order to maintain a constant angle with respect to the Sun. However, the spin of the sail and spacecraft creates an angular momentum vector whose direction must be changed in order to turn the entire vehicle (see Figure 5.5).

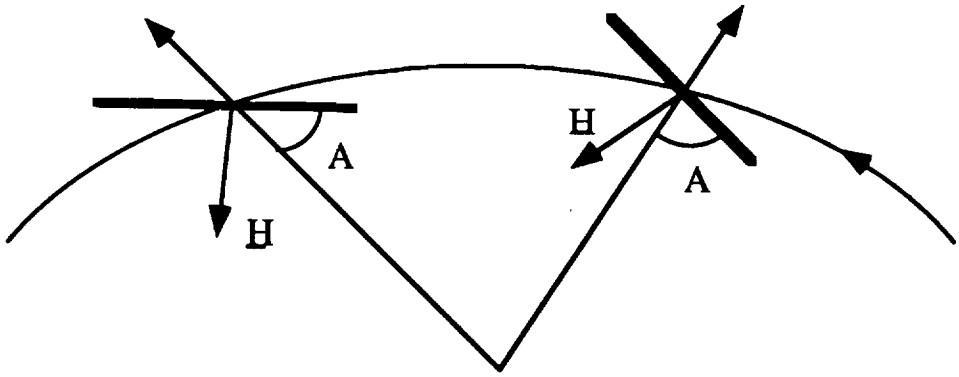

Figure 5.5. Changing angular momentum vector of the solar sail.

Sixteen control vanes on the perimeter of the sail supply the necessary moment to alter the direction of the angular momentum. Small electrical motors mounted at the base of the vanes turn the vanes perpendicular or parallel to the solar pressure so that the moment acts only on the side of the intended turn (see Figure 5.6a and 5.6b).

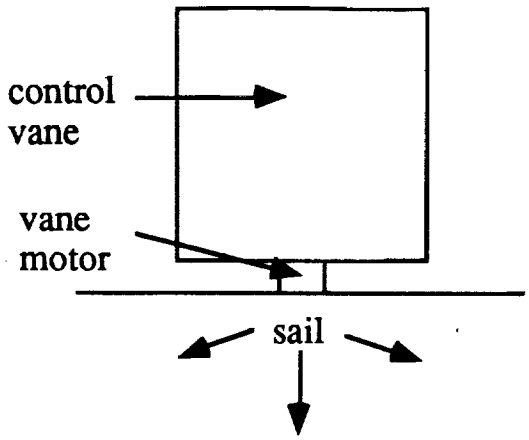

Figure 5.6a. Solar sail control vanes detailed view

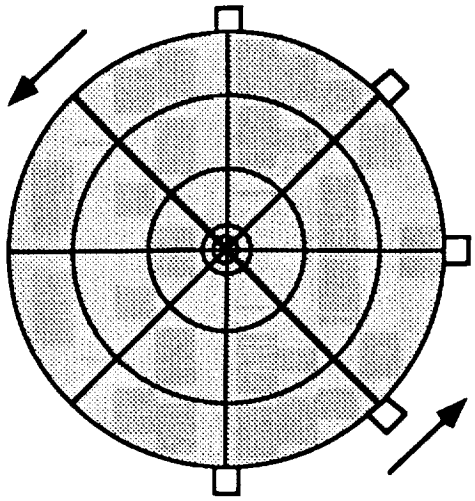

Figure 5.6b. Solar sail control vanes expanded view

The estimated mass of each motor is 0.05 to 0.1 kg and they would receive their power by a line through one of the sail stiffening supports. The size of the turning vanes is estimated by first considering the maximum turning rate required by the sail as explained in the previous section. Similarly, the moment required to turn the angular momentum vector of the sail is given by Equation (5.1) Given the spin rate, the moment of inertia of the sail, and $d\theta/dt$, the required moment is 3.874 N·m. As the craft turns, it is assumed that five of the vanes on the turning side are fully effective (i.e. maximum area exposed to the solar pressure). The other two are only partially effective because of the time required to turn the vane into place. The applied moment can then be expressed in terms of the moment arms and the force on the vanes as follows:

$$M_{applied} = \sum L_{arm} F = 0.0126 A_{cv} \left(\frac{r_o}{r} \right)^2 = 0.0905 A_{cv} \tag{5.7}$$

where r_0 is Earth's distance from the Sun, r is Mercury's distance from the Sun, and A_{cv} is the area of one control vane. Equating the required and applied moments yields a control vane area of 42.8 m^2. A square shape 6.54 m on a side was chosen because of its simplicity and use in other similar designs [18].

The GNC subsystem must have a means of detecting tears, micrometeorite damage, and severe vibrations in the sail structure and taking appropriate corrective actions to ensure proper control and navigation. Some conceptual ideas for monitoring include lasers and smart structures. Lasers could optically "sample" the sail (with small reflectors at various locations) and relay that information to the computer for interpretation. Smart structures, implemented in the support and reinforcement structure, could relay information about stresses and strains in virtually any part of the sail.

The craft must have a mechanism to discard the sail prior to injection into Mercury orbit. Explosive bolts, mounted between the main spacecraft and the cylinder that the sail is attached to, provide an inexpensive and reliable way to detach the sail and permit the remainder of the craft to continue on its mission.

5.4 Orbiter GNC

The orbiter will contain all the GNC equipment of the main spacecraft plus a horizon sensor to facilitate mapping of the planet surface. The three important GNC concerns in Mercury orbit will be proper initial orbit insertion, disturbance torques, and probe release.

Proper orbit insertion requires that the insertion burn be applied at the proper time and orientation during approach. Once the spacecraft reaches Mercury orbit, it is turned 180° for the insertion burn. Assuming the turn occurs in one axis only, the torque required equals $I\alpha$. Given an I_{zz} of 56356 $kg \cdot m^2$ and an applied torque from the thrusters of 138.6 N·m, α becomes 0.14 deg/s. Performing a bang-bang maneuver, the craft can be turned in 70 seconds using 2.9 kg of hydrazine propellant. In addition to the difficulty of proper timing

and craft orientation, some off-axis disturbances occur during firing that have to be corrected. The mass of propellant needed for corrections during this burn is given by Equation (5.8).

$$M_{\Delta V} = K_v M_{s/c} \Delta V \, l_v \, \alpha_v / (L_t g I_{sp}) \tag{5.8}$$

K_v is the effectivity which is usually between 1 and 2, $M_{s/c}$ is the mass of the spacecraft, l_v is the distance from the motor to the mass center, α_v is the angular offset of the motor, and L_t is the lever arm of the control thruster [20]. The mass of propellant for this is 2.6 kg and is large because much of the craft's mass is concentrated in the landers.

Three important disturbances in Mercury orbit will be gravity gradients, solar pressure, and magnetic field torques. Equation (5.6) defines the torque caused by the gravity gradient,

$$T_g = (3\mu/R^3) \cdot / I_z - I_y / \theta \tag{5.9}$$

where μ is 22,320 km^3/s^2, R is the orbit radius, I_z and I_y are the moments of inertia, and θ is the deviation from the local vertical [20]. Since the craft must remain fixed towards the Sun for power and thermal considerations, the gravity gradient torque experiences two maxima of 0.22 Nm each orbit. Because this torque is higher than the rating for the momentum wheels, the thrusters will have to be used to make corrections each orbit. However, once the orbiters are released, the torque becomes insignificant.

In orbit around Mercury, solar pressure, instead of being a control problem, can actually be used to orient the craft towards the Sun at all times. Because of Mercury's proximity to the Sun, solar pressure is high enough on the solar panels to exert an equal moment on each of the four panels. The moment works on each of the opposing panels to keep the craft pointing out of the plane of the panels. Hence, the craft will be stabilized along one of its axes. This control, of course, only works when the craft is not eclipsed.

The torque from the solar pressure is significant because the solar pressure at Mercury is nearly seven times that of earth. The formula for the amount of torque is,

$$T_{sp} = P_s A_s L_s (1 + q) \tag{5.10}$$

where $P_s = 5.889 \times 10^{-4}$ N/m^2 (solar constant at Mercury), A_s is area exposed to the solar pressure, L_s is moment arm, and q is a reflectance factor (0.6) [20]. Given an array size of 4.44 m^2 and a moment arm of 2.5 m, the torque is 0.0104 Nm. This torque can easily be countered by the reaction wheels. Another effect of solar pressure is the disturbances that occur when the craft emerges from eclipse. This sudden presence of solar pressure will cause a control problem as well as a pointing error that will require experiments, mapping, and communications activities to cease for a brief period. The magnetic field torque is difficult to quantify because of a lack of good "mapping" of the magnetic field around Mercury. As an approximation, the magnitude of the torque is assumed to be small compared to the gravity gradient [21].

Because the probes are landing at several different locations on Mercury, they must be released at different times and at different orbit inclinations. Also, in order to map the polar regions of Mercury, the orbit must be inclined sufficiently for those regions to pass under the orbiter camera's field of vision. Because of these requirements, extra propellant must be supplied to incline the orbit and control the craft during the change. The formula for the ΔV required is given in Equation (5.11).

$$\Delta V = 2V \sin\left(\frac{\Delta i}{2}\right) \tag{5.11}$$

A maximum inclination of 60° must be established to allow the polar areas to be mapped. Given an orbit velocity of 2.7557 km/s, the ΔV required is 2.7557 km/s. The mass of propellant required is 705 kg. A final orbiter GNC consideration is that the release of the

probes will significantly reduce all of the moments of inertia of the entire craft. This reduction translates to overall easier control and a corresponding longer functional life of the orbiter.

5.5 Probe GNC

The GNC of the surface probes on the Mercury mission depends on factors such as probe mass, slew rate, and descent velocity relative to the surface. For an approximate probe sizing, a spherical shape and a diameter of 1.5 m was chosen as an initial geometry. Due to the placement of the various on board systems, the center of mass was calculated to be 0.36 m from the base. The four main descent thrusters were uniformly positioned around the probe base at the height of the center of mass. A small thruster pack on the top of the probe will serve as a backup in case one of the descent thrusters fail, and also will work to counteract roll rates too fast for the gyros to handle. It was also determined that to save propellant and best utilize the descent thrusters for descent rather than orientation, small thrusters should be placed at the top of the probe for rotation counteraction. The low center of gravity of the probes will stabilize the craft during descent, facilitating fewer thruster corrections, thus saving propellant.

Torque, T = I*alpha

I = 46.46 kg*m^2

alpha ≈ 1.0 rad/s^2

M = F*L = Thrust*1.14 m

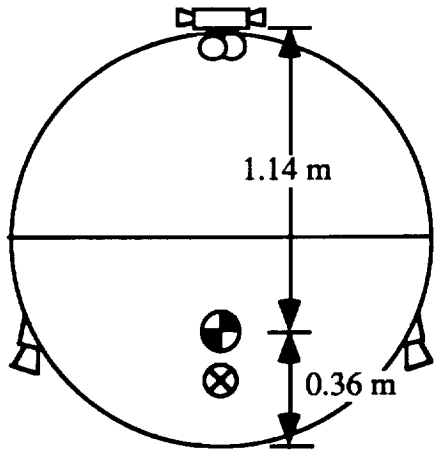

Figure 5.7. Probe with some dimensions

For a very fast rotation of 1.0 rad/s, a moment of inertia of 46.46 kg-m^2, and using a moment arm of 1.14 m, it was calculated that the thruster pack would need eight Leros 20 thrusters. If the rotation were 0.5 rad/s, only four Leros 20 thrusters would be needed. However the eight thruster configuration would provide a margin of safety for thruster failure and also allow for a more accurate stabilization burn. These thrusters must be placed in a symmetric configuration.

The Leros 20 thrusters are a second generation bipropellant attitude control thruster. Previous use in other systems has shown the Leros 20 has good steady state and pulsed performance over a wide thrust range. The dry mass of each thruster is 0.45 kg and each uses a MON_3 oxidizer at 4.8 g/s flow rate and a MMH fuel at 2.9 g/s flow rate. The propellant feed will be accomplished using a helium pressure system. The thrust produced by each thruster is 22.2 N with a specific impulse of 295 seconds (vacuum nominal) [11].

The probes also use an inertial guidance system which will require 20 watts of power and has a mass of 4 kg and a radar range finder/altimeter requiring approximately 5 watts of power with a mass of approximately 1 kg. The momentum wheels used will be the smallest size offered by Honeywell [22] and will have a mass of 2.3 kg and require 6 watts static and 40 watts start up power. Appendix F lists all GNC hardware and specifications for the both the spacecraft and the probes.

6.0 Command and Data Handling (C&DH) Subsystem

6.1 C&DH Requirements

The command and data handling capabilities of a mission to Mercury must be able to successfully process and relay data to and from the spacecraft and Earth, and from the spacecraft to each of the four landers. The C&DH subsystem is also responsible for general housekeeping, telemetry, timing, and storage of data. Project Firefly requires a C&DH subsystem for both the orbiter and the lander.

6.2 Orbiter C&DH System

The complexity and capabilities of the C&DH subsystem were determined by the mission objectives. For Project Firefly, the factors that were used to choose the C&DH subsystem include communications, payload, data storage, and guidance and navigation requirements. The interfaces of these factors with the C&DH subsystem are shown in Figure 6.1.

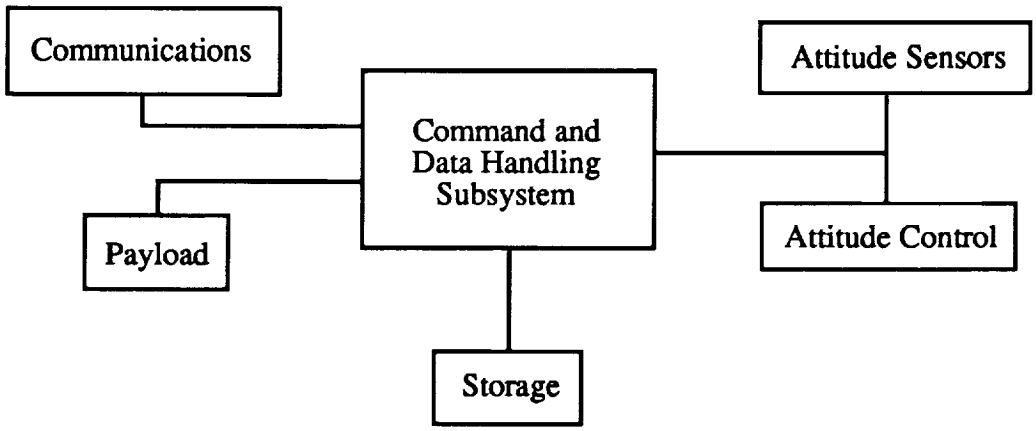

Figure 6.1. Subsystem Interfaces with the C&DH System

Each of the factors of data rate, data size, and timing were considered to help define the C&DH subsystem. The data rates varied from 1 kbps for the radar altimeter up to 350 kbps for the camera and are listed in Table 6.1 for each of the subsystems.

Table 6.1. Subsystem Data Rate Requirements

System	Data rate (kbps)
Payload (Sci. Instruments)	
Magnetometer	3.6
IR Spectrometer	8 Packets
IR Thermal Mapper	8 Packets
Cameras (2) Wide and Narrow Lenses	6.2-350 each
Radar Altimeter	3.2
Communications	150
Guidance, Navigation and Control	
Sun Sensor	1
Star Tracker	2
Inertial Guidance	10
Control (Thrusters)	100
Thermal Control and General Housekeeping	31

6.2.1 Computer

In selecting a computer for Project Firefly, the major concerns were mass, size, power, and throughput. Computers that were capable of holding more than 5 Mbytes were not considered since the maximum amount of memory required for this mission would not exceed this value. The computers under consideration are listed in Table 6.2.

Table 6.2. Computer options

Option	Computer	Size (cm^3)	Mass (kg)	Power (W)	Throughput (MIPS)	Memory (Mb)
1	Fairchild FS1750	4693	3.6	15	0.44	0.141
2	AlTech 950	3500	4	8	4	0.5
3	Honeywell ASCM-CPM	5899	8.98	25.3	3	1-5
4	Honeywell ASCM-ATIM	5899	7.8	25	35	2-6
5	IBM GVSC	1280	8.2	23	4.5	3.906
6	Rockwell RI-1750A/B	2050	2.5	6.6	1.8	3.906

A trade study (Table 6.3) was performed on these computers, and the lowest value corresponded to option 6, the Rockwell RI-1750A/B. This computer has enough memory and throughput to handle the necessary data, as well as keeping the power and mass to a minimum. It is also small enough to easily find a location for it on the main craft.

$$J = K_1(mass) + K_2(size) + K_3(power) - K_4(throughput) \qquad (6.1)$$

K_1=4, K_2=5, K_3=4, K_4=3
1=Best, 5=Worst

Table 6.3. C&DH Computer Trade Study

Option	Mass	Size	Power	Throughput	J
1	3	4	3	1	41
2	3	3	4	4	31
3	5	5	5	5	50
4	4	5	5	5	46
5	4	2	5	4	34
6	2	2	3	3	21

6.2.2 Spaceflight Recorder

Since the orbiter will not be in direct contact with Earth during certain periods of time, the data received from the probes and the scientific instruments needs to be stored. Therefore, a space flight data recorder is required. Manufactures such as Eldec Corp., RCA, Amptek, and IBM have been contacted to obtain information on recorders (see Table 6.4).

Table 6.4. Spaceflight recorder options

Option	Recorder	Memory (Mbyte)	Data rates (kbps)	Power (W)	Mass (kg)	Volume (cm^3)	Error rate
1	Odetis DDS5000	2	3000	40	9.07	14450	1.0 E-6
2	Amptek FDR8200	2 & 10	1000	18	7.3	10442	1.0 E-13
3	Lockheed 4200	0.08	512	4	2.95	4365	1.0 E-6
4	RCA STR108	0.5	2560	17	3.18	2276	1.0 E-6
6	Fairchild SSR	0.128	10000	3	6.17	6842	1.0 E-10

A trade study was performed to determine which recorder would be most applicable to Project Firefly. The factors considered were mass, volume, power required, and memory capacity. Cost and heritage were not used as factors since the components are "off-the-shelf" products, they would have similar values. The trade study is shown in Table 6.5.

$$J = K_1(mass) + K_2(size) + K_3(power) - K_4(throughput) \qquad (6.2)$$

K_1=4, K_2=5, K_3=4, K_4=3
1=Best, 5=Worst

Table 6.5. C&DH computer trade study

Option	Mass	Volume	Power	Capacity	J
1	5	5	5	4	53
2	4	5	5	5	46
3	2	3	2	2	25
4	3	2	4	4	26
5	3	4	2	3	31

The results of the trade study shows that option 3 (Lockheed), option 4 (RCA), and option 5 (Fairchild) are the best components to use. The final choice for which product to use was based on the power consumed and the bit error rate. Since the Fairchild solid state recorder has the lowest power requirement and the lowest bit error rate of the remaining three options, it was selected for this mission.

6.3 Lander C&DH System

The four probes that will be utilized for Project Firefly will have subsystem requirements similar to the orbiter. They will contain their own power supply, communications, GNC, scientific instruments, and C&DH. However, the scientific instrumentation is slightly different. The components and data rates are listed in Table 6.6.

Table 6.6. Scientific instrument data rates

Instrument	Data rate
Alpha particle instrument	0.5 kbps
Seismometer	5 kbps
Surface sampler	N/A
In-situ imaging system	15-20 Mbits in packets of 8 kbps
Temperature recorder	10 bps

The components for C&DH were basically selected from the same options as the orbiter, with the addition of one more computer: the Honeywell DSBC. This computer was chosen since the most important considerations are the low power required and the small volume of the components. The specifications are shown in Table 6.7.

Table 6.7. Honeywell DSBC computer specifications

Volume (cm^3)	1200
Mass (kg)	1.2
Power (W)	4
Throughput (MIPS)	1.2
Memory (Mbyte)	0.256

The landers will each require a recorder for times when communication is not possible. The same products were considered as with the orbiter. Mercury capacity was not considered in the trade study because each product met the landers' requirements. Otherwise, the trade study is the same as the one listed in Table 6.5; since the probes are smaller, the Lockheed 4200 series tape recorder was chosen. The volume and the power required are lower than most of the other choices, and its mass is the lowest of them all.

6.4 C&DH Design Summary

The C&DH for the orbiter will be required to interface information with all the other subsystems. The subsystem will consist of a computer to handle all commands and a space flight data recorder to store information. The computer selected is the Rockwell RI-1750A/B and the space flight recorder is the Fairchild solid state recorder. The components for each of the four landers will also include a computer and a recorder (Honeywell DSBC computer and Lockheed 4200 series tape recorder).

7.0 Communications

7.1 Communications Requirements

The communication subsystem is tasked with the job of establishing links between ground control and the spacecraft; as well as between the spacecraft and the probes. A continually spinning spacecraft, whose orientation with respect to the Earth is also constantly changing, requires many options for uninterrupted communications. Communication relay from as many as four probes on the planet's surface also requires filtering and delineation of data.

7.2 High-Gain Communications Design

Table 7.1 shows some of the possible options which could be used for the communications subsystem. A trade study for the communications requirements was performed for the options in Table 7.1 are presented in Table 7.2. Usability refers to the technological level of the system. The more usable the system, the more communications options it can perform. Steerability is a measure of the communication readiness. A steerable antenna can align itself and process communications at any time without the need for spacecraft reorientation.

Table 7.1. Possible options for communications

Option	Usage	Frequency Range	Orientation
(1) One Antenna	transmitting & receiving combined	X - band (5200-10900 MHz) S - band (1550-5200 MHz)	steerable
(2) One Antenna	transmitting & receiving combined	X - band (5200-10900 MHz) S - band (1550-5200 MHz)	fixed
(3) Two Antennas	transmitting & receiving individually	X - band (5200-10900 MHz)	steerable
(4) Two Antennas	transmitting & receiving combined	X - band (5200-10900 MHz)	steerable
(5) Two Antennas	transmitting & receiving individually	X - band (5200-10900 MHz)	fixed
(6) Two Antennas	transmitting & receiving individually	X - band (5200-10900 MHz)	fixed & steerable

$$J = K_1(mass) + K_2(cost) - K_3(usability) - K_4(steerability) \qquad (7.1)$$

K_1=1, K_2=2, K_3=3, K_4=4
1=Best, 5=Worst

Table 7.2. Option trade study

Option	Mass	Cost	Usability	Steerability	J
1	1	3	1	2	-4
2	1	2	1	1	-2
3	3	4	3	5	-18
4	3	4	4	5	-21
5	3	4	2	3	-7
6	3	5	3	4	-6

From the trade study performed on the antennas, the best option for the spacecraft is the use of two high-gain antennas capable of combined transmitting and receiving with steerable mounts (option 4). Due to the rotation and changing orientation of the spacecraft while enroute to Mercury, only one of these high-gain antennas will be used at any one time. Additionally, since one antenna will need to be placed on each side of the solar sail for continuous communications, the antenna on the far side of the solar sail with respect to the main spacecraft will need to be ejected with the solar sail upon arrival in Mercury orbit.

Due to the need for two antennas, a high performance, but low mass antenna system is preferred. Many options of antenna type are available, ranging from traditional rigid parabolic antennas to inflatable reflector antennas which are still being developed. A combination of these different types may be used, as one of the antennas will only be used during certain communication black out periods.

Utilization of two rigid parabolic antenna would create both high cost and mass. The mass for one rigid high-gain communication system is approximately 85 kg [23]. This approximation includes all harnessing and wiring necessary for the system. For the purpose of mass reduction, one of the best options to fulfill the communications requirements may be the use of inflatable antennas. Several factors, other than mass, support the choice of this option. Some factors include: storage of antennas during launch, cost, and versatility of antenna systems. The inflatable antenna system which has been investigated contains many distinct features that traditional rigid systems lack. The primary construction material consists of layers of a Kevlar/Kapton composition. The antenna system has been successfully tested on a frequency range from 1.6 to 22.0 GHz. The inflatable antenna's space when stowed is less that 0.27 cubic meters for launch with a total mass of 30 kg each, which includes the attachments needed to harness the antenna to the spacecraft. A pressurization system, used to inflate the antenna, will require an additional mass of 35 kg. Thus a final mass estimate for the total communications subsystem comes to less that 100 kg for two inflatable reflector antennas [24]. By contrast, the mass estimate for two rigid

antennas is 170 kg. Once deployed in space, the pressurization system will initiate, inflating the structure, causing the ribs to lock into place, and allowing the system to become rigid. This releases the need for continued pressurization. The specifications of the inflatable antenna system are found in Figure 7.1. Data rates to be used by the high-gain antenna systems require an upper limit of approximately 150 kbps in order to insure adequate communication windows to and from the SPF-2000 spacecraft. The X-band frequency range, from 5.2 to 10.9 GHz, will be used by the high-gain antenna systems [25].

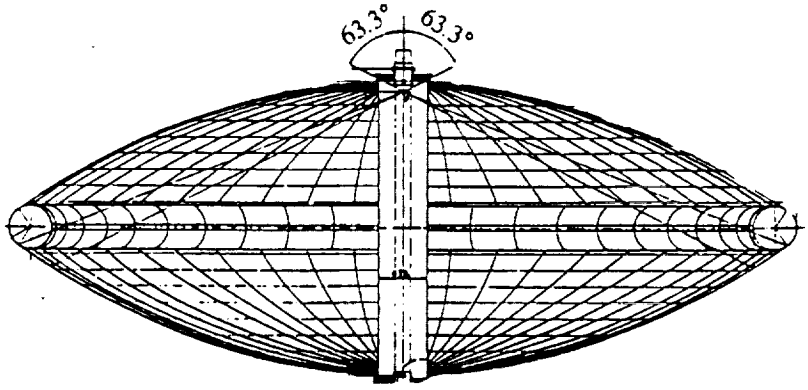

Figure 7.1. 5.83 m Inflatable reflector antenna [E. Pagana and P.G. Mantica, *ESA Journal*, Vol. 14, No. 2, 1990, p. 211]

Power requirements for the high-gain communication system are dependent upon the maximum distance between the spacecraft and Earth, the antenna diameter, and the transmission frequencies used by the system. A factor of ten must also be included in the maximum transmission power level to account for solar noise, due to the close proximity of Mercury to the Sun [7]. The approximate power required for the entire high-gain system, with the utilization of inflatable antennas, is 125 W. For a rigid parabolic antenna system, the required power is approximately 100 W [26]. Additional power loads for the high-gain antenna systems will be need for the thermal control of each system.

Temperature requirements for the high-gain communication system are between -80 and +100 °C [27]. These temperature requirements are primarily for the operating efficiency of the components. At extreme temperature limits, greater possibility of error is introduced into communications due to the antenna materials, and particularly in the construction of the inflatable antenna. Proper shielding of the equipment on board the spacecraft also provides thermal insulation for the spacecraft and probes. If the solar sail requires the spacecraft to be spinning, the communication booms will need to be placed on de-spun platforms so the antennas can be positioned and oriented to enable communications with ground control.

The Deep Space Network (DSN) will handle the ground control communications with the SPF-2000 spacecraft for its entire mission. Transmissions to and from the spacecraft, using the spacecraft transmission frequencies and the necessary data rates, may be readily incorporated into the present DSN system for interplanetary missions. The DSN will also be capable of efficiently managing the necessary transmissions to and from the spacecraft through the restrictive communication windows during the mission to Mercury, and while the spacecraft is in Mercury orbit.

7.3 Low-Gain Communications Design

Communications between each of the probes and the main spacecraft will be handled via low-gain antennas. This requires that each probe have a low-gain antenna, as well as one on the main spacecraft. Different transponder codes will be used to distinguish each probe's transmissions. This will enable the command and data handling subsystem to accurately process and store the data from each probe for later transmission to ground control via the high-gain communication system. Due to the close proximity of the main spacecraft to Mercury, a high transmission power level is not necessary. However, given the short period of rotation around Mercury, a high rate of transmission is preferred for probe to main spacecraft communications. A directional parabolic low-gain antenna system for each probe

and for the main spacecraft will be used to fulfill all of the requirements of the probe to main spacecraft communications.

The approximate mass of each low-gain system is 15 kg, and the estimated diameter needed is 0.33 m. Maximum power required is approximately 25 to 40 W [28]. The limiting temperatures for the thermal control of the low-gain systems are the same as for the high-gain systems, from -80 to +110 °C [27].

7.4 Communications Design Summary

In order to fulfill all of the communication requirements of the SPF-2000 spacecraft during its mission, many different options are needed. Multiple factors in the mission require consideration, such as the solar sail, the spinning of the main spacecraft, the changing orientation of the spacecraft while enroute to Mercury. Several high-gain communication systems were considered and selection of the final system was based on minimum mass, approximate costs, technological complexity, and operability of the system for the needs of the mission. Several low-gain system were also investigated based on size, mass, and capabilities of the system.

The selected communication system for the mission includes two high-gain antennas: one rigid parabolic and one inflatable reflector antenna. The rigid system will be placed on the near side of the solar sail with respect to the orbiter while the inflatable antenna system will be placed on the far side of the solar sail and will be ejected with the solar sail upon arrival at Mercury. Lander communications with the main spacecraft will be handled via low-gain antennas. The high-gain systems will communicate with the DSN on Earth. Since the main spacecraft will be spinning in order to maintain the rigidity of the solar sail, the antenna booms require despun platforms

8.0 Thermal Control

8.1 Requirements

Thermal control is an especially important design parameter of this mission due to the uncommonly high thermal loading associated with Mercury's proximity to the Sun. The spacecraft will experience a solar flux at Mercury of approximately 9000 W/m^2 (Appendix G) and the landers will be subjected to surface temperatures on Mercury as high as 467 °C and as low as -183 °C [29]. In addition to these external loads, the spacecraft will experience varying internal thermal loads throughout the mission. The thermal control system (TCS) will compensate for these loads and maintain spacecraft subsystem operational and nonoperational temperatures. Table 8.1 shows the allowable temperature ranges for the components of the spacecraft.

Table 8.1. Typical Temperature Limits (Agrawal, Brij, Design of Geosynchronous Spacecraft. Prentice-Hall, Inc., Englewood Cliffs, NJ, 1986)

Subsystem/Equip.	Nonoperating Temp (°C)	Operating Temp (°C)
Communications		
Receiver	-30/+55	+10/+45
Input multiplex	-30/+55	-10/+30
Output multiplex	-30/+55	-10/+40
Antenna	-170/+90	-170/+90
Attitude Control		
Earth/Sun sensor	-30/+55	-30/+50
Angular rate assembly	-30/+55	+1/+55
Momentum wheel	-15/+55	+1/+45
Propulsion		
Solid apogee motor	+5/+35	—
Propellant tank	+10/+50	+10/+50
Thruster catalyst bed	+10/+120	+10/+120
Structure		
Pyrotechnic mech.	-170/+55	-115/+55
Separation clamp	-40/+40	-15/+40
Scientific Instruments		
Orbiter	-15/+40	-15/+41
Lander	-30/+40	-30/+40

8.2 Thermal Loading

Each mission phase is defined by unique thermal loadings. During pre-launch phase the payload bay and the spacecraft will be kept at 15 °C by launch pad refrigeration systems. As the spacecraft is launched, the temperature of the payload fairing will increase to approximately 204 °C due to launch vehicle interactions with the atmosphere [31]. Solar flux and several of the internal subsystems will be the primary thermal loading for a low Earth orbit (LEO) system check. Solar sail radiation will increase the thermal loading slightly once the sail is deployed. In passage to Mercury, the solar flux will increase from 1350 W/m^2 at Earth to approximately 9000 W/m^2 at Mercury. Once in orbit around Mercury, increased waste heat from the solar panels and scientific instruments will cause a larger internal thermal loading.

The landers will experience a significant external load from the regolith and an internal load from the RTGs. The thermal loading of each phase of the mission is shown in Table 8.2.

Table 8.2. Thermal Loads on the Spacecraft

	Pre-Launch	Launch	Earth Orbit	Earth to Mercury	Mercury Orbit	Mercury Surface
External Loads						
Solar Flux (W/m^2)	0	0	1350	1350-9000	9000	0-9000
Flux from Solar sail (W/m^2)	0	0	0	5	33	—
Temp. Surroundings (°C)	15	15-204	—	—	—	-183/687
Internal Loads (W)						
Orbiter						
Solar Panels	0	0	486	486	12773	—
Propulsion	n	n	n	n	n	—
Communications	n	n	165	165	165	—
GNC	n	n	548	548	548	—
C&DH	n	n	177	177	177	—
Sci. Instr.	n	n	n	n	140	—
Thermal Control	n	n	54	54	54	—
Lander						
RTGs	0	0	0	0	2800	2800
Communications	n	n	n	n	n	65
GNC	n	n	n	n	n	10
Sci. Instr.	n	n	n	n	n	55
Thermal Control	n	n	n	n	n	20
Propulsion	n	n	n	n	n	n
C&DH	n	n	n	n	n	50

n - negligible

8.3 Discussion of Design

The thermal control for this mission is accomplished primarily through the use of louvers on the orbiter and heat pipes with thermal switches on the landers. The choice of coatings for the orbiter and the landers is also an integral part of the thermal control system.

8.3.1 Spacecraft

To maintain the necessary operational temperatures while subjected to the solar flux of 9000 W/m^2 at Mercury, the Optical Solar Reflector (OSR) coating is chosen for the spacecraft. This coating will minimize the flux absorbed while maximizing the energy

emitted (OSR has the lowest available absorptivity to emissivity ratio (0.1)) [31]. Radiation properties of several materials and coatings are shown in Table 8.3.

Table 8.3. Radiation Properties (Wertz, James R., and Wiley, J. Larson, Space Mission Analysis and Design, Norwell, MA, 1991, p. 382)

Material	Surface Condition	Solar Absorptivity	Infrared Emissivity	Absorp./Emiss.
Aluminum (6061-T6)	As received	0.379	0.0346	10.95
Aluminum (6061-T6)	Polished	0.2	0.031	6.45
Gold	As rolled	0.299	0.023	13
Steel (AM 350)	As received	0.567	0.267	2.12
Steel (AM 350)	Polished	0.357	0.095	3.76
Titanium (6AL-45)	As received	0.766	0.472	1.62
Titanium (6AL-45)	Polished	0.448	0.129	3.47
White Enamel	Al Substrate	0.252	0.853	0.3
White Epoxy	Al Substrate	0.248	0.924	0.27
Black Paint	Al Substrate	0.975	0.874	1.12
Optical Solar Reflector		0.077	0.79	0.1

However, with this coating, the equilibrium temperature of the spacecraft in orbit around Mercury is above the allowable range. To lower the temperature, louvers are incorporated into the orbiter thermal control design. Louvers will be rotated on the side of the spacecraft facing away from the Sun to expose a surface coated with white epoxy. White epoxy, having a higher emissivity that OSR, will allow the spacecraft to emit more energy. White epoxy also absorbs more energy than OSR, so it can only be exposed on the shaded side of the spacecraft (see Table 8.3). As shown in detail in Appendix G, 16.5 m^2 of white louver area will be exposed at Mercury to give an equilibrium temperature of approximately 38 °C. An analysis of the eclipse phase of the Mercury orbit indicates that the spacecraft temperature will drop only 0.05 °C, which is within the allowable range (Appendix G).

The OSR coating causes a significantly lower temperature than allowed while the spacecraft is in orbit around Earth. To raise the equilibrium temperature during this mission

phase, the longitudinal louvers are designed to have 3 surfaces: OSR, white epoxy, and gold (see Figure 8.1). The gold surface will be exposed to absorb more solar flux while at Earth. Gold has the highest absorptivity to emissivity ratio as well as the maximum absorptivity per unit area, which minimizes the amount of exposed louver area required (see Table 8.3). In orbit around Earth, 33 m^2 of gold louvers will be exposed to bring the spacecraft equilibrium temperature to 15 °C (Appendix G). for Earth orbit eclipse, as with the Mercury eclipse, the spacecraft temperature will drop by only a small amount (1 °C), which is well within the allowable temperature range.

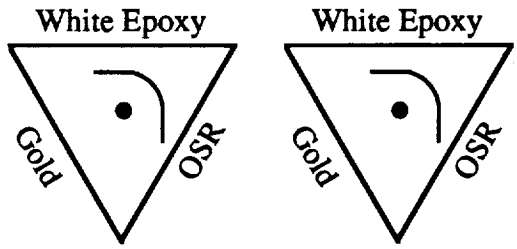

Figure 8.1. Louver Design

Because the sail is bowed away from the spacecraft and only a 4 m diameter section directly behind the spacecraft is rigid, the product of the area and view factor for the sail is very small. This, coupled with nearly a specular reflecting sail, yields only a small loading on the spacecraft from the solar sail. The solar flux reflected by the bowed part of the sail passes in front of the spacecraft while the portion reflected by the rigid section passes behind the spacecraft. Thus, the only thermal load on the spacecraft from the sail comes from energy emitted by the rigid portion. The heat radiated to the spacecraft from the sail is approximately 5 W at Earth and 33 W at Mercury. This additional loading is compensated for by decreasing the area of exposed gold louvers. Appendix G shows the effects of these loads on the spacecraft and gives the thermal load calculations for the solar sail in detail.

During thrusts to escape Earth orbit and to insert into an orbit around Mercury, the thrusters produce a significant amount of heat. Consequently, the Earth escape thruster and propellant tank will be thermally insulated from the rest of the spacecraft. The Mercury insertion thruster will be insulated from its propellant tank and shroud with a blanket of multilayer insulation (MLI); the shroud and propellant tank will not be insulated from the spacecraft in order to absorb more solar flux while at Earth and in transit to Mercury.

8.3.2 Orbiter Booms

The thermal control for the four booms will be accomplished by several methods. The magnetometer will be covered with white epoxy, keeping the instrument within operating temperatures while in Mercury orbit. At Earth, it is assumed that the magnetometer will be kept warm via conduction of heat from the spacecraft through the boom. The solar array will be maintained at the required temperature using a highly emissive coating on the back side of the panel and a heat pipe (4 cm diameter) within the boom to pump the panel's waste heat into a heat sink on the spacecraft. the heat sink will distribute this energy throughout the structure. The instruments on the scientific instruments boom will have polished aluminum surfaces to absorb sufficient solar flux at Earth to maintain allowable temperatures. The excess heat absorbed by the instrument boom at Mercury will be pumped into the spacecraft structure with a heat pipe (1.26 cm diameter) similar to the solar array boom. The communication system and boom have their own TCS, so none is required.

8.3.3 Landers

The landers will be coated with OSR to protect the instruments from the solar flux and the high surface temperatures of the Mercury terminator. The instruments and lander structure will be protected from the internal loads generated by the RTGs with a MLI blanket wrapped around the RTGs. The instruments will be kept at operational temperatures throughout the Mercury night by running heat pipes with thermal switches from the RTG

section to instrument section. These switches allow a varying amount of heat to transfer between the RTGs and the spacecraft. For example, when the surface temperature is minimum (90 K), 1711 W will be allowed to flow from the RTGs to keep the instruments at 288 K (this requires a combined cross-sectional heat pipe area of 17.2 cm^2). With all of the thermal switches open, the instruments will receive a heat flow of less than 5 W from the RTGs. With this configuration, the lander can withstand surface temperatures as high as 530 K while maintaining the instruments' operational temperatures. It can be seen from Figure 8.2 that given this maximum surface temperature, this phase of the mission could last for up to 136 Earth days (from 13 days before sunset to 35 days after sunrise) for this maximum surface temperature. See Appendix G for detailed calculations of lander thermal control. The thrusters are insulated from the spacecraft with an MLI blanket to avoid any waste heat entering the lander during the landing sequence. Appendix G also shows that the thermal loading from the atmosphere during landing is negligible. This lander TCS will provide ample time for the scientific experiments to be carried out.

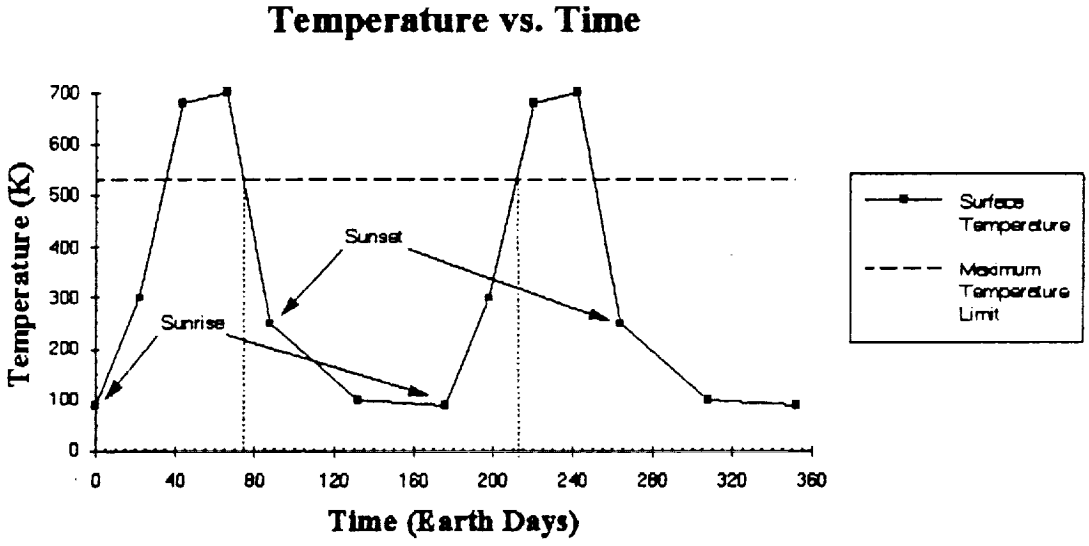

Figure 8.2. Temperature versus time for the spacecraft on Mercury's surface (Surface temperatures compiled from Strom, Robert G., Mercury, The Elusive Planet, Smithsonian Institution Press, Washington, D.C., 1987)

8.4 Summary of Design

The spacecraft will be protected from the high solar flux at Mercury with a low absorptivity to emissivity ratio paint coupled with white epoxy louvers exposed in the shadow of the spacecraft. To keep the spacecraft warm near Earth, gold louvers (highly absorptive and minimally emissive) will be exposed. The thrusters will be insulated from the spacecraft to avoid excessive thermal loads during thrust phases. The booms requiring thermal control are maintained at operational temperatures through the use of coatings and heat pipes where necessary. finally, the landers are kept at operational temperatures on the Mercury surface for 136 Earth days through the use of OSR coating and by insulating the RTGs from the instrumentation with a blanket of multilayer insulation. In addition, heat pipes with thermal switches will allow variable amounts of heat to be transferred from the RTGs to the instruments as the surface temperature changes. The rest of the RTG waste heat is radiated away from the lander.

9.0 Scientific Instruments

Mercury is a planet unique in physical appearance and geological features. Magnetic and surface experiments may provide answers to the many mysteries about Mercury that have puzzled scientists for years. These unknowns include the formation of various regions of the planet, the presence of ice in the craters, and the elemental composition of the regolith.

9.1 Requirements

For a full understanding of the origins of the planet, it is necessary to visit multiple sites. Different regions for landing sites have been determined by analyzing photographs returned by Mariner 10. Upon arrival, the orbiter instruments will map the surface to pinpoint four landing sites. Each site is unique in physical characteristics and will provide different clues as to how Mercury became a part of the solar system [29]. At each site, local seismic and tectonic activity will be monitored and regolith will be studied to determine its magnetic properties and chemical composition. After lander deployment, the orbiter will map Mercury's magnetic field and relay lander data to Earth. Instrument selection will be determined by these parameters.

9.2 Landing Sites

The landing sites determined by analyzing Mariner 10 photographs include the Caloris Basin, Hilly and Lineated Terrain, Intercrater Plains, and Smooth Plains [29]. A description of these regions and their scientific interests follow.

9.2.1 Caloris Basin

One lander will be deployed to the center of this large impact basin near 30° N latitude, 190° W longitude [32]. Measurements in this area will determine if deformation

occurred after the initial impact and also explain why fracture widths increase toward the basin's center [33].

9.2.2 Hilly and Lineated Terrain

This area is located at 30° S latitude, 25° W longitude. This is the only area on Mercury with both "hilly" and "lineated" terrain. Scientists believe the formation of this region stems from seismic activity or tectonic shifts because gravity would have prevented Caloris impact ejecta from reaching this area. Seismography experiments will give scientists more insight into this region's formation [32].

9.2.3 Intercrater Plains

Intercrater Plains are located mostly in the Southwest quadrant of Mercury. A lander will be deployed to Bernini, a crater located at 80° S latitude, 136° W longitude. This is the largest crater located close to the south polar point of Mercury. Investigations in this region will prove or disprove scientist's speculations that there is ice in the craters near the poles [34]. Investigations inside the crater may also determine if the craters are of endogenic origin [32].

9.2.4 Smooth Plains

Smooth plains are spread over the planet. One of the larger plain areas is Borealis Planitia (located at 75° N latitude, 85° W longitude). Experiments done in this area will ascertain how the plains were formed. Also, by determining the ages of the plains, scientists can conclude if surface impacts are the result of comets or asteroids [29].

9.3 Orbiter Instruments and Operations

The orbiter's main functions include planet mapping and magnetic studies. These tasks will be performed primarily with a magnetometer and instruments located on a High-Precision Scan Platform (HPSP).

9.3.1 High-Precision Scan Platform

Upon Mercury capture, suitable landing areas within the selected sites will be found using instruments located on the High-Precision Scan Platform (HPSP) similar to the one used on the Rosetta spacecraft [35]. The HPSP will be configured as shown in Figure 9.1 and mounted on a universal gimbal to allow rotational motion along two axes. Performance characteristics for the HPSP are given in Table 9.1. Table 9.2 lists specifications for orbiter and HPSP scientific instruments. Because the HPSP also contains the star tracker and sun sensors, the platform must be despun during the transfer from Earth orbit to Mercury orbit. At Mercury, the HPSP will map the entire planet in 757 orbits (Appendix H).

	Dimensions (cm)
RIS Electronics	32x22x15
Radiometer	44.8x19.1x32.7
IR Spectral Mapper	20x30x7
RCT	15.7x13.3x13.3
Star Tracker	10.8x18.1x10.8
Sun Sensor	10.9x6.4x2.8

	Dimensions (cm)
WAC	28x32x60
NAC	30x41x95
RA Micro/Digital	40x40x20
Laser	7000 cm^3
Radar Altimeter	56 cm diam
	l=40 cm

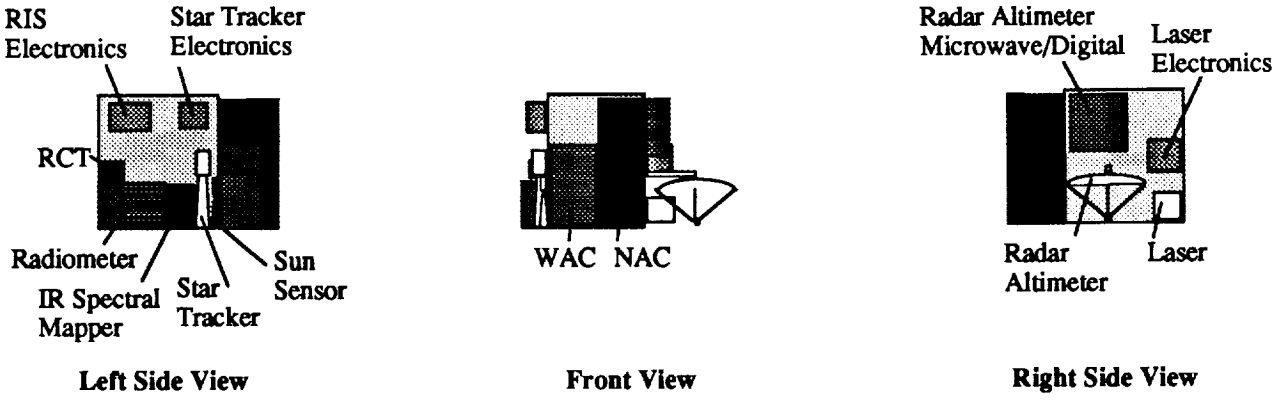

Figure 9.1. High-Precision Scan Platform

Table 9.1. High-Precision Scan Platform Performance Characteristics (Rosetta/CNSR, "A Comet/ Nucleus Sample/ Return Mission," ESA SP1125, June 1991.)

Pointing Range	±45° elevation, 360° azimuth
Pointing Accuracy	2.0 mrad after 2 hr
Point Knowledge	0.25 mrad at update, 1.0 mrad after 2 hr
Pointing Stability	10 mrad over 1 sec
Slew Rate	0 to 17.5 mrad/s

Table 9.2. Orbiter Instrument Specifications (unless otherwise noted all information taken from Rosetta /CNSR, "A Comet/ Nucleus Sample/ Return Mission," ESA SP1125, June 1991.)

Orbiter Instrument	Mass (kg)	Power (W)	Thermal Range (°C)	Dimensions (cm)	Data rate
Magnetometer	3[a]	3.1[a]	-15 to 110[b]		3.6 kbps[a]
Infrared Mapper					
Radiometer	4.8	12	-30 to 40	44.8x19.1x32.7	0.035 kbps
RCT	0.4	1.5		15.7x13.3x13.3	
Laser Range Finder	12	30 op; 5 nonop	-30 to 40	7000	3.2 kbps
Cooler	1	27 op			
IR Spectral Mapper	7	10 op; 2 nonop	-30 to 40	20x30x7	10-120 Mbits
RIS					
WAC	13.3	15 op; 7 nonop	-20 to 0	28x32x60	6.2-350 kbps
NAC	15	16.3 op; 7 nonop	-20 to 0	30x41x95	6.2-350 kbps
CCD detectors			-70		
Electronics Harness	8			32x22x15	
Radar Altimeter					
Antenna	10.2	57 op; 5 nonop	-30 to 40	diam. 56	
Microwave/Digital	11.5		-30 to 40	40x40x20	1 kbps

Notes: a. "Report on ESA's Scientific Satellites," Space Science Dept., ESA Publications - Division, 1989.
b. Stultz, James W., "Thermal Design of the Galileo Spun & Despun Science," Journal of Spacecraft & Rockets, Vol. 28, No. 2, March - April, 1991, p. 141.

9.3.2 Site Selection

Site selection for the landers is accomplished using the HPSP Remote Imaging System (RIS). There are two mapping phases involved in site selection: global and detailed. During the global mapping phase, the surface of Mercury is mapped using a Wide Angle Camera (WAC), a thermal-infrared spectrometer, a near-infrared spectrometer, and a radar altimeter. From a 500 km orbit, 757 passes will be required to map the entire surface of Mercury. The WAC will map the surface in 20.774 km by 20.774 km elements, with a resolution of 20.774 m per pixel (Appendix H). The infrared thermal mapper is used to determine the thermal inertia of the surface. An infrared mapping spectrometer will be used for site selection, also returning the spectral characteristics of Mercury's surface [35].

The radar altimeter will determine the approximate distance between the spacecraft and the surface, surface physical characteristics, and radar reflectivity. In order to determine possible landing sites within the defined areas of interest, it is imperative that the roughness and the slope of the surface be known. The regolith composition and possible presence of ice may be determined by microwave-reflection [35]. The presence of ice or detection of some unidentifiable substance will aid in determining the landing sites (landing in a region containing ice is desirable) [34].

After the entire planet is mapped (≈29.3 Earth days), a ground support team will designate candidate landing sites based on radar reflectivity and visual, thermal, and spectral characteristics. Candidate sites will be ranked based on probability for successful lander operations. After candidate sites in each of the proposed areas have been selected, a detailed mapping phase using a Narrow Angle Camera (NAC) and a laser altimeter will begin. The NAC will map the candidate sites in 5 km by 5 km elements with a resolution of 5 m per pixel. The laser altimeter will enable three-dimensional mapping on the scale of a few decimeters. Additionally, the altimeter data will provide complete topographic maps of the 20 km by 20 km candidate landing areas with a vertical and spatial resolution of about 50 cm [35]. The laser must be mounted on the HPSP to provide the two degrees of freedom

required for three-dimensional mapping. After the detailed mapping phase is completed, a ground support team will determine the four specific landing sites most suitable for mission success.

9.3.3 Additional Orbiter Operations

After the specific landing sites are selected, the HPSP instruments will continue to observe Mercury. The thermal infrared mapper will determine the effects of changing solar flux on the thermal conductivity of the surface layers. For an accurate determination of thermal conductivity, observations are required at different times during the Mercury day. Radar reflectivity also may give information on any surface changes due to drastic temperature changes. The laser altimeter and NAC also may be used during times when exchanges between the orbiter and landers are minimal to map the surface in more detail.

Apart from the HPSP, a magnetometer is used to determine the extent of Mercury's magnetic field. The magnetometer has a mass of 3 kg and is located at the end of a 3.1 m boom [38]. Once in orbit around Mercury, the magnetometer will begin taking measurements and continue for the duration of the mission. The information returned will disclose the size and shape of the magnetic field and any effects due to solar phenomena.

9.4 Lander Instruments and Operations

Once each lander has landed, various instruments will conduct tests to determine regolith composition and magnetic properties while monitoring seismic and tectonic activity. Cameras are used to photograph and record the local landscape features of Mercury. Figure 9.2 shows size and location of the scientific instruments on each lander and Table 9.3 gives specifications for the lander's scientific instruments.

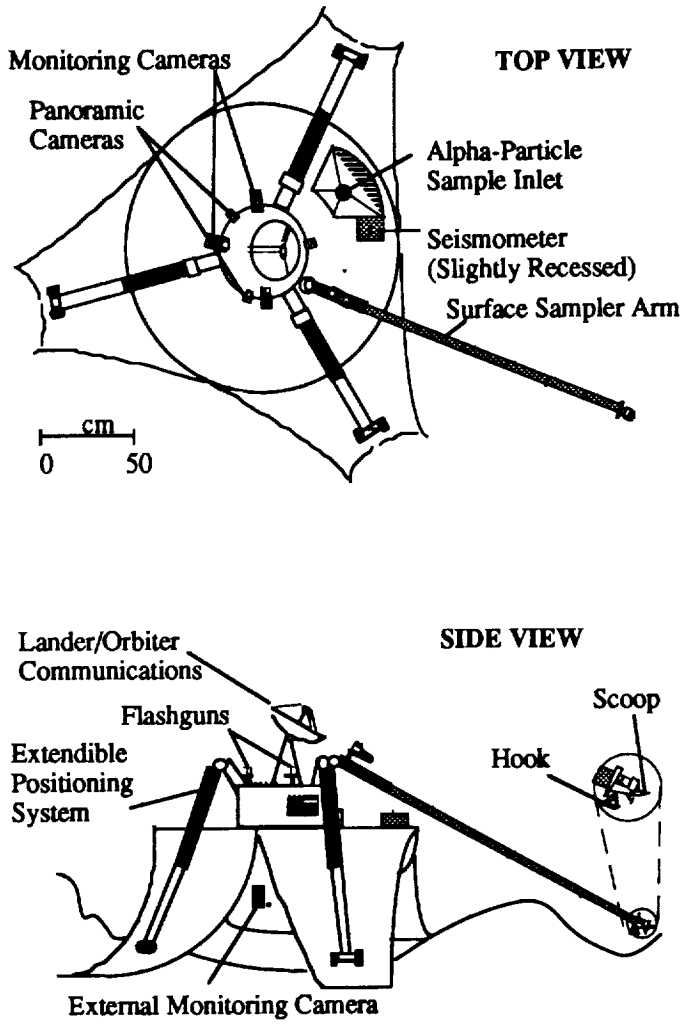

Figure 9.2. Scientific Instruments on Landers

Table 9.3. Lander Instrument Specifications (unless otherwise noted all information taken from Rosetta /CNSR, " A Comet/ Nucleus Sample/ Return Mission," ESA SP1125, June 1991.)

Lander Instrument	Mass (kg)	Power (W)	Thermal Range (°C)	Dimensions (cm)	Data rate
Surface Sampler	15[a]	15[c]	-30 to 40[c]		
Alpha Particle X-Ray	1[b]	2[b]	-30 to 40[b]	15.24x7.62x25.4[b]	
Seismometer	2.2[c]	3[c]		10.16x15.24x12.7[d]	
Imaging system					15-20 Mbits
Monitoring Camera (5)	1.575	1 op; 0 nonop	> -20	12x6x4	
Flash gun (5)	0.5				
Panoramic Camera (4)		1 op; 0 nonop	> -20	6x4x3	
Harness	1				
Thermal Logger					0.01 kbps
Thermistors (3)	0.6	1	< -113.15		

Notes: a. Stultz, James W., "Thermal Design of the Galileo Spun & Despun Science," Journal of Spacecraft & Rockets, Vol. 28, No. 2, March - April, 1991, p. 141.
b. Hord, Michael R., CRC Handbook of NASA Future Missions and Payloads, Vol. II, CRC Press, Inc., Boca Raton, FL, p. 53.
c. Martin Marietta Corporation, The Viking Mission to Mars, Denver, CO, pp (III): 32-69.

9.4.1 Regolith Sample

A regolith scoop is located on the end of an extendible-maneuvering surface sampler arm [36]. The arm is capable of extending 1.9 m, with a maximum vertical deflection angle of 40°. This will enable a sample to be taken as far as 0.83 m below the sampler arm base (Appendix H). During sampling the regolith will be acquired and transferred to an alpha particle x-ray instrument inlet while being observed by a small camera located on the surface sampler arm. The alpha particle x-ray instrument is recessed in the lander so that any stray samples can be funneled into the instrument. Once the regolith is transferred, the alpha particle instrument will conduct elemental chemical analyses [37].

9.4.2 Seismic and Tectonic Activity

A seismometer will be used to measure any seismic and/or tectonic activity. Initially, the seismometer will be recessed in a small compartment located next to the alpha particle instrument inlet. It will be transferred to the planet's surface with a hook located on the surface sampler arm. Once on the surface the instrument will record any seismic and/or tectonic activity.

9.4.3 Thermal Properties

In addition to the thermal measurements taken from orbit, small thermistors will be used to measure the temperature variations and thermal conductivity of the regolith. Measurements are monitored during three phases: before the regolith is removed, during transfer to the alpha particle instrument inlet, and during the analysis. The temperatures will be recorded every three seconds using a thermal recorder.

9.4.4 Local Landscape

During descent to the surface, a camera located on the side of the lander will record images of the landing site. After landing, the entire site will be photographed using panoramic and monitoring cameras containing flashguns. One camera will be located on the surface sampler arm and three other cameras will be positioned to view the entire landing area. Flashguns will be used to vary shadow patterns or eliminate darkness [35].

9.5 Summary of Design

Four landers will be deployed to different sites on the planet. These sites will have been narrowed down from general regions to specific sites using mapping instruments located on a high-precision scan platform on the orbiter. After the landers reach the surface they will use various instruments to measure seismic and tectonic activity as well as determine regolith chemical composition and magnetic properties. The results from these

experiments will provide answers as to how and when Mercury was formed, and why there are many physically different regions on Mercury.

10.0 Launch Vehicles

10.1 Launch Vehicle Requirements

The launch vehicle chosen for this mission is the Titan IV. The main requirement for this vehicle is to boost the SPF-2000 and probes into LEO

10.2 Properties of the Titan IV

Due to the length and the large mass of the spacecraft, many of the previously studied launch vehicles were eliminated. The only launch vehicle that will fit the specified spacecraft dimensions is the Titan IV. The Titan IV program was initiated in 1985 by the Air Force as a means of launching Shuttle-class payloads. The first launch of the Titan IV was on June 14, 1989. As of today the Titan IV has a 100% success rate [11].

Normally the Titan IV has three stages;. a fourth stage, or an upper stage can be added. The first three stages allow the vehicle to carry its payload to LEO, a more detailed flight sequence is listed in Table 10.1.

Table 10.1. Titan IV Typical Flight Sequence [Isakowitz, Steven J., *International Reference Guide to Space Launch Systems*, AIAA, 1981.]

Time (min:sec)	Event	Altitude (ft)
00:00	Stage 0 Ignition	0
02:00	Stage 1 Ignition	158375
02:12	Stage 0 Separation	186398
03:50	Payload Faring Separation	383614
05:08	Stage 2 Ignition	501535
05:09	Stage 1 Separation	502624
08:52	Stage 2 Shutdown	608391
09:18	Stage 2 Jettison	607604

The lift-off thrust of the Titan IV is provided solely by two SRMs. This constitutes the initial state, Stage 0, of the vehicle. Stage 1 consists of an LR87 liquid propellant rocket engine attached to an airframe. This includes the fuel and oxidizer tank, inner-tank structure, forward skirt and aft skirt. Stage 2 uses an LR91 liquid propellant rocket engine attached to an airframe similar in construction to that of Stage 1. The specifications for the Titan IV can be seen in Table 10.2. The faring design is shown in Figure 10.1.

Table 10.2. Titan IV Specifications [Isakowitz, Steven J., *International Reference Guide to Space Launch Systems*, AIAA, 1981.]

Vehicle	
System height	up to 204 ft (62.2 m)
Payload fairing size	16.7 ft (5.1 m) diameter 86 ft (26.2 m) height
Gross mass	1900000 lb (860000 kg)
Planned enhancements	Centaur-based Honeywell single-string avionics and the Hercules Solid Rocket Motor upgrade (SRMU) by 1993
Operations	
Primary missions	Polar, LEO, or GEO missions
Compatible upper stages	IUS, Centaur
Launch azimuth	93-112° (LC-40/41) 147-210° (SLC-4E)
Financial status	
Estimated launch price	$154M for Titan IV, no upper stage $214M for Titan IV, IUS $227M for Titan IV, Centaur

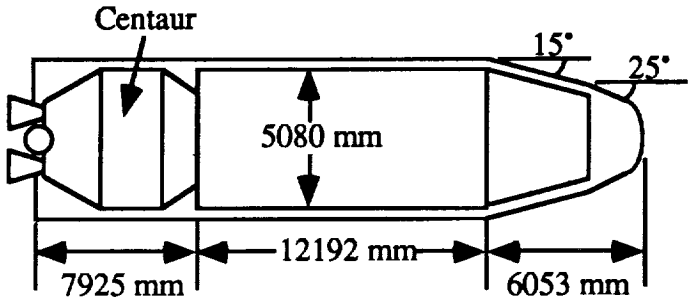

Figure 10.1. Titan IV Payload Faring

11.0 References

[1] Wertz, J.R. and W.J. Larsons, eds., Space Mission Analysis and Design, Norwell, MA, Klewer Academic Publishers, 1991, pp. 383, 624-625.

[2] Agarwal, B.D. and L.J. Brontman, Analysis and Performance of Fiber Composites, Wiley Publishing, 1990, p. 437.

[3] Personal correspondence with J. Leslie, Advanced Composite Products and Technology, Inc., Huntington Beach, CA.

[4] Wertz, p. 365.

[5] Wertz, p. 366.

[6] Wertz, p. 367.

[7] Aerospace 401 Class Notes, The Pennsylvania State University, University Park, PA, Fall 1992.

[8] Friedman, L., Star Sailing, Solar Sails, and Interplanetary Travel, 1989, p. 30.

[9] Foward, R.L., "Solar Photon Thruster," *Journal of Spacecraft and Rockets*, Vol. 27, No. 4, June/August 1990, pp. 411-413.

[10] Bate, Mueller, and White, Fundamentals of Astrodynamics, Dover Publications, Inc., New York, NY, 1971, pp. 390-396.

[11] Wilson, A., Interavia Space Directory - 1991-1992, Jane's Information Group, Alexandria, VA, 1991, pp. 281-282, 318.

[12] Sutton, G.P., Rocket Propulsion Elements - An Introduction to the Engineering of Rockets, Sixth Edition, John Wiley & Sons, Inc., 1992, pp. 251-252, 256.

[13] French, J.R., and J. Wright, "Solar Sail Mission to Mercury," *Journal of Interplanetary Society*, Vol. 40, No. 12, January 1987, pp. 543-550.

[14] The Marquardt Company, R-40B Specifications, September 1985.

[15] Aerojet Tech Systems, XLR-132A Specifications, August 1991.

[16] Aerojet Tech Systems, Transtar Specifications, January 1989.

[17] Honeywell, RLGA Specifications, 1991.

[18] Wertz, p. 162.

[19] Friedman, L., et al, "Solar Sailing - The Concept Made Realistic," JPL Feasibility Research, AIAA Paper 8-82, 1978.

[20] Friedman, 1989, p. 34-35.

[21] Groves, G.V., "Sailing to Mars on Sunlight," *Spaceflight*, The British Interplanetary Society, Vol. 32, No. 6, June 1990, p. 188.

[22] Honeywell, HR01 Specifications, 1991.

[23] Wertz, p. 341.

[24] Pagana, E. and P.G. Mantica, "An Inflatable Parabolic Reflector Antenna: Its Realization and Electrical Predictions," *ESA Journal*, European Space Agency, Vol. 14, No. 2, 1990, pp. 211-216.

[25] Wertz, pp. 332, 340.

[26] Wertz, p. 341.

[27] Williamson, M., The Communications Satellite, IOP Publishing Ltd., New York, NY, 1990, pp. 96-143.

[28] Wertz, p. 482.

[29] Murray, B., Earthlike Planets, W.H. Freeman and Company, San Francisco, CA, 1981, pp. 239-265.

[30] Agrawal, B., Design of Geosychronous Spacecraft, Prentice-Hall, Inc., Englewood Cliffs, NJ, 1986, p. 282.

[31] Martin Marietta Corporation, The Viking Mission to Mars, Denver, CO, pp. III:32-69.

[32] Moore and Hunt, The Atlas of the Solar System, Royal Astronomy Society, New York, NY, 1990, pp. 78-79.

[33] Surkov, Y.A., Exploration of Terrestrial Planets from Spacecraft, Eilis Horwood, New York, NY, 1990, pp. 32-41.

[34] Wilford, N.J., The New York Times, printed in *The Planetary Report*, Vol. 12, No. 1, Jan./Feb. 1992, p. 26.

[35] "Rosetta/CNSR — A Comet Nucleus Sample Return Mission," ESA SP-1125, June 1991.

[36] "Report on ESA's Scientific Satellites," Space Science Dept., ESA Publications Division, 1989.

[37] Stultz, J.W., "Thermal Design of the Galileo Spun & Despun Science," *Journal of Spacecraft and Rockets*, Vol. 28, No. 2, March/April 1991, p. 141.

[38] Hord, M.R., CRC Handbook of NASA Future Missions and Payloads, Vol. II, CRC Press, Inc., Boca Raton, FL, p. 53.

[39] Bell Aerospace Group, "New Generation Stellar Attitude Sensors," NASA Technical Report, 1991.

[40] Honeywell, HR20M Specifications, 1991.

[41] Honeywell, HR01 Specifications, 1991.

Appendix A: Spacecraft Structures

Modeling where the main body is supported by payload fairing and sail canister is not.

1. Dimensions of beams needed for Leros thrusters on sail canister

sf = safety factor
M = moment caused by thrusters
F = force caused by thrusters
d = distance of thrusters from hub of canister
S = bh^3/6 for a rectangle
b = base
h = height

M=F*d

Stress=M*sf/S

523E6 = (1.5 m)(20 N) (1.5)/((0.02 m)(0.03m)^3/6)

Beam dimensions = 0.02 m x 0.03 m x 2.12 m

Mass of each beam = 3.56 kg

2. Dimensions of main beams connecting propellant tank and sail canister

sf = safety factor
F = force on the 4 beams
m = mass of sail canister and communications dish
a = acceleration = 10 g estimated in tension
Fe = force on each beam
s = maximum stress
A = area

F = m*a
F = (960+11.125)(10)(9.81)
F = 95267.4 N

Fe = F/4 = 23817 N

s = F*sf/A
523E6 = (23817)(1.5)/(6.83E-5 m^2)

Beam dimensions = 0.008 m x 0.008 m x 1.625 m

Mass of each beam = 0.2912 kg

3. Dimensions of angled beams connecting propellant tank to sail canister

sf = safety factor = 1.5
Foa = off-axis force = 0.25 axial force
Fb = force in the beam
s = maximum stress
A = area

Foa = (0.25)(23817)(1.5)
Foa = 8931.4 N

Fb*sin(42.13) = 8931.4 N
Fb = 13314 N

s = Fb/A
523E6 = 13314/(2.55E-5 m^2)

Beam dimensions = 0.005 m x 0.005 m x 2.19 m

Mass of each beam = 0.1533 kg

4. Dimensions of beams connecting propellant tank to platform

F = force on each beam
m = mass of propellant, tank, canister, thruster, and communications dish
a = acceleration = 10 g estimated
sf = safety factor
A = area
s = maximum stress

F = m*a
F = (2242+120+960+11.125+57.27)(10)(9.81)/4
F = 83149 N

s = F*sf/A
523E6 = (83149)(1.5)/(2.38E-4 m^2)

Beam dimensions = 0.0154 m x 0.0154 m x 0.475 m

Mass of each beam = 0.317 kg

5. Dimensions of tube connecting propellant tank platform to main body

F = mass of everything behind tube (i.e. canister, propellant)
A = area
s = maximum stress
sf = safety factor

ro = outside radius = 0.65 m
ri = inside radius
t = maximum shear stress
h = height

s = sf*F/A
523E6 = (2242+57.27+960+11.125+120+10)(9.81)(10)(1.5)/(9.57E-4 m^2)

A=π*(ro^2-ri^2)
ri = 0.6497 m

t = s/2 = 2*M*ro/(π*(ro^4-ri^4))
ri=0.6499 m

Tube dimensions: ri = 0.64 m due to unknown forces caused by despun platform
ro = 0.65 m
h = 0.3 m

Tube mass = 34 kg

6. Dimensions of beams holding landers (these are in compression)

s = maximum stress
F = force on beams
m = mass of landers that produce F
a = acceleration = 10 g estimated
P = critical load
E = Young's modulus
I = moment of inertia = b*h^3/12
b = base
h = height
A = area

s = F/A
523E6 = ((2000)(10)(9.81)/3)/(0.125E-4)

P = E*I*π^2/(L^2)
let b = 0.1 so landers can be attached to beam h =0.09 m

Beam dimensions = 0.1 m x 0.09 m x 6.4 m

Mass of each beam = 161.3 kg

7. Dimensions of main body beam

s = maximum stress
A = area
F = force

sf = safety factor
r = radius
h = height

s = F*sf/A
523E6 = (500368-196200)(1.5)/(8.724E-4 m^2)

Beam dimensions: r = 0.2 m
h = 1.25 m

Mass of beam = 3.05 kg

8. Mass of main body

ρ = density
ro = outside radius
ri = inside radius
l = length
h = height of end caps
m = mass of main body structure

m = ρ*π*(ro^2-ri^2)*l+ρ*π*ro^2*h
m = (2800)π(0.8^2-0.77^2)(1.15)+(2800)π(0.64)(0.04)

m = 701.7 kg

Appendix B: Solar Array Sizing

Three cases examined:

I. Provide 600 W at LEO for GNC and instrument standby
II. Provide a minimum of 600 W during travel to Mercury
III. Provide a peak power of 1295 W at Mercury

CASE I

$$P_{out} = f_{in} X A (1 - d) \cos q \tag{B.1}$$

$$d = (d_1 + d_2) t \tag{B.2}$$

P_{out} = power from arrays (W)
f_{in} = solar flux
X = 0.21 (BOL efficiency of GaAr)
A = area of array panel (m^2)
d = solar cell degradation
d_1 = degradation due to thermal cycling
d_2 = degradation due to radiation
t = length of mission (years)
q = array angle relative to the Sun

Pout needs to be twice the maximum power to account for efficiencies of the power distribution, regulation, and control system. Therefore, P_{out} equals 1200 W. The solar flux at Earth is 1358 W/m^2. The degradation term, d, is a combination of degradation due to thermal cycling and radiation. The thermal cycling term for GaAr is 2.5% per year. The radiation term is 1.25% per year at Earth. To calculate overall degradation, the time spent in LEO was assumed to be a conservative 6 months. So, d equals 1.875%. Sizing was done assuming θ of only 10°, since high radiation is not as much as a concern in Earth orbit. Solving the power equation for area results in A = 4.35 m^2.

CASE II

The solar flux term in Equation B.1 is inversely proportional to distance from the Sun squared. The degradation of the solar arrays are directly proportional to the distance from the Sun. Therefore, as the spacecraft approaches Mercury, the increased power output will offset the increased degradation of the arrays due to the increased radiation and a minimum of 600 W will be provided with a 4.35 m^2 array panel.

CASE III

Pout of the solar arrays at Mercury must be 2590 W. the solar flux when scaled to a distance of 0.3871 AU from the Sun, Mercury's semi-major axis, becomes 9063 W/m^2. Solar cell degradation, d, when scaled to the higher radiation environment at Mercury and assuming a maximum mission time of five years equals 47.95%. Solving the power equation for area, with an array angle of 10° equals 2.65 m^2.

This shows that the LEO power requirement is the limiting case. Therefore, an array area of 4.4 m^2 was chosen. This size allows for an angle of incidence of up to 14° at Earth and 50° at Mercury.

Appendix C: Battery Sizing

Two cases examined:

I. Provide 600 W at LEO for GNC and instrument standby
II. Provide a peak power of 1295 W at Mercury

CASE I

$$Mass = \frac{P_{out}t}{33W - hr/kg} \tag{C.1}$$

$$Volume = \frac{P_{out}t}{0.4W - hr/cm^3} \tag{C.2}$$

P_{out} = power from batteries (W)
t = eclipse time (hrs)

At Earth, P_{out} equals 600 W, and there is an eclipse time of 85 minutes, 1.42 hours. This results in a mass of 26 kg, and a volume of 2130 cm^3.

CASE II

At Mercury, P_{out} equals 1295 W, and the orbiter eclipse time is 35 minutes, 0.58 hours. This results in a mass of 23 kg, and a volume of 1888 cm^3. The power required at Earth is the limiting factor, therefore, the batteries will have a mass of 26 kg and occupy a volume of 2130 cm^3.

Appendix D: Encke Program

ENCKE PROGRAM VARIABLE DIRECTORY

nu0 - the initial true anomaly
mus - gravitational parameter of the Sun
mum - gravitational parameter of Mercury
mue - gravitational parameter of Earth
muv - gravitational parameter of Venus
icount - counting variable
r - distance between the Sun and the spacecraft
rdot - velocity of the spacecraft
rho - radius (from the Sun) of the osculating orbit
rhodot - velocity of the osculating orbit
xn - initial condition for fourth order Runge-Kutta
g1, g2, g3, g4 - constants used to calculate the fourth order Runge-Kutta
r0 - initial radius of the spacecraft
theta0 - initial mean anomaly
w0 - initial rotational velocity
e0 - eccentric anomaly
a - semi-major axis
e - eccentricity
t0 - initial time
itype - counter
nstep - initial step
dt - change in time
ndim - dimensions
nvar - number of variables
f0 - acceleration of the sail
f - force on the sail
zoom - angle of the sail with respect to the solar flux
s - solar flux
rm - distance of Mercury from the Sun
omegam - rotational velocity of Mercury
anglem0 - initial angle of Mercury
re - distance of Earth from the Sun
omegae - rotational velocity of Earth
angle0 - initial angle of Earth
rv - distance of Venus from the Sun
omegav - rotational velocity of Venus
angleV - initial angle of Venus
rms - distance between Mercury and the spacecraft
rvs - distance between Venus and the spacecraft
res - distance between Earth and the spacecraft

ENCKE PROGRAM INPUT FILE

ndim - number of dimensions	2
dt - change in time	100 seconds
anglm0 - initial angular position of Mercury	0 rad
anglv0 - initial angular position of Venus	0 rad
angle0 - initial angular position of Earth	6.d-2 rad
r1 - initial radial component of the position of the spacecraft	1.495 d+8 km
r2 - initial tangential component of the position of the spacecraft	0.d0 km
rdot1 - initial radial component of the velocity of the spacecraft	0.d0 km/s
rdot2 - initial tangential component of the velocity of the spacecraft	29.262 km/s

ENCKE PROGRAM

```
      program encke

      implicit real*8 (a-h,o-z)
      real*8 nu0,mus,mum,muv,mue
      integer icount
c
      dimension r(3),rdot(3),rho(3),rhodot(3)
      dimension xn(6),step(6),g1(6),g2(6),g3(6),g4(6)
c
      common /rhodat/r0,theta0,w0,nu0,e0,a,e,t0,itype
      common /param/dt,ndim,nvar
      common /grav/mus,f0,f,zoom,s,icount
      common /merc/mum,rm,omegam,anglm0
      common /venus/muv,rv,omegav,anglv0
      common /earth/mue,re,omegae,angle0
      common /sc/rms(3),rvs(3),res(3)
c
      data r,rdot,rho,rhodot/3*0.d0,3*0.d0,3*0.d0,3*0.d0/
      data xn,step/6*0.d0,6*0.d0/
      data g1,g2,g3,g4/6*0.d0,6*0.d0,6*0.d0,6*0.d0/
c
      open(unit=5, file="enke.in", status="unknown")
      open(unit=6, file="enke.out", status="unknown")
c
c
      open(unit=7, file="flyby.out", status="unknown")
      open(unit=8, file="rho.out", status="unknown")
      open(unit=10, file="r0.out", status="unknown")
c
c       write any headings to the files
c
      write(7,700)
c
c       initialize the data for the osculating orbit
c
      r0=0.d0
      w0=0.d0
      theta0=0.d0
      nu0=0.d0
```

```
      e0=0.d0
      a=0.d0
      e=0.d0
      t0=0.d0
      itype=0
      nstep=0
      zoom=1.04719755
      icount=1
c
c       initialize the data for the planets
c
      mus=1.327d+11
      mum=2.232d+4
      muv=3.257d+5
      mue=3.986012d+5
c      mue=0.d0
c      mum=0.d0
c      muv=0.d0
      rm=57.9d+6
      rv=108.1d+6
      re=149.5d+6
      omegam=8.268326464d-7
      omegav=3.241133505d-7
      omegae=1.992845693d-7
c
      t=0.d0
      rmax=2.279d8
      rmin=57.9d+6
      maxstp=10000000
c
c         read the initialization data and the governing parameters
c
      read(5,*) ndim,dt
      nvar=2*ndim
      read(5,*) anglm0,anglv0,angle0
      read(5,*) (r(i),i=1,ndim)
      read(5,*) (rdot(i),i=1,ndim)
c
c        now determine the osculating orbit to begin the integration
c
      call kiss(r,rdot,t)
c
c        begin the integration
c
   10 continue
      call rk4(xn,step,g1,g2,g3,g4,t)
c
c        the integration has now completed a time step
c        now calculate the new true orbit position and velocity
c        vectors
c
      nstep=nstep+1
      if(nstep .gt. maxstp)  then
        write(6,900)
        go to 999
      endif
c
      call rhocal(rho,rhodot,t)
```

```
      do 20 i=1,ndim
      r(i)=rho(i)+xn(i)
      rdot(i)=rhodot(i)+xn(i+ndim)
      if (r(1) .eq. 0.d0) then
         count = count +1
         write(6,1234)
      endif
   20 continue
c
c        calculate the distance from the planets to see if the
c        spacecraft has entered the sphere of influence.  If it
c        has entered the sphere of influence, stop the program.
c
      r1=r(1)
      r2=r(2)
      call planet(r1,r2,t,rm1,rm2,rdms,rv1,rv2,rdvs,re1,re2,rdes)
      write(7,710) t,rdms,rdvs,rdes
c
c
c        check for arrival at Mercury or Mars
c
      radius=dsqrt(r1**2+r2**2)
      if(radius .gt. rmax)  then
        write(6,600) t
        go to 999
      endif
      if(radius .lt. rmin)  then
        write(6,601) t
        go to 999
      endif
c
c        now determine if a new osculating orbit is required
c
      rhomag=dsqrt(dot(rho,rho,ndim))
      delr=dsqrt(dot(xn,xn,ndim))
c>>>>>>>>>>>>>>>>>>>>>>>>>>>>>>>>>>>>>>>>>>>>>>>>>>>>>>>>>>>>>>>>>>>>
      if(nstep .eq. nstep/50*50) then
      write(8,6080) t,rhomag
      write(6,6100) t,r1,r2
      am1=mum*(rms(1)/rdms**3+rm1/rm**3)
      av1=muv*(rvs(1)/rdvs**3+rv1/rv**3)
      ae1=mue*(res(1)/rdes**3+re1/re**3)
      am2=mum*(rms(2)/rdms**3+rm2/rm**3)
      av2=muv*(rvs(2)/rdvs**3+rv2/rv**3)
      ae2=mue*(res(2)/rdes**3+re2/re**3)
      am=dsqrt(am1**2+am2**2)
      av=dsqrt(av1**2+av2**2)
      ae=dsqrt(ae1**2+ae2**2)
      write(6,6110) am,av,ae
      endif
 6080 format(2x,'T = ',f10.1,5x,'rho = ',d15.5)
 6100 format(//2x,'T = ',f10.1,2x/
     1         2x,'r    = ',d13.5,' N1 + ',d13.5,' N2')
 6110 format(2x,'am = ',d13.5,5x,'av = ',d13.5,5x,
     1           'ae = ',d13.5)
c<<<<<<<<<<<<<<<<<<<<<<<<<<<<<<<<<<<<<<<<<<<<<<<<<<<<<<<<<<<<<<<<<<<<
      if(dabs(delr/rhomag) .gt. 0.01d0)  then
        call kiss(r,rdot,t)
```

```
        do 30 i=1,nvar
   30   xn(i)=0.d0
        endif
        go to 10
  999 continue
c
c            F  O  R  M  A  T          S  T  A  T  E  M  E  N  T  S
c
  600 format(//5x,'For a Mars transfer, the time is: ',d15.5/)
  601 format(//5x,'For a Mercury transfer, the time is: ',d15.5/)
  610 format(2x,'Rectification occurred at t = ',f10.1)
  700 format(t10,'T ',t25,'Rms',t45,'Rvs',t65,'Res')
  710 format(2x,f10.1,3(5x,d15.5))
  900 format(5x,'the program executed the maximum number of steps'/
     1       5x,'before reaching the prescribed radius'//)
c
c
      stop
      end
c
c
c*********************************************************************
c
c         this subroutine is the 4-order Runga-Kutta integrator
c
c---------------------------------------------------------------------
c
      subroutine rk4(xn,step,g1,g2,g3,g4,t)
      implicit real*8 (a-h,o-z)
c
      dimension xn(nvar),step(nvar),g1(nvar),g2(nvar),g3(nvar),g4(nvar)
c
      common /param/dt,ndim,nvar
c
      time=t
      do 10 i=1,nvar
   10 step(i)=xn(i)
      call rhs(step,g1,time)
      do 20 i=1,nvar
   20 step(i)=xn(i)+g1(i)*dt/2.d0
      time=t+dt/2.d0
      call rhs(step,g2,time)
      do 30 i=1,nvar
   30 step(i)=xn(i)+g2(i)*dt/2.d0
      call rhs(step,g3,time)
      do 40 i=1,nvar
   40 step(i)=xn(i)+g3(i)*dt
      time=t+dt
      call rhs(step,g4,time)
c
      do 50 i=1,nvar
   50 xn(i)=xn(i)+(g1(i)+2.d0*(g2(i)+g3(i))+g4(i))*dt/6.d0
      t=t+dt
c
      return
      end
c
c
```

```
c**********************************************************************
c
c         this subroutine calculates rhs of the differential equations
c
c----------------------------------------------------------------------
c
      subroutine rhs(x,xdot,t)
      implicit real*8 (a-h,o-z)
      real*8 nu0,mus,mum,muv,mue
      integer icount
c
      dimension x(nvar),xdot(nvar),wk(3)
c
      common /rhodat/r0,theta0,w0,nu0,e0,a,e,t0,itype
      common /param/dt,ndim,nvar
      common /grav/mus,f0,f,zoom,icount
      common /merc/mum,rm,omegam,anglm0
      common /venus/muv,rv,omegav,anglv0
      common /earth/mue,re,omegae,angle0
      common /sc/rms(3),rvs(3),res(3)
c
c
      x1=x(1)
      x2=x(2)
c
c        calculate rho(t) and r(t)
c
      call rhocal(wk,xdot,t)
      rho1=wk(1)
      rho2=wk(2)
      rho=dsqrt(rho1**2+rho2**2)
      r1=rho1+x1
      r2=rho2+x2
      r=dsqrt(r1**2+r2**2)
c
c        calculate the positions of the planets and the distance
c        from each planet to the spacecraft
c
      call planet(r1,r2,t,rm1,rm2,rdms,rv1,rv2,rdvs,re1,re2,rdes)
      s=1.4d3*(re/r)**2
      f0=((2*(sin(zoom))**2*s*1.067d-7)*icount)/2500
c
c       calculate q(t) and fq(t)
c
      q=-(x1*(rho1+x1/2.d0)+x2*(rho2+x2/2.d0))/rho**2
      fq=1.d0-1.d0/dsqrt((1.d0-2.d0*q)**3)
c
c       now calculate the xdot vector
c
      xdot(1)=x(3)
      xdot(2)=x(4)
      xdot(3)=mus*(fq*r1-x1)/rho**3-mum*(rms(1)/rdms**3+rm1/rm**3)-
     1         muv*(rvs(1)/rdvs**3+rv1/rv**3)-
     2         mue*(res(1)/rdes**3+re1/re**3)+
     3         f0*cos(zoom)/r*(r2-r1)
      xdot(4)=mus*(fq*r2-x2)/rho**3-mum*(rms(2)/rdms**3+rm2/rm**3)-
     1         muv*(rvs(2)/rdvs**3+rv2/rv**3)-
     2         mue*(res(2)/rdes**3+re2/re**3)-
```

```
     3        f0*sin(zoom)/r*(r2+r1)
c
c
      return
      end
c
c
c*********************************************************************
c
c         this subroutine calculates the positions of the planets
c         and the distance from each planet to the spacecraft
c
c---------------------------------------------------------------------
c
      subroutine planet(r1,r2,t,rm1,rm2,rdms,rv1,rv2,rdvs,re1,re2,rdes)
      implicit real*8 (a-h,o-z)
      real*8 mum,muv,mue
c
      common /merc/mum,rm,omegam,anglm0
      common /venus/muv,rv,omegav,anglv0
      common /earth/mue,re,omegae,angle0
      common /sc/rms(3),rvs(3),res(3)
c
c       calculate rm(t) and rms(t)
c
      rm1=rm*dcos(anglm0+omegam*t)
      rm2=rm*dsin(anglm0+omegam*t)
      rms(1)=r1-rm1
      rms(2)=r2-rm2
      rdms=dsqrt(rms(1)**2+rms(2)**2)
c
c       calculate rv(t) and rvs(t)
c
      rv1=rv*dcos(anglv0+omegav*t)
      rv2=rv*dsin(anglv0+omegav*t)
      rvs(1)=r1-rv1
      rvs(2)=r2-rv2
      rdvs=dsqrt(rvs(1)**2+rvs(2)**2)
c
c       calculate re(t) and res(t)
c
      re1=re*dcos(angle0+omegae*t)
      re2=re*dsin(angle0+omegae*t)
      res(1)=r1-re1
      res(2)=r2-re2
      rdes=dsqrt(res(1)**2+res(2)**2)
c
c
      return
      end
c
c
c*********************************************************************
c
c         this subroutine calculates the orbital parameters of the
c         osculating orbit
c
c---------------------------------------------------------------------
```

```
c
      subroutine kiss(r,rdot,t)
      implicit real*8 (a-h,o-z)
      real*8 nu0,mus
      integer icount
c
      dimension r(ndim),rdot(ndim),eccvec(3)
c
      common /rhodat/r0,theta0,w0,nu0,e0,a,e,t0,itype
      common /grav/mus,f0,f,zoom,s,icount
      common /param/dt,ndim,nvar
c
c       calculate the angular momentum and the eccentricity vectors
c
      pi=dacos(-1.d0)
      rdotv=dot(r,rdot,ndim)
      r0=dsqrt(dot(r,r,ndim))
      vsq=dot(rdot,rdot,ndim)
      coeff=vsq-mus/r0
      do 10 i=1,ndim
   10 eccvec(i)=(coeff*r(i)-rdotv*rdot(i))/mus
      e=dsqrt(dot(eccvec,eccvec,ndim))
c
c        The following section sets up the prediction problem for the
c        osculating orbit IN A ZERO INCLINATION ORBIT.  If the orbit
c        plane is inclined, this section must be changed
c
      theta0=atan2(r(2),r(1))
      if(e .le. 0.001d0) then
           w0=dsqrt(vsq)/r0
           itype=0
        else
            edotr=dot(eccvec,r,ndim)
            arg=edotr/e/r0
            if(dabs(arg) .gt. 1.d0)   arg=dsign(1.d0,arg)
            nu0=dacos(arg)
            if(rdotv .lt. 0.d0)  nu0=2.d0*pi-nu0
            energy=vsq/2.d0-mus/r0
            a=-mus/2.d0/energy
            e0=dacos((e+dcos(nu0))/(1.d0+e*dcos(nu0)))
            if(nu0 .gt. pi)  e0=2.d0*pi-e0
            itype=1
      endif
      t0=t
c>>>>>>>>>>>>>>>>>>>>>>>>>>>>>>>>>>>>>>>>>>>>>>>>>>>>>>>>>>>>>>>>>>>>
      write(8,6010) t
      write(8,6012) r(1),r(2),rdot(1),rdot(2)
      write(8,6015) r0,dsqrt(vsq)
      if(itype.eq.0) then
         write(8,6000) r0,theta0,w0
      else
         write(8,6005) r0,nu0,e0,a,e
      endif
 6000 format(//2x,'The radius is:            ',d15.5/
     1             2x,'The initial angle is:    ',d15.5/
     2             2x,'the angular velocity is: ',d15.5)
 6005 format(//2x,'The radius is:                 ',d15.5/
     1             2x,'The initial true anomaly is:    ',d15.5/
```

```
     2              2x,'the eccentric anomaly is:       ',d15.5/
     3              2x,'The semi-major axis is:         ',d15.5/
     4              2x,'The eccentricity is:            ',d15.5)
 6010 format(///5x,'The osculating orbit has been found at t = ',
     1                  f10.1)
 6012 format(/2x,'r    = ',d13.5,' N1 + ',d13.5,' N2'/
     2        2x,'rdot = ',d13.5,' N1 + ',d13.5,' N2')
 6015 format(//2x,'r = ',d15.5,5x,'v = ',d15.5)
c<<<<<<<<<<<<<<<<<<<<<<<<<<<<<<<<<<<<<<<<<<<<<<<<<<<<<<<<<<<<<<<<<<<<<<<
c
      return
      end
c
c
c**********************************************************************
c
c         this subroutine determines the value of rho and rhodot at the
c         specified time
c
c----------------------------------------------------------------------
c
      subroutine rhocal(rho,rhodot,t)
      implicit real*8 (a-h,o-z)
      real*8 nu0,mus
c
      dimension rho(ndim),rhodot(ndim)
c
      common /rhodat/r0,theta0,w0,nu0,e0,a,e,t0,itype
      common /grav/mus,f0
      common /param/dt,ndim,nvar
c
      pi=dacos(-1.d0)
      if(itype .eq. 0) then
          angle=w0*(t-t0)+theta0
          rho(1)=r0*dcos(angle)
          rho(2)=r0*dsin(angle)
          rhodot(1)=-r0*w0*dsin(angle)
          rhodot(2)=r0*w0*dcos(angle)
      else
c
c          use newton's method to solve for the eccentric anomaly
c
          const=dsqrt(mus/a**3)*(t-t0)
          k=const/2.d0/pi
          const=const-2.d0*pi*dfloat(k)+e0-e*dsin(e0)
          call newton(en,const)
c
          rn=a*(1.d0-e*dcos(en))
          csnu=(e-dcos(en))/(e*dcos(en)-1.d0)
          snnu=a*dsqrt(1.d0-e**2)*dsin(en)/rn
          csphi=dcos(theta0-nu0)
          snphi=dsin(theta0-nu0)
c
          coeff=dsqrt(mus/(a*(1.d0-e**2)))
          rho(1)=rn*(csnu*csphi-snnu*snphi)
          rho(2)=rn*(snnu*csphi+csnu*snphi)
          rhodot(1)=coeff*(-snnu*csphi-(e+csnu)*snphi)
          rhodot(2)=coeff*(-snnu*snphi+(e+csnu)*csphi)
```

```
c
      endif
c
      return
      end
c
c
c*********************************************************************
c
c         this subroutine determines the value of rho and rhodot at the
c         specified time
c
c---------------------------------------------------------------------
c
      subroutine newton(en,const)
      implicit real*8 (a-h,o-z)
c
      real*8 nu0
      common /rhodat/r0,theta0,w0,nu0,e0,a,e,t0,itype
c
c
      en=const
      ncount=0
   10 continue
      f=en-e*dsin(en)-const
      df=1.d0-e*dcos(en)
      en=en-f/df
      if(dabs(f/df/en) .gt. 1.d-4) then
          ncount=ncount+1
          if(ncount .gt. 50) then
             write(6,900)
c>>>>>>>>>>>>>>>>>>>>>>>>>>>>>>>>>>>>>>>>>>>>>>>>>>>>>>>>>>>>>>>>>>>>
      write(6,6005) const
 6005 format(///2x,'Subroutine Newton entered. Const = ',d15.5)
      write(6,6000) ncount,en,f,df
 6000 format(2x,'Newton iteration no.',i3/5x,'E = ',d15.5,5x,
     1       'F = ',d15.5,5x,'F''= ',d15.5)
c<<<<<<<<<<<<<<<<<<<<<<<<<<<<<<<<<<<<<<<<<<<<<<<<<<<<<<<<<<<<<<<<<<<<<
             stop
          endif
          go to 10
      endif
c
  900 format(///5x,'Newton''s method failed to converge'//)
c
      return
      end
c
c
c*********************************************************************
c
c         this function calculates the dot-product of two vectors
c
c---------------------------------------------------------------------
c
      function dot(a,b,ndim)
      implicit real*8 (a-h,o-z)
c
```

```
      dimension a(ndim),b(ndim)
c
c
      dot=0.d0
      do 10 i=1,ndim
   10 dot=dot+a(i)*b(i)
c
      return
      end
```

Appendix E: Rocket Motors

MERCURY CAPTURE

$\Delta V = 2.14149$ km/s

	Propellant mass (kg)	Burn time (sec)	Escape mass* (kg)
Two R-40B	2939.2	1124.51	7887.92
XLR-132A	2774.48	555.80	7757.75
Transtar	2840.49	548.94	7841.49

*$M_{esc} = M_{sail} + M_{orbiter} + M_{landers} + M_{capture\ engines} + M_{capture\ propellant}$

EARTH ESCAPE

$\Delta V = 3.4046$ km/s

Propellant mass (kg)

Motor	RL-10A	Proton	Tsyklon	Ariane
Two R-40B	9301.16	13275.78	14643.35	9343.38
XLR-132A	**9147.67**	13056.70	14404.70	9189.19
Transtar	9246.42	13197.64	14557.15	9288.38

Burn time (sec)

Motor	RL-10A	Proton	Tsyklon	Ariane
Two R-40B	554.43	539.33	609.60	654.12
XLR-132A	**545.28**	530.43	599.54	643.32
Transtar	551.16	536.15	606.01	650.27

Mass at LEO** (kg)

Motor	RL-10A	Proton	Tsyklon	Ariane
Two R-40B	17327.43	21466.70	22689.27	17386.63
XLR-132A	17043.77	21117.45	22317.45	17101.94
Transtar	17226.26	21342.13	22556.64	17284.87

**$M_{LEO} = M_{escape} + M_{escape\ engines} + M_{escape\ propellant}$

Appendix F: GNC Hardware

Table F.1. GNC Hardware list for the SPF-2000 spacecraft

	Power required (W)	Mass (kg)
1. LEO to Earth escape		
a. Thrusters to align craft for escape burn are internal to booster		
2. Earth escape to Mercury capture		
a. Sun sensor (0.05° accuracy)	3 (max)	2
b. Star tracker (high accuracy CT-601 from Bell) [39]	12 (max)	8
c. Inertial guidance (RLGA from Honeywell) [17]	14	5.9
d. Sail control actuators (≈16?)	16 x 5	16 x 0.25
e. Sail control sensors (≈16?)	8 x 1	16 x 0.25
f. Four Honeywell HR20M reaction wheels		
Torque: 0.105 Nm; (operating/holding power) [40]	4 x (80/30)	4 x 10.4
h. 24 MRE-5 thrusters (12 pairs) [41]	NA	12 x 1.14
4 MRE-15 thrusters [11]	NA	4 x 1.13
3. Mercury orbiter		
a. Steerable horizon sensor (static/moving power)	(2.5/7.5)	1.6
4. Lander		
a. Inertial guidance	20	4
b. Radar range finder/altimeter	≈5	≈1
c. Momentum wheels (smallest size offered by Honeywell) [41]	(6/40)	2.3
d. Leros 20 thrusters [11]	NA	8 x 0.45
TOTALS	509 max	96.2

Table F.2. Specifications for MRE-5 and MRE-15 thrusters

Parameter	MRE-5 Thruster	MRE-15 Thruster
Thrust	12-24.5 N	44.5-82 N
Isp	235 sec	225 sec
Propellant catalyst	MMH w/ Shell 405 catalyst	MMH w/ Shell 405 catalyst
Stead burn capability	yes	yes

Table F.3. GNC Propellant Masses (kg)

Thrusters (MRE-5 and MRE-15)	
Initial spin-up	0.7
Sail deployment	558
Margin for losses due to flexible nature of sail	10%*(558)
180° turn before capture burn	2.9
Off-axis perturbations during capture burn	2.6
Subtotal	620
Margin to account for losses due to flexible structures, despun booms, propellant slosh, and imbalanced spinning	10%*(620)
Total	682
Capture motor (inclination change)	705
TOTAL propellant mass	1387

Appendix G: Thermal Control Subsystem

1. To evaluate the solar flux at Mercury the following equation is used:

$$\phi_m = \phi_e \left(\frac{R_e}{R_m} \right)^2 \tag{G.1}$$

ϕ_m = solar flux at Mercury
ϕ_e = solar flux at Earth = 1350 W/m^2
R_e = radius of Earth's orbit = 149600000 km
R_m = radius of Mercury's orbit = 57910000 km

2. The equilibrium temperature is calculated from the following equation:

$$T_E = \left[\frac{Q + \phi \sum_i \alpha_i \mu_i a}{\sigma \sum_i \varepsilon_i A_i} \right]^{\frac{1}{4}} \tag{G.2}$$

T_E = equilibrium temperature
Q = internal thermal load
S = solar flux
α = absorptivity
$\mu_i a$ = incident area
ε = emissivity

The time constant is found via

$$\tau = \frac{\sum_i M_i C_p}{4 \sigma T_E^3 \sum_i \varepsilon_i A_i} \tag{G.3}$$

τ = time constant
C_p = average specific heat of spacecraft
M_i = mass of spacecraft
ε_i = emissivity
σ = Stefan-Boltzmann constant
A_i = total surface area of spacecraft
T_E = equilibrium temperature of the spacecraft

Finally, the transient temperature can be found by integrating the following relationship

$$\frac{dT}{dt} = \frac{T_E^4 - T^4}{4\tau T_E} \tag{G.4}$$

dT/dt = rate of temperature change
T = spacecraft transient temperature
t = time

When integrated, the following expression is generated which can be iterated to find the final temperature (T2) knowing the initial temperature (T1) and the time interval (Δt).

$$\Delta t = 2\left[\ln\left(\frac{T_2 - T_E}{T_2 + T_E}\right) - 2\tan^{-1}\left(\frac{T_2}{T_E}\right) - \ln\left(\frac{T_1 - T_E}{T_1 + T_E}\right) + 2\tan^{-1}\left(\frac{T_1}{T_E}\right)\right] \tag{G.5}$$

3. To evaluate the thermal loading due to the solar sail, the following equations are used:

$$F_{ij} = \frac{1 + \frac{r_j}{r_i} - \left[1 + \left(\frac{r_j}{r_i}\right)^2\right]^{\frac{1}{2}}}{2} - \frac{1 + \frac{r_p}{r_i} - \left[1 + \left(\frac{r_p}{r_i}\right)^2\right]^{\frac{1}{2}}}{2} \tag{G.6}$$

F_{ij} = shape factor of sail to s/c
r_j = 13 m = distance from sail to front of s/c
r_i = 1.32 m = radius of rigid portion of sail

r_p = 3 m = distance from sail to aft end of s/c

F_{ij} = 0.138

4. For the thermal analysis of the landers on the surface they will be approximated as spheres divided vertically by insulation. One portion will contain the scientific instrumentation at a temperature of T_i and the other portion containing the RTGs at a temperature of T_r. During the Mercury night the thermal balance for instruments portion of the lander is as follows:

$$Q_i + R + \frac{\alpha_L \varepsilon_m \sigma A_i T_m^4}{2} = \varepsilon_L \sigma A_i T_i^4 \qquad \text{(G.7)}$$

Q_i = load from instruments = 200 W
R = flux from RTG portion
α_L = absorptivity of lander = 0.077
ε_m = emissivity of regolith = 0.9
σ = 5.87E-06
A_i = surface area of instrument portion of lander = $4\pi r^2 - 2\pi rh$ = 6.44 m^2
r = radius of lander = 0.75
h = width of RTG section = 0.133
T_m = temperature of regolith
ε_L = emissivity of lander = 0.79
T_i = temperature of lander = 288 K

To maintain a T_i temperature of 288 K the following Rs are required

Sunset T_m = 250 K
R = 1659 W

Sunrise T_m = 90 K
R = 1711 W

The thermal balance for the RTG portion of the lander during the Mercury night will be

$$Q_r + \frac{\alpha_L \varepsilon_m \sigma A_r T_m^4}{2} = R + \varepsilon_L \sigma A_r T_r^4 \qquad \text{(G.8)}$$

Q_r = load from RTGs = 2800 W

A_r = surface area of RTG portion of lander = $2\pi rh$ = 0.626 m^2
T_m = temperature of regolith
R = flux to scientific instrument section
T_r = temperature of RTG section of layer

At sunset with T_m = 250 K and R = 1659 W, T_r = 449.6 K

At sunrise with T_m = 90 K and R = 1711 W, T_r = 443.9 K

During the Mercury day the thermal balance for the instrument portion of the lander is

$$Q_i + R + \alpha_L \varepsilon_m \sigma A_i T_m^4 + \alpha_L \phi A_i = \varepsilon_L \sigma A_i T_i^4 \qquad \text{(G.9)}$$

Q_i = load from scientific instruments = 200 W
ϕ = solar flux = 9000 W/m^2
A_i = incident area of instrument portion of landers = 1.77 m^2

By setting R to a minimal value of 4.5 W, setting T_i at 574.1 its maximum of 303 K and solving for T_m, it can be seen that the landers can withstand a maximum surface temperature of T_m = 530 K = 257 °C.

The thermal balance for the RTG section of the landers during the Mercury day will be

$$Q_r + \alpha_L \varepsilon_m \sigma A_r T_m^4 + \alpha_L \phi A_{ri} = \varepsilon_L \sigma A_r T_r^4 + R \qquad \text{(G.10)}$$

where A_{ri} = incident area of RTG portion of lander at the surface temperature of 530 K found to be the maximum.

T_m = 530 K
T_r = 577 K

The minimum value for R can be found in the equation

$$R = K\frac{dT}{dx}A \qquad \text{(G.11)}$$

K = conductivity of insulation between the RTG and instrument section = 0.00029 W/mK
dT = temperature difference between the two sections = 57 K - 303 K = 274 K
dx = thickness of the insulation = 0.01 m
A = cross-sectional area of contact between the two sections = 0.57 m^2
R = 4.5 W

5. To evaluate the thermal loading during lander entry the following equations were used:

The atmosphere is primarily helium.
Entry velocity is between 2000 and 3000 m/s
p = 10^{-12} millibar
Temperature is between -183° C and 450° C
Assume spherical geometry with diameter of 1.5 m

To determine if gas is rarefied, check Knudsen number:

$$K_n = \frac{l}{\sqrt{2}L\pi d^2 n} \qquad \text{(G.11)}$$

d = 2e-10 m
n = molecules/m^3 = ρ/μ
m = 7e-27 kg

$$\rho = \frac{P}{RT} = \frac{10^{-10}N/m^2}{(2079)723K} = 6.7x10^{-17}kg/m^3$$

$\therefore$ n≈1010 molecules/m3

$$\therefore K_n \approx \frac{6x10^8}{1.5} = 4x10^8$$

Flow is rarefied if K_n>0.1 and "free molecular" for K_n>1

Appendix H: Scientific Instruments

MAPPING

The Narrow Angle Camera (NAC) at 10 km maps a 122 m x 122 m square element. However, Rosetta only uses 81.85% of this element, probably due to the curvature of the comet. To meet $\Delta\lambda$ requirements, Firefly will use an 85% effective element area for the Wide Angle Camera (WAC) and an 81.85% effective area for the NAC.

From a 500 km orbit, the WAC will map a 20.774 km x 20.774 km element, and the NAC will map a 5 km x 5 km element. The corresponding resolution for these cameras are 20.774 m/pixel and 5 m/pixel, respectively. Figure H.1 shows the dimensions for the WAC and NAC mapping elements.

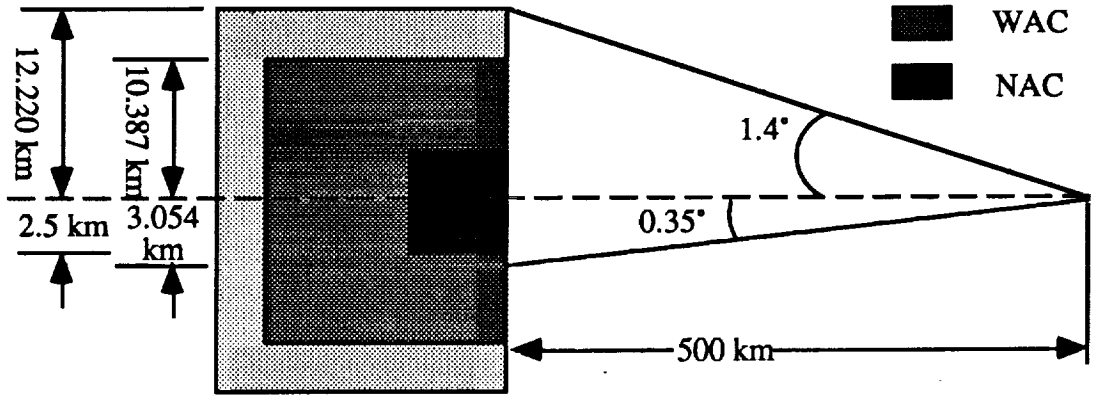

Figure H.1. Mapping Area Diagram for WAC and NAC at 500 km Altitude

Mercury rotates once every 58.65 Earth days. Since the radius is 2439 km, Mercury moves through 15324.689 km at the equator in one Mercury day. This means that the surface velocity at the equator is 3.0242e-3 km/s. Assuming $R\omega=V$, then ω = 1.2399e-6 rad/s. The period of Firefly is defined by

$$T = 2\pi\sqrt{\frac{a^3}{\mu}} \tag{H.1}$$

where a = 2939 km and μ = 2.232e4 km^3/m^2. The displacement of the surface relative to each pass of Firefly, $\Delta\lambda$, can be found

$$\Delta\lambda = \omega T = \omega(2\pi)\sqrt{\frac{a^3}{\mu}} \tag{H.2}$$

Figure H.2 represents the definition of $\Delta\lambda$ corresponding to two consecutive orbits.

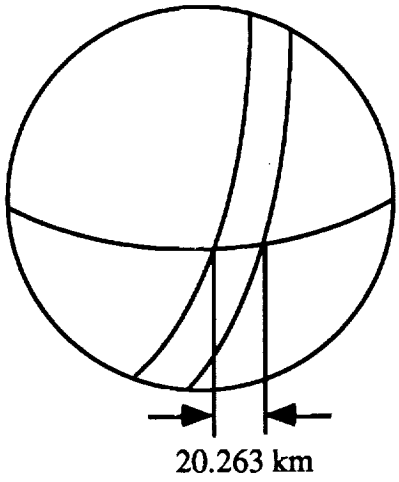

Figure H.2. Surface Displacement for Two Consecutive Orbits at 500 km.

Since the WAC element is 20.774 km x 20.774 km, there will be a minimum overlapping area of 500 m per orbit. The number of passes required to map Mercury can be determined by dividing 2π by $\Delta\lambda$

$$2\pi/\Delta\lambda = 756.242 \text{ passes}$$

Since Firefly will be mapping continually during its orbit, the required time for mapping can be halved. This will result in a required global mapping time of 29 days, 7 hours, and 50 minutes. The duration of the detailed mapping phase is dependent on the location of the four candidate sites at the onset of this phase.

EXTENDIBLE SAMPLER ARM REQUIREMENTS

For successful sampling operations, the sampler arm must be able to gather regolith samples when the extendible positioning system (EPS) is at its maximum. Each EPS boom is mounted 0.347 m radially in from the edge of the lander, and 0.347 m above the lander base platform. Figure H.3 illustrates the EPS configuration.

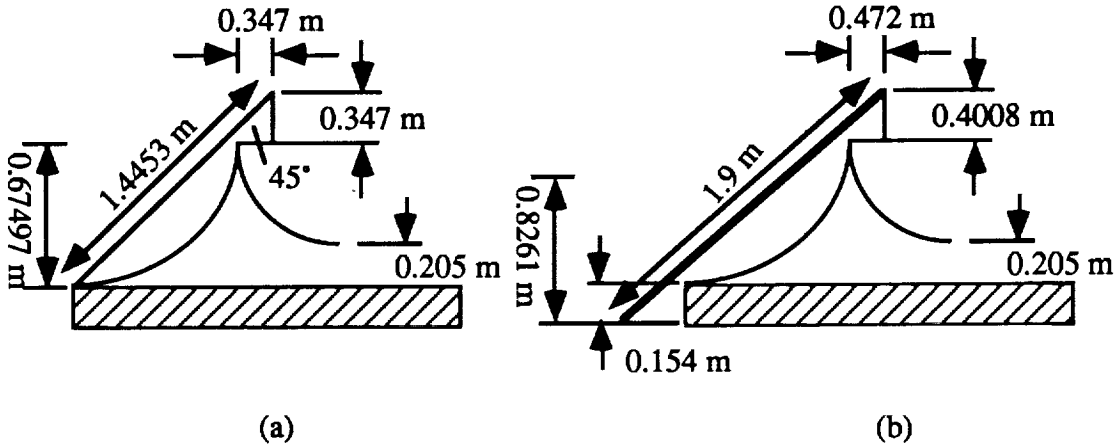

Figure H.3. Extendible Boom Dimensions - (a) Extendible Positioning System (EPS) in maximum configuration; (b) Surface sampler arm in maximum configuration

The EPS configuration will allow a maximum angular displacement of 45° from the horizontal plane. In this position, the EPS will be able to support the lander 0.205 m above the surface, assuming it is level.

The surface sampler arm is mounted 0.472 m from the edge of the lander and 0.4008 m above the lander base platform. The arm is shown fully extended in Figure H.3(b). It is capable of a 40.3° angular displacement from the horizontal plane, allowing subsurface sampling.

Volume II

Project Arma: Mission to the Moons of Mars (Phobos and Deimos)

The Pennsylvania State University

Department of Aerospace Engineering

MISSION TO THE MOONS OF MARS — PHOBOS AND DEIMOS

(Project Arma)

by

Christopher Calhoun, Robert Colbert, Matthew Cummings, Jeffrey Foley, Michael Gallagher, Christopher Giersch, Kelly Jandrisovits, Jeffrey Keller, Thomas Klein, Andrew Loser, Chad McFarland, Kent Mitterer, Dan Mouer, Simon Nagel, Larry Scislowicz, Brock Spigelmyer, Brian Wanger, Wendy Zeitz

July 1993

Table of Contents

List of Figures

List of Tables

1.0 Introduction

Very little is known about the moons of Mars; Phobos and Deimos. Many previous missions to Mars have primarily focused on retrieving information about Mars with little information regarding the moons. Some of these missions include Viking, Mariner 9, and the recently launched Mars Observer. Of all the missions to the Mars system, only one has focused on Phobos. This mission was performed by the former Soviet Union which launched two satellites, Phobos-1 and Phobos-2, to study the moon. Unfortunately, contact with Phobos-1 was lost during interplanetary transfer, and contact with Phobos-2 was lost shortly after Mars capture. With Mars being a destination for future manned missions, propellant and other raw materials will be needed. If Phobos and Deimos have oxygen and hydrogen as expected, propellant for return trips to Earth can be extracted from the two moons [1]. Thus, a scientific mission to Phobos and Deimos (Project Arma) has been developed to analyze regolith and other moon properties, which may be of concern for future manned missions.

The primary goal of Project Arma is to perform an in-situ analysis of each moon's regolith. Other goals of Project Arma include: (1) achieving a better understanding of the geology, geophysics, and climatology of the moons [2]; (2) shedding light on the origin and early history of the moons and the solar system [3]; (3) achieving a more accurate determination of their orbital characteristics; (4) obtaining a better understanding of the interactions between the moons and the solar wind [4]; and (5) studying the effects of one complete solar cycle in the absence of an atmosphere.

Project Arma will be launched on a Proton rocket in the year 2010. The spacecraft consists of one orbiter, one lander per moon, and one penetrator. Upon arrival at the Mars system, an aerobraking maneuver will be implemented to slow the spacecraft and place it in an orbit about Mars. After capture into a Martian orbit, the orbiter will transfer to Deimos, map its surface, and perform other regolith analyses from orbit. When the orbiter finishes its mapping and regolith analysis of Deimos, the orbiter will release the first lander to the

surface. The orbiter, second lander, and penetrator, will then transfer to an orbit about Phobos.

At Phobos, the orbiter will map and perform regolith analysis. Upon completion, the orbiter will release the second lander and the penetrator to Phobos' surface. The orbiter will then transfer to a final parking orbit between Phobos and Deimos. From the parking orbit, the orbiter will perform long term measurements of the Martian system and act as a communications link between the landing packages (landers and penetrator) and Earth. The mission scenario is depicted in Figure 1.1.

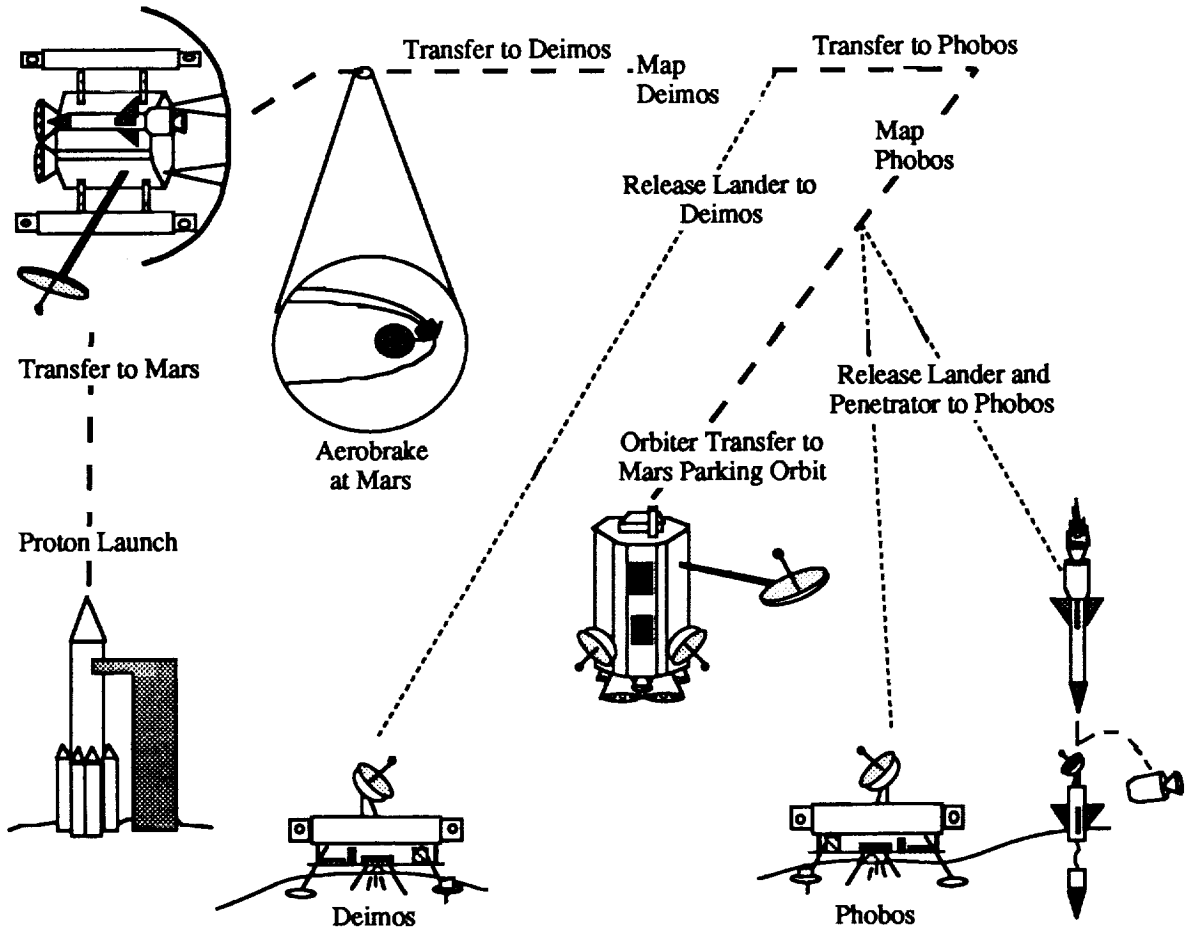

Figure 1.1. Project Arma Mission Scenario

2.0 Structures

2.1 Introduction

Selection of materials for the orbiter and landers is broken down into three distinct categories. The first category, Support Structure, consists of the materials which are used as support between the subsystems of the spacecraft as well as the internal and external framework. These structures include struts, tubing, and panels. The bulk of the spacecraft is formed by these structures that enclose and support the scientific instrument packages located inside the body of the orbiter and landers.

The Appendages category contains the materials which will be used as booms. Scientific instruments, RTGs, and the communications systems will be mounted on these booms for use away from the main body of the spacecraft.

The final category, Thrust Structure, consists of the materials which are used for the absorption of the thrust loads. These loads are experienced during the launch of the Proton rocket which places the spacecraft directly on a transfer orbit to Mars. The structures which fall into this category includes the thrust cones and their supporting rings. Also included in this category will be the material used for the propellant tanks.

In addition, the materials chosen for each of the structures in the three categories must be able to withstand the launch loads as well as protect the scientific instruments during launch. Research was also conducted on the materials to be used for the aerobraking shroud. This topic is discussed in its own section. The materials for the penetrator were also chosen. Also, a study was done on the effects of the high velocity impact including the effects of cratering and predictions of penetration depth. The placement of subsystem components in the spacecraft was also investigated for structural reasons and to ensure that the components would meet their operating requirements.

2.2 Orbiter and Lander Material Attributes

Table 2.1 lists the materials and their properties which will be studied for use in the various components of the landers and the orbiter. The selection of which material will used for each individual structure will be discussed in its own section.

Table 2.1. Material Properties (Agrawal, Brij, N. Design of Geosynchronous Spacecraft, Prentice-Hall, Inc., Englewood Cliffs, NJ, 1986., p.245)

Material	Density ($Kg/m^3 \times 10^3$)	Long. Ult. Str. ($Nm/Kg \times 10^3$)	Young's Modulus ($N/m^2 \times 10^9$)	Specific Stiffness ($Nm/Kg \times 10^3$)	Thermal Expansion (1×10^{-6} / K)
Al 6061-T6	2.71	106.8	67	24.9	23.4
Al 2014-T6	2.8	157.6	72	25.9	22.51
Beryllium					
Extrusion	1.85	335.4	293	158.4	11.5
Sheet	1.85	242.2	293	158.4	11.5
Wrought		150.6	293	160.1	11.5
Lockalloy Be 38% Al	2.1		186	88.6	11.5
Boron Epoxy [0]	2.01	665.4	206	102.9	4.2
Graphite/Epoxy [0] UHM	1.69	367.1	289	171.3	-1
Graphite / Epoxy [0] Vf 55%	1.49	897.6	151	101.7	-0.36
Kevlar 49 [0]	1.38	999.06	75	54.9	-4

[0] denotes 0 degree fiber orientation

Table 2.2 lists the attributes for the materials that are being studied for use in the lander and orbiter components. These material attributes were considered for the trade studies .

Table 2.2. Material Attributes

Material	Advantages	Disadvantages	Uses
Aluminum	- Low cost - Low natural frequency	- Low specific stiffness - Low modulus of elasticity	- Panels
Beryllium	- High specific stiffness - High strength	- Brittle and notch sensitive - Toxic - Cost	- Panels - Appendages - Thrust Cone - Rings
Beryllium/ Lockalloy	- Ductility of Al w/ high strength of Be - High temp. applications - Low density	- Cost	- Panels
Boron/ Aluminum	- High strength after buckling - High Modulus	- High density	- Struts & Tubes
Boron/ Epoxy	- Low density - High Modulus - High specific stiffness	- Difficult to machine	- Struts & Tubes
Graphite/ Epoxy	- Low thermal - High Strength - High specific stiffness	- Average Modulus	- Struts & Tubes - Appendages - Thrust Cone - Rings
Kevlar 49	- Good strength, weight, toughness - Low thermal expansion - Damage tolerance	- Low compression strength	- Struts & tubes - Areas of possible space debris damage
Titanium	- Good thermal compatibility w/ Be and graphite/epoxy	- Difficult to machine - Poor fracture toughness	- Rings

Cost is important in selecting any material. Spacecraft materials are often expensive due to their specialized nature. Perhaps the least expensive of the materials being considered is aluminum which costs about $0.60 per pound [6]. This is the cost for the aluminum itself and does not take into account the costs of fabricating the components. Estimated raw material costs of some of the other more advanced materials are as follows: Beryllium $900-2200/lb. [6] , Graphite / Epoxy $45/lb. [7], and Titanium $25/lb [6].

2.3 Material Selection Trade Studies

The following equation is used all the trade studies used for selection of orbiter and lander materials:

$$J = K_1*(Cost) - K_2*(Properties) + K_3*(Manufacture) \quad (2.1)$$

The cost was considered to be the most important factor in selecting a material so K_1 was set to 5. Desirable properties was considered the second most important attribute so K_2 was set to 4. Manufacture was considered to be the ease of fabrication and was considered to be the least important factor and was set to 2 which is K_3.

2.4 Materials for Support Structure

2.4.1 Struts & Tubes for Orbiter and Landers

The struts and tubes are designed to provide support to the internal framework of the spacecraft. The materials are chosen to withstand buckling stresses. Design criteria also include light weight and a high unidirectional strength/mass ratio. The trade study for the materials being considered for these components are listed in Table 2.3.

Table 2.3. Struts & Tubes Trade Study

Material	Cost	Properties	Manufacture	J
Boron/Epoxy	3	2	5	17
Graphite/Epoxy	3	4	2	3
Kevlar 49	4	3	4	16
Boron/Al	3	4	3	5

From this trade study it was found that graphite/epoxy was the best material to be used as for the struts & tubes. Graphite/epoxy is easily shaped, has a high specific stiffness and ultimate strength, and a low thermal expansion coefficient.

2.4.2 Panels for Orbiter and Lander

The panels are used to support the subsystem components. They are designed to have low natural frequencies. This is to ensure that vibrations are not transmitted along the spacecraft body where they could interfere with the operation of certain scientific instruments which are sensitive to this phenomenon. Also, electrical and thermal conductivity are an important consideration. Electrical conductivity is a concern since the accumulation of charge on the body of the spacecraft may damage the on-board instrumentation. Thermal conductivity, in the same regard, is an important subject since some scientific instruments are vulnerable to excess heat. Table 2.4 shows the material trade study done for the panels.

Table 2.4. Trade Study for Panels

Material	Cost	Properties	Manufacture	J
Al 6061 T6	1	2	1	-1
Al 2014 T6	1	3	1	-5
Beryllium				
Sheet	5	5	5	15
Wrought	5	5	5	15
Lockalloy Be 38% Al	5	4	5	19

Thus from the trade study it was found that Aluminum 6061-T6 proved to be the best material to be used as the panels. Aluminum is relatively inexpensive and has been a primary material used for past space missions.

2.5 Materials for Appendages for Orbiter and Lander

Appendages are generally designed with high stiffness materials, required for the high pointing accuracies of the antenna structure and other scientific instruments. They allow little deflection in the booms, even at the ends, an thus provide a stable platform for the antenna and other instruments. These materials allow the appendages to be deployed with little interaction between vibrations and the attitude control system. In addition, low thermal distortion is required by the antenna structure and other scientific instruments in order to achieve high pointing accuracies. Table 2.5 shows the trade study done for the appendages.

Table 2.5. Appendage Trade Study

Material	Cost	Properties	Manufacture	J
Beryllium				
Sheet	5	3	5	23
Wrought	5	4	5	19
Extrusion	5	3	5	23
Graphite/Epoxy UHM	2	5	3	-4

Graphite/Epoxy UHM was found to be by far the best material to be used as appendages. This material has a very high specific stiffness and a low coefficient of thermal expansion making it a perfect choice as a material for booms.

2.6 Materials for Thrust Structure

2.6.1 Thrust Cone for Orbiter

The thrust cone forms the center of the structure of the spacecraft. Materials for this component are designed to withstand the axial compressive loads and bending moments

caused by the firing of the booster rocket. They are also chosen to avoid buckling in the thrust cone shells. Graphite/Epoxy [0] Vf 55% was chosen for this application due to its high ultimate strength, high specific stiffness and low thermal expansion.

2.6.2 Rings

The rings are the supporting structures for the thrust cone. They are required to have a high strength and are designed to be thermally compatible with the materials used for the thrust cones. Titanium is usually used with thrust cones made of graphite/epoxy [5]. Titanium is used due to its thermal compatibility with these materials as well as its high strength.

2.6.3 Propellant Tanks

The propellant tanks must be constructed of a material that is temperature resistant, and able to withstand the low temperatures of cryogenic propellants, as well as being resistant to corrosion. It must also be able to withstand the pressures created by the propellant and be relatively lightweight. The material selected, that fulfills those requirements, was stainless steel with a glass coated interior for corrosion resistance.

2.7 Aerobraking Shroud

Three materials were considered for use as the primary heat absorbing material of the aerobraking shroud. These materials were (1) ceramic tiles, (2) carbon/carbon composites, and (3) ablative materials.

Ceramic tiles are currently in use as the heat shields for Space Shuttles. They have been proven to work through numerous missions and are tough enough to be reused multiple times (an asset that is not important to this mission, however, since the aerobraking maneuver will be performed only once and then the shroud will be jettisoned). In the future, it is predicted that ceramic tiles will be able to withstand temperatures of up to 3500° F [8].

Carbon/carbon composites exhibit a high resistance to thermal shock, are relatively tough, and provide uniform and predictable thermal insulation. They can also be reinforced with plies of Kevlar for damage resistance to space debris. However, the main disadvantage of carbon/carbon composite is their high cost [9].

The ablative materials are the materials which have been used as spacecraft heat shields many times in the past. They absorb heating loads by charring and evaporating off the surface of the heat shield. Ablative heat shields were used on the Apollo missions and the materials used on them are still state of the art in the ablative category. A trade study was performed to choose a material for the aerobraking shroud according to the equation below:

$$J = K_1*(Cost) - K_2*(Performance) - K_3*(Experience) \quad (2.2)$$

Cost was decided to be most important therefore, K_1 was given a value of 5. The value of K_2 for performance was set to 2 since the shroud only needed to be used once and would not be subjected to the heating load of a full re-entry. Experience, or the relative number of times the material has been used in the past, was considered to be important and was set to 4. It was felt that since aerobraking is a new technique greater success could be obtained with a material that exhibits the most predictable and studied behavior. Table 2.6 below, shows the results of this trade study.

Table 2.6. Aerobraking Shroud Material Trade Study

Material	Cost	Performance	Experience	J
Ceramic Tiles	3	4	4	-9
Carbon/Carbon	5	5	2	7
Ablative	2	2	5	-14

The ablative materials were found to have the lowest trade value. They are relatively inexpensive to make and have been used with acceptable safety for numerous years on previous space flight missions. For these reasons ablative materials were chosen for use as the heat absorbing surface of the aerobraking shroud.

2.8 Penetrator

2.8.1 Penetrator Tip Material

Depleted uranium was chosen as the primary impacting material for use in the tip of the penetrator because it exhibits an extremely high density, allowing for a high concentration of mass in a small area. Since the mass of the projectile is directly proportional to penetration depth upon impact this is a valuable attribute. Depleted uranium has been used in armor-piercing and ballistic ordnance applications. Figure 2.1 shows the dimensions for the penetrator tip. Appendix A presents calculations for the mass of the penetrator tip with the dimensions from Figure 2.1. Table 2.7 shows some of the properties of depleted uranium.

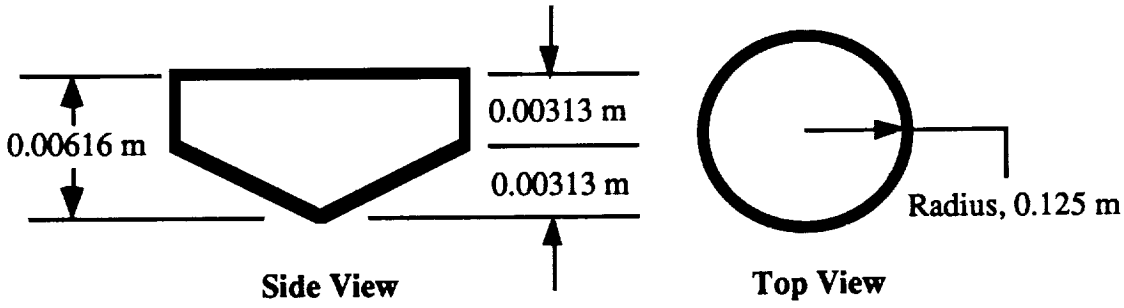

Figure 2.1. Depleted Uranium Tip Dimensions

Table 2.7. Properties of Depleted Uranium (Metals Handbook, American Society for Metals, Columbus, Ohio, 1990, pp. 20,35)

Density (Mg/m3)	19
Melting Point (°C)	1130
Hardness (HBR)	50 - 100

The body of the penetrator will be made of boron/aluminum due to its high strength after buckling. This is an important attribute since after impact the body of the penetrator will have to withstand considerable buckling stresses.

2.8.2 Penetrator Impact Crater

Upon impacting with the surface of Phobos the penetrator will most likely form a small conical crater. The conical shape of the crater will be created by compression waves that are formed during impact. The communications package of the penetrator must come to rest on the surface of the crater so that there will be no interference with the signal of the low gain antenna. For this reason the communications package has been fitted with an inhibitor so that it will rest on top of the crater. The inhibitor will be made of Kevlar 49 since this material is known for its damage tolerance through a cushioning effect.. This is important since the a great deal of the impact must be withstood by the inhibitor to allow it to arrest the descent of the upper portion of the penetrator. Figure 2.2 shows the resting configuration of the penetrator on the surface of Phobos.

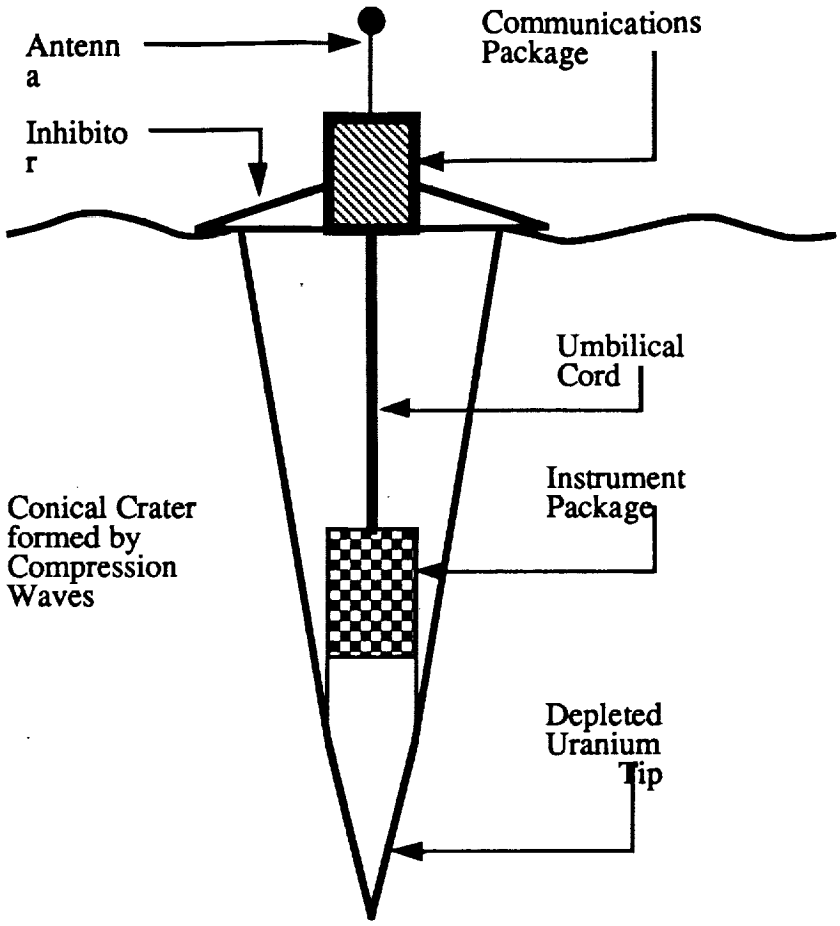

Figure 2.2. Resting Configuration of Phobos Penetrator

2.8.3 Penetration Depth

It was desired that a penetration depth of approximately three meters was to be obtained by the penetrator. To estimate the impact velocity required to achieve this depth (with the given mass of the depleted uranium tip), the Herrman Jones Logarithmic Penetration Law was utilized. These predictions were based entirely on the mass of the depleted uranium tip without taking into account the mass of the other impacting structures. Also, the hardness of the surface of Phobos was estimated from the assumption that the surface was composed primarily of fragmentary rock with the underlying core only

approximately twice the density of water. The details of these calculations are shown in Appendix A. Table 2.8, below, shows the resulting velocity required to achieve a three meter surface penetration of Phobos:

Table 2.8. Penetration Calculation Results

Penetration Depth (m)	3
Projectile Mass (kg)	3.044
Penetration Velocity (m/s)	675

2.9 Spacecraft Configuration

2.9.1 Introduction

The placement of all the subsystem components presented a challenging task for various structural reasons, such as easy accessibility, size, frequency response, weight, shape, radiation, and individual instrument requirements. In order to properly place all of the components, research was completed to produce the preliminary arrangement of the various scientific instruments, antennas, GN&C components, RTGs, Command and Data Handling (C&DH), and thermal control packages to present drawings of the spacecraft's configuration. Figures 2.3, 2.4 and 2.5 illustrate the three-dimensional views of the orbiter, lander and penetrator, respectively, for Project Arma's spacecraft using the IDEAS 3-D solid modeling computer program. A more detailed discussion of the instruments' placement is presented next.

2.9.2 Orbiter

Several components will be placed on the orbiter's 5 booms to satisfy operating requirements (see Figure 2.3 for the three-dimensional view of the orbiter). For example, both Radioisotope Thermoelectric Generators (RTGs) will be placed on separate booms, on opposite sides of the spacecraft, to protect the spacecraft from their generated heat. The High-Gain Antenna (HGA) will be on its own boom, unobstructed, to achieve the best communication performance back to Earth. This boom will be allowed to rotate to obtain the best pointing accuracy. It will also be stowed during launch and the aerobraking maneuver, and deployed while in transit to Mars.

Finally, many scientific instruments will also be located on booms, such as the radar sounder and the magnetometer (one boom); plus the Gamma-Ray Spectrometer (GRS) and the near-infrared mapping spectrometer's telescope (on a separate boom). One primary reason for using booms is to prevent the orbiter's materials from interfering with the instruments' measurements in addition to protecting the rest of the spacecraft from harmful radiation generated by these instruments.

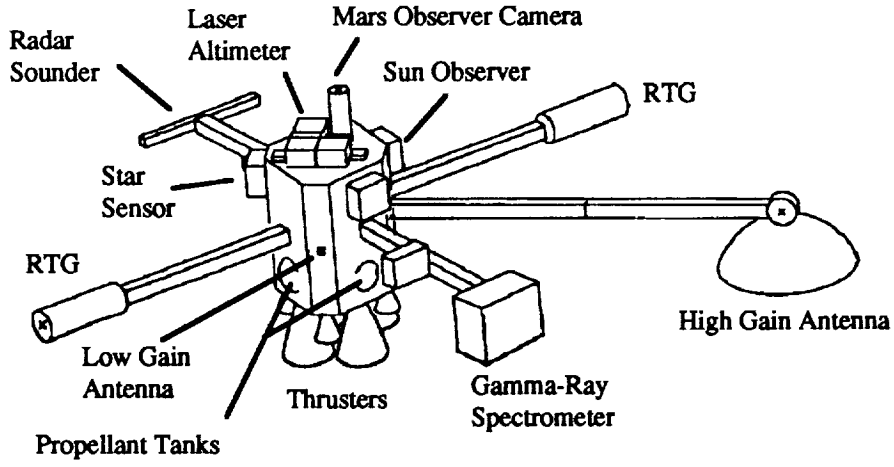

Figure 2.3. Three-Dimensional View of the Arma Orbiter

Several components need to be placed towards the top of the spacecraft to permit the following: sensing and correcting navigation of the spacecraft's position relative to the moons, taking pictures/ground sciences, and performing topographical mapping, as well as other experiments. Instruments including the retarding potential analyzer, gravity gradiometer, Mars Observer Camera (MOC), laser altimeter, DION (mass spectrometry of secondary ions), both sun sensors, and the mass spectrometer's sensors and laser are positioned here.

The components of the C&DH subsystem (computers and data storage recorders) will be located in the center of the spacecraft to shield them against harmful radiation, which degrades their memory levels. Their interfacing wire bundles will also be packed closely to these components to save weight [11].

Both of the orbiter's low-gain, parabolic antennas will be placed on opposite sides of the spacecraft to achieve the most coverage for communication links. Also, their electronic equipment (transponders, a filter and a waveguide), in addition to other electronic equipment from other instruments, will be positioned somewhat close to the antennas towards the bottom of the orbiter to minimize wire lengths and simplify component interfaces, which will ultimately reduce the overall weight and cost [11].

The four propellant tanks will be located in the bottom corners to preserve some symmetry (thus also helping to reduce some of the overall weight) about the orbiter.

For placement of the GN&C components, each of the principal axes will have at least two smaller thrusters for control, while the base of the spacecraft will have a larger array of thrusters (primary and secondary) to provide greater thrust for tangential orbital maneuvers. The reaction wheels will be placed orthogonally for three-axis control while a fourth wheel will be placed on a skewed axis in a backup mode. The three Sun sensors will be placed 120° apart, while the star sensors will be approximately 180° apart to provide accurate tracking during any maneuvers.

Most of the thermal control components (heat sinks, pipes, and louvers, etc.) will be positioned in surrounding structural skin panels with stiffeners to help control the spacecraft's temperature variations [11].

2.9.3 Lander

Figure 2.4 illustrates the three-dimensional view of the lander. Many instruments need to be placed on the top of the landers. For example, the low-gain antenna will be located directly on the top of the spacecraft to achieve the maximum coverage. Also, both panoramic cameras will be positioned on opposite sides of the lander to obtain pictures of the moons' surfaces. The lander's wide-angle camera will be placed out on a boom so it will not interfere with the low-gain antenna's coverage. The boom will rotate allowing the camera to take pictures of Mars for one complete solar cycle. All of the antenna's equipment (both transponders, a filter, and a waveguide) will be positioned in close proximity to the dish in order to reduce the length of the electric cables, thus reducing the overall weight.

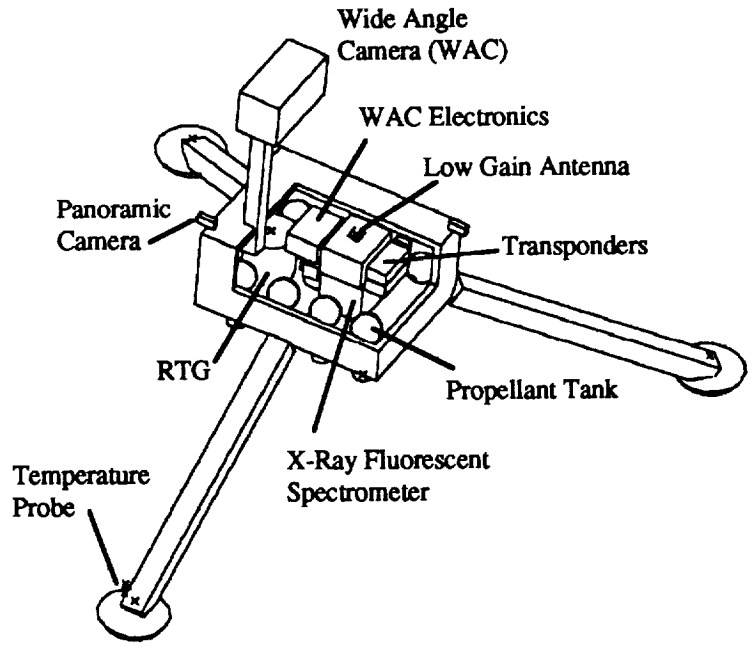

Figure 2.4. Three-Dimensional View of an Arma Lander

As with the orbiter, the C&DH package (computer and data storage recorder) will be located in the center of the lander to shield it from harmful thermal radiation [11].

For GN&C components, the 4 roll control thrusters will be placed on opposite sides of the lander, while the 3 groups of 4 small thrusters will be placed 120° apart on each leg for attitude control to the moons' surfaces.

Each lander will have an RTG for its power supply, which will be placed in a back corner, as far away from the other instruments as possible, to protect them from the RTGs heat fluxes.

The seismometer, X-ray fluorescent spectrometer, and radiation detector instruments will be placed on an experiment platform, located at the bottom of each lander, so that they are near the surface. This platform will be deployed from a bay in the bottom of the lander.

For the propulsion system, seven propellant tanks will be placed on the perimeter of the lander, close to the thrusters.

Lastly, the temperature probe will be positioned on one of the foot pads so that it just slightly protrudes into the top layer of the moons' surface to record accurate temperature readings and variations. Also, its electronic converter will be located on the top of the leg, close to the probe in order to reduce losses and the data inaccuracies from the shorter length of the electronic lines.

2.9.4 Penetrator

A Solid Rocket Thruster (SRT) will be placed at the top of the penetrator to launch it toward Phobos. During penetration, the SRT will be detached in order to expose the low-gain antenna. Directly underneath the antenna will be two transponders, a filter and waveguide, in order to keep the interfacing wire lengths to a minimum. This will, again, reduce the overall weight of the penetrator.

The battery was placed in between the waveguide and the C&DH computer so it could be close to all the equipment to which it will supply power. The computer will again be located towards the middle of the penetrator to protect it from harmful radiation.

The last instrument, the X-Ray Fluorescent Spectrometer (XRFS), was positioned at the bottom of the penetrator. After the penetrator embeds itself into the moon's surface, a panel will open to expose the XRFS to the moon's inner composition, thus allowing it to perform experiments.

Finally, four small thrusters will be placed on all four sides of the penetrator to provide guidance control during the descent towards Phobos. Figure 2.5 illustrates the Phobos penetrator.

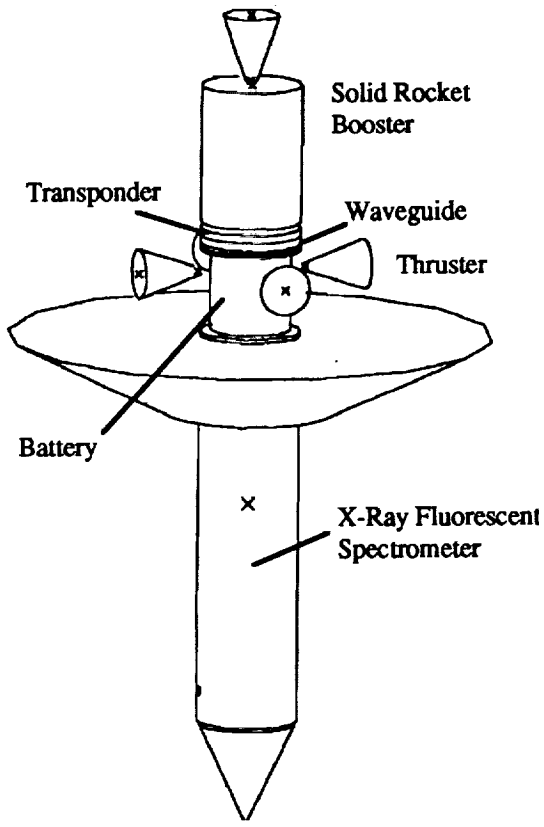

Figure 2.5. Three-Dimensional View of the Phobos Penetrator

3.0 Power Subsystem

3.1 Power Requirements

By means of a trade study, the Modular Radioisotope Thermoelectric Generator (MOD-RTG) was selected to power the orbiter and each of the two mission landers. A lithium thionyl chloride primary battery will power the penetrator. These selections were based on the peak power requirements of the four spacecraft, as well as requirements for minimal cost, risk, and complexity and maximal performance. A breakdown of the power requirements for each spacecraft follows.

3.1.1 Lander Power Requirements

Listings of the lander power requirements are provided in Tables 3.1 and 3.2. The beginning of life peak power requirements for the Phobos and Deimos landers are 98 W and 80 W, respectively. The GNC and propulsion subsystems will operate only prior to landing, and the XRFSs and panoramic cameras will operate for only a short time following landing. Minus these subsystems and instruments, the end of life requirements for the Phobos and Deimos landers are 63 W and 45 W, respectively. A design margin of 10% was included to allow for additional requirements including thermal control and regulation, distribution, and control of power.

3.1.2 Orbiter Power Requirements

The orbiter's power requirements are divided into three mission phases: transit, orbit about the moons, and orbit about Mars. The "transit" phase is comprised of all periods when the spacecraft is not in orbit about either of the moons or Mars. The requirements for the phases are similar to each other and only contain differences in the number and type of operational scientific instruments; in addition, the horizon sensor will only be operational during the "orbiting moons" phase. The maximum power requirement is 657 W and occurs

during the orbiting of the moons. Tables 3.3 through 3.5 list the requirements for each of the phases. A design margin of 10% was added to allow for additional requirements.

Table 3.1. Power Requirements for the Phobos Lander

Equipment	Power (W)
COMMUNICATIONS	
Low-Gain Antenna	15
COMMAND & DATA HANDLING	
Computer	6.6
Data Storage Unit	3
SCIENTIFIC INSTRUMENTS	
Seismometer	10
Temperature Probe with Converter	1
Radiation Detector	5
X-Ray Fluorescence Spectrometer (XRFS)	10
Wide Angle Camera	16.3
Panoramic Cameras (2)	2
GNC & PROPULSION	
Cold Gas Thrusters	20
BOL SUBTOTAL	88.9
	Add 10% Margin
BOL TOTAL	98.0
EOL SUBTOTAL	40.6
	Add 10% Margin
EOL TOTAL	45.0

Table 3.2. Power Requirements for Deimos Lander

Equipment	Power (W)
COMMUNICATIONS	
Low-Gain Antenna	15
COMMAND & DATA HANDLING	
Computer	6.6
Data Storage Unit	3
SCIENTIFIC INSTRUMENTS	
Seismometer	10
Temperature Probe with Converter	1
Radiation Detector	5
X-Ray Fluorescence Spectrometer (XRFS)	10
Panoramic Cameras (2)	2
GNC & PROPULSION	
Cold Gas Thrusters	20
BOL SUBTOTAL	72.6
	Add 10% Margin
BOL TOTAL	80
EOL SUBTOTAL	40.6
	Add 10% Margin
EOL TOTAL	45

Table 3.3. Power Requirements for Orbiter "Transit"

Equipment	Power (W)
GNC	
Reaction Wheel	100
Inertial Measurement Unit (IMU)	100
Star Sensors (2)	10
Sun Sensors (3)	6
COMMUNICATIONS	
Low-Gain Antennas (2)	3
High-Gain Antenna	45
COMMAND & DATA HANDLING	
Computer	23
Data Storage Units (2)	6
SCIENTIFIC INSTRUMENTS	
Magnetometer	3.1
Near-Infrared Mapping Spectrometer (stand-by)	6
Laser Altimeter (stand-by)	5
PROPULSION	
Thrusters	60
SUBTOTAL	367.1
	Add 10% Margin
TOTAL	404

Table 3.4. Power Requirements for Orbiter "Orbiting Moons"

Equipment	Power (W)
GNC	
Reaction Wheel	100
Inertial Measurement Unit (IMU)	100
Horizon Sensor	5
Star Sensors (2)	10
Sun Sensors (3)	6
COMMUNICATIONS	
Low-Gain Antennas (2)	30
High-Gain Antenna	45
COMMAND & DATA HANDLING	
Computer	23
Data Storage Units (2)	6
SCIENTIFIC INSTRUMENTS	
Radar Sounder	50
Magnetometer	3.1
Gravity Gradiometer	50
Visual Instruments	29.8
Mass Spectrometer	15.01
Near-Infrared Mapping Spectrometer	12
Laser Altimeter	30
Gamma Ray Spectrometer	2
DION	20
PROPULSION	
Thrusters	60
SUBTOTAL	596.91
	Add 10% Margin
TOTAL	657

Table 3.5. Power Requirements for Orbiter "Orbiting Mars"

Equipment	Power (W)
GNC	
Reaction Wheel	100
Inertial Measurement Unit (IMU)	100
Star Sensors (2)	10
Sun Sensors (3)	6
COMMUNICATIONS	
Low-Gain Antennas (2)	30
High-Gain Antenna	45
COMMAND & DATA HANDLING	
Computer	23
Data Storage Units (2)	6
SCIENTIFIC INSTRUMENTS	
Magnetometer	3.1
Near-Infrared Mapping Spectrometer	12
Gravity Gradiometer	50
Retarding Potential Analyzer	4.5
PROPULSION	
Thrusters	60
SUBTOTAL	449.6
	Add 10% Margin
TOTAL	495

3.1.3 Penetrator Power Requirements

Power requirements for the penetrator are listed in Table 3.6. The peak requirement is 42 W including a 10% design margin. The selected power source must operate for approximately two hours and be able to withstand penetrator impact. In addition, the source must fit within the penetrator diameter of 0.25 m.

Table 3.6. Power Requirements for Penetrator

Equipment	Power (W)
COMMUNICATIONS	
Low-Gain Antenna	15
COMMAND & DATA HANDLING	
Computer	6.6
SCIENTIFIC INSTRUMENTS	
X-Ray Fluorescence Spectrometer (XRFS)	8
GNC & PROPULSION	
Solid Rocket	2
Cold Gas Thrusters (4)	4
THERMAL CONTROL	
5% of Total Power Required	1.78
SUBTOTAL	37.38
	Add 10% Margin
TOTAL	42

3.2 Power Source Selection

The only power supplies which satisfy the above requirements for the orbiter and landers are the solar array, General Purpose Heat Source RTG (GPHS-RTG), and the MOD-RTG. Trade studies were conducted to determine the best selections using:

$$J = 2\,(cost) + 3\,(risk) - 3\,(performance) + 1\,(complexity) \qquad (3.1)$$

In this case, complexity refers to the necessity of the added hardware and maneuvers required for solar dependent sources (i.e. batteries and GNC to keep the arrays pointed in the proper direction). Risk applies to the ability of the sources to withstand such harsh conditions as radiation, extreme temperatures, and micrometeoroid collisions. Since the mission is of such long duration (11 years), a harsh operating environment was assumed. Risk also refers to the generation of the technology (i.e. the MOD-RTG has never flown on a

mission, therefore it has a higher risk than the GPHS-RTG). Trade studies and design parameters are provided in the following sections.

The only sources which satisfy the above requirements for the penetrator are the GPHS-RTG, MOD-RTG, solar array, and primary battery. A trade study was not conducted because other restrictions eliminated all but one choice: the primary battery.

3.2.1 Lander Power Source Selection

The trade study parameters and values for each option are provided in Table 3.7. The MOD-RTG was selected primarily because of the proven reliability of past generations of RTGs and their hardness to hazardous space environments. Such performance is required of a source which will operate for 11 years. The RTG power outputs for the Phobos and Deimos landers are 114 W and 95 W, respectively. Design parameters for each RTG are listed in Tables 3.8 and 3.9.

Table 3.7. Lander Trade Study Parameters and Values

	Solar Array	GPHS-RTG	MOD-RTG
Risk	3	1	2
Cost	4	5	3
Performance	3	4	5
Complexity	4	2	2
J	12	3	-1

Although solar arrays are relatively inexpensive, the mass of the required storage batteries (about 100 kg per lander) makes the overall mass of a solar array power system much greater than that of an RTG system. This higher mass would translate to higher cost

due to the required added propellant. Therefore, despite its seemingly high cost, the MOD-RTG is the most cost-effective option.

Table 3.8. Phobos Lander MOD-RTG Design Parameters (Modified from Robert F. Hartman, "Modular RTG Technology Status," General Electric Company, Philadelphia, PA, 1990.)

Load Voltage, Volts	30.8
Power Output, Watts	114
Specific Power, W/kg	7.9
Cold/ Hot Junction Temperature, K	573 / 1273
Converter Efficiency, %	7.5
Waste Heat, W	1380.0
Number of GPHS Modules	6
Number of Multicouples	48
Length, m	0.443
Overall Diameter, m	0.33
Weight, kg	14.43
Cost, dollars	1,938,000

Table 3.9. Deimos Lander MOD-RTG Design Parameters (Modified from Robert F. Hartman, "Modular RTG Technology Status," General Electric Company, Philadelphia, PA, 1990.)

Load Voltage, Volts	30.8
Power Output, Watts	95
Specific Power, W/kg	7.9
Cold/ Hot Junction Temperature, K	573 / 1273
Converter Efficiency, %	7.5
Waste Heat, W	1150.0
Number of GPHS Modules	5
Number of Multicouples	40
Length, m	0.390
Overall Diameter, m	0.33
Weight, kg	12.03
Cost, dollars	1,615,000

3.2.2 Orbiter Power Source Selection

The results of the trade study conducted for the orbiter are provided in Table 3.10.

Table 3.10. Orbiter Trade Study Parameters and Values

	Solar Array	GPHS-RTG	MOD-RTG
Risk	5	1	2
Cost	1	5	4
Performance	3	4	5
Complexity	5	2	2
J	28	9	7

The MOD-RTG, again, proved to be the best selection due to its relatively low risk and high performance of operation. Solar arrays have an added risk and complexity due to the need to retract and deploy them during the aerobraking maneuvers. Because the MOD-RTG supplies a maximum of only 342 W, two 329 W RTGs are required to satisfy the orbiter's maximum power requirement of 657 W. The smallest RTG that will satisfy this 329 W requirement is an 18 module RTG which supplies 342 W. The orbiter RTG design parameters are shown in Table 3.11.

3.2.3 Penetrator Power Source Selection

The lithium thionyl chloride battery was selected to power the penetrator. This battery type was chosen because its moderate life span of a few hours satisfies the required operational time of two hours. The battery can be sized to fit the 0.25 m diameter penetrator and the average mass is approximately 0.26 kg.

The RTGs were eliminated as options due to size restrictions; the overall diameter of the penetrator was too small to accommodate either the GPHS or MOD-RTG which each

have a diameter of 0.33 m. The solar array is not a viable option because it is too fragile to withstand the penetrator impact.

Table 3.11. Design Parameters for Each Orbiter MOD-RTG (Modified from Robert F. Hartman, "Modular RTG Technology Status," General Electric Company, Philadelphia, PA, 1990.)

Load Voltage, Volts	30.8
Power Output, Watts	342
Specific Power, W/kg	7.9
Cold/ Hot Junction Temperature, K	573 / 1273
Converter Efficiency, %	7.5
Waste Heat, W	4140.0
Number of GPHS Modules	18
Number of Multicouples	144
Length, m	1.080
Overall Diameter, m	0.33
Weight, kg	43.29
Cost, dollars	5,814,000

3.3 Summary of Power Subsystem Design

Two 342 W MOD-RTGs will power the Arma orbiter, one 114 W MOD-RTG will power the Phobos lander, and one 95 W MOD-RTG will power the Deimos lander. The proven reliability and exceptional performance of past generations of RTGs, makes the MOD-RTG the best option for the three spacecraft. Although the MOD-RTG is expensive, its relatively small mass will provide cost savings in propellant consumption.

The penetrator will be equipped with a 0.26 kg lithium thionyl chloride primary battery which can be sized to fit the 0.25 m diameter penetrator. The battery will supply the required 42 W for approximately two hours. The GPHS and MOD-RTGs were eliminated as options because each have diameters (0.33 m each) which exceed the 0.25 m diameter restriction. The solar array was not a viable option due to its fragility.

4.0 Propulsion Subsystem

4.1 Requirements

The Project Arma mission requires the propulsion system to perform several diverse duties. The Launch Vehicle Subsystem team has indicated that the propulsion system will not be needed for Earth escape. The Propulsion Subsystem team is required to select an appropriate propulsion system for the orbiter. This system is required to provide the ΔV for mid-course corrections during the Hohmann transfer ellipse from Earth to Mars, for Mars capture with the aid of aerobraking, and for maneuvers around Phobos and Deimos. In addition, the Propulsion Subsystem team is required to select an appropriate propulsion system for the landers and the penetrator. The landers' propulsion systems are required to transport the landers from the orbiter to the surface of their designated moon. The penetrator's propulsion system is required to transport the penetrator from the orbiter to Phobos and provide the ΔV to penetrate three meters into the surface. Finally, the Propulsion Subsystem team is required to select attitude control thrusters as dictated by the Guidance, Navigation, and Control (GNC) Subsystem team.

4.2 ΔV Determination

Selecting an appropriate propulsion system is dependent on determining the ΔV budget required for the mission. The GNC Subsystem team is responsible for determining the total ΔV for Project Arma. According to the GNC team, the total ΔV for the mission sums to 2.9 km/sec. This new estimate includes: 2.0 km/sec for insertion into Martian orbit; 0.1 km/sec for mid-course corrections; 1.0 km/sec for an inclination change; and 0.8 km/sec for maneuvers around Phobos and Deimos. An aerobrake maneuver at Mars is assumed to reduce the ΔV required for Martian capture to 1.0 km/sec. To include a contingency, the total ΔV used to calculate propellant mass is 3.0 km/sec. This number includes only the ΔV

for impulsive maneuvers to be performed by the spacecraft as a whole, and does not include maneuvers to be performed by the landers.

4.3 Orbiter Propulsion System Trade Study

After the total ΔV budget is estimated, a trade study of different propulsion system types is performed based on several different options. The results of this trade study are presented in Table 4.1.

Table 4.1. Orbiter Propulsion System Trade Study

Category	Performance	Risk	Cost	J
Solid	6	5	4	-1.8
Monopropellant	7	4	5	-2.4
Bipropellant	9	6	6	-3.0
Electric	5	6	8	-0.2
Solar Sail	2	7	8	1.8
Nuclear	4	8	9	1.0

Areas of performance (P), risk (R), and cost (C) are rated on a scale from one to ten (1.0 = low; 10.0 = high). A high performance, low cost and low risk propulsion system is desired, represented by Equation 4.1.

$$J = -0.6(P) + 0.2(R) + 0.2(C) \tag{4.1}$$

This equation is used to determine the trade values (J) that appear in Table 4.1. The lowest trade value, -3.0, occurs for the bipropellant category. Therefore, it is selected as the main propulsion system for Project Arma.

4.4 Orbiter Component Selection

Four large thrusters, modeled after the thrusters utilized on the Mars Observer Mission, are used on Project Arma for the main orbiter maneuvers. The thrusters are the multistart TRW VTE (Variable Thrust Engine), and have a mass of 6.8 kg [13]. The single greatest advantage of these engines is that they are throttlable from 58 to 579 N. This range allows "ramp-up" starts which minimize propellant slosh and precisely deliver the required thrust [13]. The TRW VTE provides a specific impulse of 306 seconds at maximum thrust, utilizes N_2O_4 / MMH at an oxidizer to fuel ratio of 1.64, and uses less than 20 Watts of power when firing [13]. Each engine is slightly less than 1 m in length, and has an exit diameter of about 27 cm [13]. In addition, four N_2O_4 / MMH thrusters built by Marquardt, are used as backups. Each provides 22 N of thrust, has a specific impulse of 290 sec, and a mass of 0.7 kg [14].

The Propulsion Subsystem team is responsible for selecting attitude control thrusters. According to the GNC Subsystem team, a total of 12 attitude control thrusters (six pairs) are required, based on the Mars Observer mission. It is assumed that these thrusters could be placed on the principal axes of the spacecraft (four per axis). The thrusters selected are the TRW MRE-1 monopropellant thrusters [15]. Each thruster provides 5 N of thrust, has a mass of 1 kg, and a specific impulse of 220 sec [15].

4.5 Main Propellant and Tankage Mass Determination

Using an I_{sp} of 306 seconds and a spacecraft dry mass estimate of 1500 kg, propellant mass of 2575 kg is required to perform the ΔV of 3.0 km/sec [16]. Propellant tank mass is estimated as 10% of the total propellant mass or 257.5 kg total [11]. Assuming Project Arma uses four TRW VTE's, the burn time at maximum thrust to provide the ΔV of 1.0 km/sec for Mars capture is estimated as 2088 sec [17].

4.6 Lander Propulsion System Trade Study

A trade study was conducted to determine the type of propulsion system to be used on the landers. The three propulsion systems evaluated were solid, monopropellant, and bipropellant. These systems were rated with Equation 4.1. The results of the trade study are presented in Table 4.2.

Table 4.2. Lander Propulsion System Trade Study

Category	Performance	Risk	Cost	J
Solid	4	5	4	-0.6
Monopropellant	8	3	5	-3.2
Bipropellant	9	6	6	-3.0

The lowest trade value, -3.2, occurs for the monopropellant category. Therefore, a monopropellant propulsion system is incorporated into each lander.

4.7 Lander Component Selection

Based on the Viking mission to Mars, several groupings of small thrusters are used on the landers for descent to the surfaces of Phobos and Deimos. These small thrusters will disturb the regolith less than a single large engine. Three groupings of four thrusters each are sufficient to provide soft landings on the moons. The thrusters chosen for these groupings are the TRW MRE-1 monopropellant thrusters, which are also used for attitude control on the orbiter.

According to the GNC Subsystem team, a total of four attitude control thrusters are needed for each lander. The thrusters selected for the landers are the TRW MRE-1 thrusters.

The total propellant mass for each lander could not be determined because of the difficulty in quantifying the propellant needed for maneuvering the landers around their moons.

4.8 Penetrator Propulsion System

For the penetrator, a solid propellant system is used to accelerate the penetrator to a speed of 675 m/sec, in order to penetrate 3 m into Phobos' surface [18]. A solid propellant system is necessary due to the limited structural size of the penetrator. This system will provide adequate ΔV to penetrate Phobos, and will contain no moving parts and no liquid propellants which may lead to catastrophic failure. Using an estimated dry mass of 200 kg for the penetrator and an estimated Isp of 190 sec for small motors with polybutadiene and ammonium perchlorate propellant, an estimated propellant mass of 87.3 kg is determined [11]. Mass of the structure to contain this propellant is not determined due to lack of information.

4.9 Summary of the Design

The Propulsion Subsystem team is responsible for selecting appropriate propulsion systems for the Project Arma spacecraft. These include systems for the orbiter, landers, and the penetrator.

For the orbiter, four large bipropellant engines will each provide 579 N of thrust for the inclination change, Mars capture, and maneuvers around the moons. Also, four smaller bipropellant engines, each providing 22 N of thrust, will serve as backups. A total of 12 attitude control thrusters are incorporated into the orbiter and each uses monopropellant hydrazine.

For each lander, a reliable monopropellant system is used for transport from the orbiter to the surface of its designated moon. Based on the Viking lander, groupings of small thrusters are used for descent to the surface to minimize disturbance of the regolith. Three groupings of 5 N thrusters (four per grouping) are used for this purpose. In addition, four

thrusters, each identical to those used in the groupings, will provide attitude control over each lander.

Finally, a solid propellant rocket motor is implemented to enable the penetrator to lodge into Phobos' surface at a depth of 3 m. The propellant used is ammonium perchlorate and polybutadiene.

5.0 Guidance, Navigation, & Control and Trajectory Design

5.1 Requirements

The design of the Guidance, Navigation, and Control subsystem (GN&C) includes the selection of the stabilization method, the control actuation systems, and the spacecraft sensors. The entire mission to Phobos and Deimos requires extreme accuracy during all phases. The most critical phases include the orbit control around the moons, and the aerobraking maneuver. The accuracy required for the orbits about the moons is specified by the scientific instruments. The scientific instrument platform is required to be continuously nadir pointed. Aerobraking utilizes the Martian atmosphere to capture the spacecraft into an orbit about Mars from the Hohmann transfer. However, an accurate GN&C system is critical to maintaining control of the vehicle throughout the atmospheric encounter to provide accurate orbital conditions while maintaining certain critical parameters to be discussed below [8].

5.2 Orbiter GN&C

5.2.1 Stabilization Method

The three different stabilization methods considered for Project Arma are the gravity gradient, spin stabilization, and three-axis stabilization. Table 5.1 shows the results of a trade study, determining the type of stabilization that will be used for Project Arma. The following formula was used to determine the best method of control with k_1=5, k_2=3, and k_3=4.

$$J = k_1(cost) - k_2(risk) - k_3(perform) \tag{5.1}$$

Table 5.1. Trade Study Results for Stabilization System

Option	Cost	Risk	Performance	Trade Value
Gravity Gradient	1	5	1	16
Spin Stabilized	2	3	2	11
Three Axis	5	1	5	8

The results of this study show that three-axis stabilization should be utilized. The gravity gradient method is too inaccurate as well as impractical for an interplanetary mission. The three-axis stabilization method was chosen primarily because of its high accuracy, within 0.001 degrees, and the freedom to make rapid changes in orientation.

5.2.2 Actuators

The orbiter will include two types of actuation systems for control. The primary method of control will be momentum wheels for the slewing requirements needed for any orientation changes. Three momentum wheels will be used and are placed orthogonally for three-axis control while a fourth wheel will be oriented at a skewed angle in a backup mode. The operation of the momentum wheels will be entirely automatic. The control system for Project Arma will use the momentum wheels to maintain the pointing of the spacecraft in the presence of perturbations from atmospheric drag (while near Mars), gravity gradients, and solar pressure torques.

Secondary control will be provided by a thruster assortment which will also provide large changes in the velocity of the spacecraft for orbital maneuvers. In addition, the thrusters will be used for momentum dumping of the momentum wheels when they become saturated. The process of momentum dumping will also be an autonomous operation for Project Arma due to the 40 minute delay in communications.

The thruster assortment will be similar to that used on the Mars Observer spacecraft. Table 5.2 shows the mass and the propellant for each size of thrusters.

Table 5.2. Mars Observer Thruster Assortment. (Halsell, C.A. and W.E. Bowman. "Mars Observer Trajectory and Orbit Control," *Journal of Spacecraft and Rockets,* October 1991, p. 537).

Thruster Size (N)	Quantity	Weight (kg)	Propellant
490	4	4	N_2O_4/MMH
22	4	0.7	N_2O_4/MMH
4.4	12	0.2	Hydrazine

The 490 N thrusters will be used to make large changes in the state of the spacecraft such as trajectory changes. Moderate rate maneuvers will utilize the 22 N thrusters. The 4.4 N thrusters will be used for orientation changes and momentum dumping while the scientific instruments are active; the hydrazine propellant does not corrupt the instrument measurements.

5.2.3 Sensors

The GN&C system can only be as accurate as the sensor suite. In order to maintain an accuracy of 0.001 degrees, an inertial measurement unit (IMU) was chosen to supplement the sun sensors, star sensors, and horizon sensor. The Project Arma spacecraft will have three sun sensors, two star sensors, one steerable horizon sensor, and an IMU which consists of laser gyros and accelerometers. Throughout the duration of Project Arma, the sun and star sensors will be used in conjunction to provide an inertial, three-axis position fix. Star sensor maps will be updated every four hours during the interplanetary cruise [14]. The IMU tracks

the motion of the spacecraft from the last fix until the uncertainty in the position of the spacecraft becomes too large; then another position fix is required. The horizon sensor should prove quite useful for navigation while in close proximity to Phobos and Deimos during the mapping and the lander insertion phases.

5.2.4 Disturbance Torques

The disturbances on the spacecraft that are expected to be encountered while at Mars are caused by solar radiation, aerodynamic drag (while near Mars), and the gravity gradients while orbiting Mars and at each of the moons. The gravity gradients of Mars are not accurately known but by the end of 1994, the Mars Observer should have completed its gravity calibration of the planet. The gravity measurements of the moons will be made by the spacecraft but these are not expected to cause any serious control problems due to the relatively small size of the moons. Aerodynamic drag is also not expected to cause orbit decay except in the long term parking orbit of the orbiter. The solar radiation torque has been estimated to be on the order of 10^{-4} Nm, using procedures outlined in [11]. Magnetic torques about Mars will be better defined after Mars Observer completes its mission, but it should not be greater than the solar radiation torque. The actuation systems of Project Arma will be sufficient to counteract the expected disturbance torques.

5.3 Lander GN&C

Four roll control thrusters placed on the sides and three groups of four thrusters placed on the bottom for braking will be used to control the descent and landing of the craft. This is based on the Viking mission [20] which used three groupings of eighteen nozzles for braking. Because there is negligible atmosphere and low gravitational acceleration due to the moons, this configuration was scaled down to four nozzles in each group. It is hoped that by using several smaller thrusters as opposed to one large thruster for braking the landing site

will be less disturbed. The attitude and position of the lander is determined by a horizon sensor and also tracking by the orbiter.

5.4 Penetrator GN&C

The experimental penetrator that will be used on Project Arma is designed to obtain a core sample from Phobos. The penetrator must impact Phobos with sufficient velocity to enter the surface to a depth of a few meters. Clearly, a method of deployment must be developed in order to achieve an impact velocity on the order of 600-700 m/s.

Several ideas have been developed as a means of deployment of the penetrator from the orbiter. The most reasonable methods are the following: a free fall release from the orbiter to the surface of the moon; placing the penetrator into a collision trajectory with Phobos; a large spring-like device to release the vehicle from the orbiter directly to the surface; and finally attach a solid rocket motor to the base of the penetrator to launch from orbit.

A trade study was completed to evaluate these options. The results of the study are shown in Table 5.3. The following formula was used to determine the best method of deployment with k_1=5, k_2=3, and k_3=4.

$$J = k_1(Cost) + k_2(Risk) - k_3(Perform) \tag{5.2}$$

Table 5.3. Trade Study Results for Penetrator Deployment Method

Option	Cost	Risk	Performance	Trade Value
Free Fall	1	4	1	13
Orbital Impact	1	3	2	6
Large Spring	2	5	4	9
Solid Rocket	3	2	4	5

The free fall method of deployment is not feasible because of Phobos' low mass, which results in a very low gravitational acceleration (9-10 cm/s^2). The use of a spring-like device to deploy the penetrator may not achieve a large enough velocity but more importantly, the recoil effect will require a large control force to stabilize the orbiter during release. The orbital impact method is essentially a "free ride;" however, the low mass of Phobos limits the achievable orbital velocity. The solid rocket motor at the base of the penetrator appears to be the most feasible design. The rocket motor can be designed to produce a wide range of impact velocities depending on the motor size and the amount of solid propellant. The control system that will be required for this method of deployment should be relatively simple. Small thrusters for pitch control and a gimbaled motor should be sufficient. The only strict requirement is that the penetrator impact Phobos perpendicular to the surface for maximum depth of penetration.

5.5 Mission Operations

Project Arma will begin atop a Proton booster. More than likely, the Proton will be launched from its current site, the Baikonour Cosmodome. The Proton will launch the orbiter with the two landers directly into the Hohmann transfer towards Mars. The launch azimuth and exact trajectory still need to be determined. The optimal launch point, in terms of propellant expenditure, for a Hohmann transfer to Mars is a fully three-dimensional problem that requires a more detailed simulation. Previous studies [21] suggest that a conjunction-class mission with a Hohmann transfer would be the optimal, minimum propellant mission transfer.

After some trajectory correction maneuvers during the cruise to Mars, the spacecraft will be ready for approach to the Martian system. The approach to Mars will likely be at some arbitrarily high inclination relative to the Martian equator. The approach is dependent upon exit conditions at Earth, planetary alignment, and control system performance. Orbit insertion will be achieved by using an aerobrake maneuver in the Martian atmosphere. The

spacecraft's position and velocity must be accurately known at the time of atmospheric entry for a successful aerocapture. In addition, the aerobraking maneuver will have to be entirely autonomous because of the communications delay [8]. Aerobraking is further discussed in the next section.

The exact orbital parameters following the aerobraking maneuver will not be known because they are dependent upon the success of the aerocapture. This initial orbit about Mars will tend to be highly elliptical and inclined [21]. The orbits of both Phobos and Deimos are both nearly circular and equatorial (Phobos at 6,068 km and Deimos at 20,168 km).

To transfer the spacecraft from this initial orbit to an equatorial orbit requires a sequence of transfers to lower the propellant requirements. A direct transfer to an equatorial orbit is very expensive in terms of propellant. First, the spacecraft is required to perform a plane change. This maneuver must occur at a point of intersection of the two orbit planes. In addition, it is desirable to make this plane change at the lowest velocity of the spacecraft in the orbit, apoapsis.

To insure apoapsis intersects the equatorial plane, a rotation of the line of apsides to 0 or 180° is required. An impulsive transfer at periapsis of the initial orbit is needed to rotate the line of apsides and raise apoapsis, which further reduces the spacecraft's velocity for the plane change. This new orbit is highly elliptical; apoapsis is outside of Deimos' orbit. Another impulsive transfer at this new apoapsis will be made to make the plane change to the equatorial orbit. Once in the equatorial orbit, the spacecraft will make Hohmann transfers to travel to each moon for mapping and lander insertion. A final parking orbit for the orbiter about Mars needs to be determined in order to optimize the propellant expenditure to maintain the orbit, in addition to providing a suitable communications link between the landers and Earth. This orbit should be frozen; that is, the orbit elements must be chosen such that planetary oblateness effects will maintain a nearly constant orbit eccentricity and argument of periapsis [19]. The gravity calibration being performed by the Mars Observer

will be used to refine the present models of the Mars gravity field and to calculate the correct eccentricity for a frozen orbit [2].

5.6 Aerobraking

An aerobraking maneuver will be used for this mission because of the significant savings in propellant mass it will provide by slowing the vehicle at Mars. Several issues must be taken into consideration if aerobraking is to be used, as outlined by Cooper [8]. These critical technologies include vehicle concepts and configuration, aerothermodynamics, thermal protection system, and guidance, navigation, and control. A brief summary of these considerations is presented below.

Vehicle concepts have been studied and a relatively blunt body with a Lift-to-Drag ratio (L/D) of 0.5-1.0 is necessary for Mars aerobraking [22]. The Aeroassist Flight Experiment (AFE) vehicle configuration should provide adequate L/D of around 0.5 for Project Arma. The AFE design was chosen because a significant amount of research has been conducted on the AFE. Thus, much information such as L/D, ballistic coefficient, and aerodynamic heating rates of the AFE have already been documented. The depth of penetration into the Martian atmosphere depends upon the L/D of the vehicle and the change in velocity that is required for a capture orbit. For an L/D of about 0.5, the spacecraft would need to plunge to an altitude of approximately 40-50 km from the surface in order to decrease the velocity ($\Delta V \approx 2$ km/s) enough to obtain a Mars capture orbit. This depth also significantly affects the heating of the body.

The flow field around the body needs to be accurately known so that the heat transfer rates to the body can be defined. Also, the wake behind the aeroshell must be known so that the payload can be adequately protected. Computer simulated flow field studies were presented in Reference [23] and, based on this study, it was calculated that an aerobrake shield with a diameter of approximately 10-11 meters is necessary to keep the payload in the subsonic region of the wake. Due to the large size of the shield, a method of deployment is

necessary since the largest dimension of the Proton payload bay is approximately 5 meters. One possibility is that the shield could be split into two halves and then brought together in orbit. Another possibility is to have it in pie sections that fan out to form the shield. A significant problem occurs in having a deployable aerobrake since seams are introduced. These seams must be very tight to protect the payload and must be able to withstand the intense heating which occurs during the aerobrake maneuver.

Once the heating rates have been defined, materials can be selected for the thermal protection system. This is a major concern of the Thermal Protection and Structures Subsystems and is discussed in their sections. Briefly, there is much debate over the thermal environment of Mars and therefore it is not certain whether insulative/radiative or ablative materials should be used [8]. Walberg [22] however believes that since an unmanned mission to Mars uses a near Hohmann transfer, the entry velocities at Mars are low and that ablative heat shields will be required.

GN&C will play a vital role in ensuring that the correct trajectory is followed through the Martian atmosphere during aerobraking. It is impossible to control the spacecraft from Earth during this maneuver; therefore, the on-board GN&C system will analyze the conditions in real time and compensate for variations in atmospheric density, gravitational anomalies, etc. The Analytic Predictor Corrector and Energy Controller are current GN&C systems being worked on by NASA to control aerobraking maneuvers and also are considered for Project Arma [24]. Also, a method to control the spacecraft is necessary since the lift vector needs to be rotated during the maneuver. Extendible surfaces much like those on airplanes were considered but again pose significant heating problems and add mass to the payload. It is expected that the attitude control thrusters and momentum wheels will be enough to rotate the lift vector during the maneuver thus adding no new components or weight.

Despite the technological challenges, Project Arma will use aerobraking to obtain a Mars capture orbit. Aerobraking will significantly reduce the mass of propellant by 10-25%

(depending on the performance of the aerobraking maneuver) and thus the mass of the payload. More importantly, this mission will be a proof of concept for aerobraking which is imperative for future manned missions to Mars.

5.7 Orbiting the Moons

Several studies [25,26] have shown that quasi-stable orbits about Phobos and Deimos are feasible. These studies are limited to simulating the orbits only in the equatorial plane of Mars. The orbits are typically characterized as retrograde with decay periods of approximately ten to twelve days, depending upon initial orbit conditions.

The orbits that are presented [25,26] however, are only numerical approximations to the "four-body problem." Part of Project Arma's mission is to map the gravity fields of both moons. The spacecraft will use the largest orbit calculated from the above studies as a first approximation until the gravity mapping is complete. This largest orbit will be obtained by first following the moon in its orbit about Mars. Slight maneuvers are then made to slowly decrease the separation distance between the spacecraft and the moon until the spacecraft begins to orbit the moon.

5.8 ΔV Estimates

Table 5.4 lists the ΔV estimates for Project Arma. The values listed are either from simple one dimensional approximations or from reference materials. The source for the ΔV estimates follows each maneuver description given below. The trajectory correction maneuvers will be made to correct any inaccuracies that occurred during launch or navigation [19]. Mars orbit insertion assumes a 50% effectiveness for the aerobrake maneuver [21]. The ΔV necessary for the plane change from the capture orbit to the equatorial plane is estimated from [1]. Simple one dimensional approximations were made to estimate the ΔV needed to Hohmann transfer to each moon. The exact parking orbit has not been determined, but the orbit will be a polar type orbit for the reasons described previously. Therefore, the

velocity change can be estimated as a reversal of the plane change maneuver. The maintenance of the parking orbit in the presence of perturbations has been estimated for the Mars Observer [19] and should be an adequate estimation for Project Arma.

Table 5.4. ΔV Estimates for Project Arma

Maneuver	ΔV (km/s)
Trajectory Correction Maneuvers	0.1
Mars Orbit Insertion w/Aerobraking	1
Plane Change Maneuvers	1
Hohmann Transfers to Moons	0.8
Final Parking Orbit Transfer	1
Stationkeeping	0.05

5.9 Summary

Table 5.5 summarizes the GN&C components that will be included on the Project Arma orbiter.

Table 5.5. GN&C Components

Component	Quantity	Weight (kg)	Size (cm)	Max. Power (W)
Momentum Wheels	4	12	40 x 10	100
IMU	1	12	5 x 5 x 6	100
Horizon Sensor (Steerable)	1	1	15 x 15 x 5	5
Star Sensor	2	10	17 x 15 x 31	10
Sun Sensor	3	4	38 x 36 x 20	3

6.0 Command and Data Handling

6.1 Requirements

The command and data handling subsystem (C&DH) receives and distributes command and telemetry data between the communications subsystem and the other spacecraft subsystems. These commands must be processed and distributed to the required subsystems in order to perform time critical sequences. The C&DH subsystem also collects and stores data obtained from Earth and the spacecraft subsystems.

6.1.1 Lander Requirements

Both of the landers will contain long term experiments which will collect data for a period of one solar cycle (11 years). The Deimos lander will have an approximate 13.6 hours of transmission time with the orbiter during one orbiter period of 15.45 hrs. The Phobos lander will have only 8.37 hours of transmission time during the same orbiter period. These constraints require the Deimos and Phobos landers to be able to record data for approximately 1.85 and 7.08 hours respectively. Thus, it will be necessary for each of the landers to contain a storage device. The required data storage and frequency of measurements for the long duration instruments on the Deimos lander is shown in Table 6.1. Similarly, Table 6.2 shows the required storage and frequency of measurements for the Phobos lander. An error correction factor of 215% has been added to the total stored bits. This error correction factor accounts for the encoding which will reduce possible errors incurred during storage, transfer, and transmission. During non-transmission times, all of the landers' instruments except for the mass spectrometer will be used. This allocates storage space for data collected from the other instruments. The mass spectrometer will, however, be used during times of communication with the orbiter.

Table 6.1. Data Storage During Non-Transmission Time for Deimos Lander

Instrument	Readings	Bits
		2220
Temp. Probe	1 every 30 sec	
Seismometer	1 every 30 sec	28416
Radiation Detector	1 every 30 sec	5550
XRFS	None	Not Used
Panoramic Cameras	1 for 132 sec	5.28E+08
TOTAL (Bits)		5.28E+08
w/error correction		1.66E+09

Table 6.2. Data Storage During Non-Transmission Time for Phobos Lander

Instrument	Readings	Bits
Temp. Probe	1 every 30 sec	8496
Seismometer	1 every 30 sec	108748.8
Radiation Detector	1 every 30 sec	21240
XRFS	None	Not Used
Panoramic Camera	1 for 112 sec	4.49E+08
Wide Angle Camera	1 for 224 sec	7.87E+07
TOTAL (Bits)		5.28E+08
w/error correction		1.66E+09

6.1.2 Orbiter Requirements

The orbiter will contain moon mapping and Mars observation instruments. During the mapping phase, the incoming data rate will be at its peak. Due to mission priorities, Mars observation instruments will not be operational until the mapping of the moons is completed. Also, due to data storage limitations, all lander experiments will be disabled until the orbiter has mapped both moons. The orbiter will have 10.45 hours of transmission time with the

Earth during an orbital period of 15.45 hours. This constraint requires the orbiter to have a recorder to store data for approximately five hours.

While mapping, the orbiter obtains data at a rate of 1.23 Mbps. This rate includes house keeping and an error correction value of 215% for encoding. House keeping data rates for the orbiter are shown in Table 6.3, while data rates for individual instruments are shown in Table 6.4.

Table 6.3. Orbiter House Keeping Data Rates (Wertz, J.R. and Larson, W.J., Space Mission Analysis and Design. 2nd Edition, 1993, p 607.)

Housekeeping Data	BPS
Command Processing	7
Telemetry Processing	3
Thruster Control	1.2
Power Management	5
Thermal control	3
Ephemeris Propagation	2
Complex Ephemeris	4
Orbit Propagation	20
TOTAL	45.2
w/error correction	142.38

Table 6.4. Orbiter Instrument Data Rates

Instrument	BPS
Radar Sounder	352000
Magnetometer	3600
Gravity Gradiometer	1000
Gamma Ray Spectrometer	655
Mass Spectrometer	4000
Visual Instruments	29260
DION	600
Laser Altimeter	618
Housekeeping w/error correction	142.38
TOTAL	391,733
w/error correction (bps)	1.234E+06

6.1.3 Penetrator Requirements

The X-Ray Fluorescence Spectrometer (XRFS) is the only scientific instrument aboard the penetrator. It will be used only once and is expected to transmit data for less than two hours. Due to the small amount of data taken by the spectrometer, the operations of the penetrator will only require a small computer. This computer can be designed to have storage space allocated for data collected by the XRFS. Thus a data storage device will not be necessary.

6.2 Component Selection

The orbital mapper and landers are each equipped with a C&DH module consisting of a computer and data storage device, while the penetrator has only a computer. Figure 6.1 depicts the block diagram for the command and data handling subsystem.

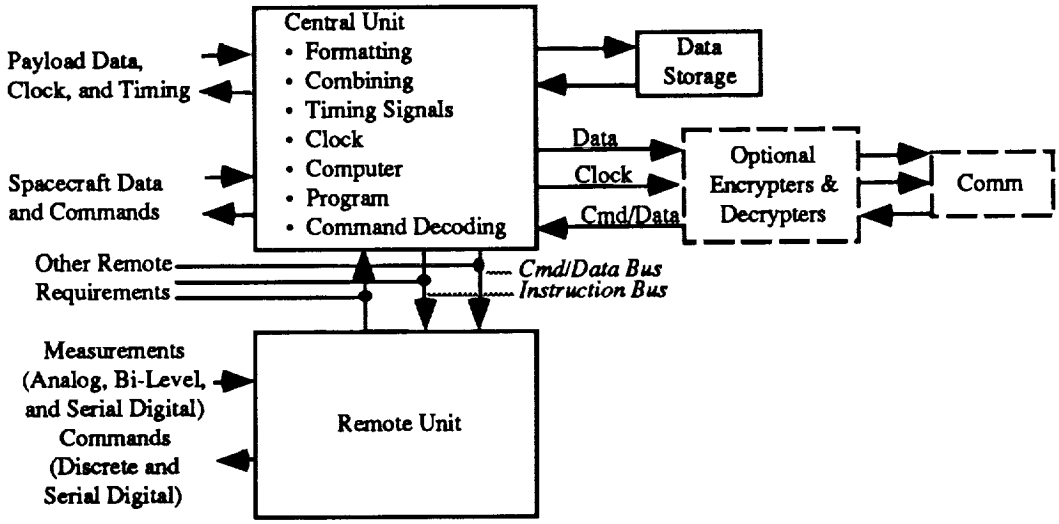

Figure 6.1. Block Diagram for a Command and Data Handling Subsystem. (Wertz, J.R. and Larson, W.J., Space Mission Analysis and Design. 1st Edition, 1993, p. 342.)

The computer system to be used for the penetrator and two landers is the Rockwell R1-1750A/B. The orbiter will use the IBM GVSC. These selections were made through a trade study of the specifications with the possible computers listed in Table 6.5. The equation for this trade study is shown below. A high power requirement as well as a large size and weight were considered to be disadvantages and a large memory and throughput were considered advantages. The computer with the highest trade study value was considered to be the best selection for Project Arma. The trade study values, J, are also listed in Table 6.5.

$$J = 1(Memory) - 0.001(Size) - 1(Weight) - 1(Power) + 1(Throughput) \quad (6.1)$$

Table 6.5. Specifications of Possible Computer Systems for Project Arma. Orbiter (Wertz, J.R. and Larson, W.J., Space Mission Analysis and Design. 2nd Edition, 1993, p 607.)

Computer System	Memory (Mbits)	Size (cm^3)	Weight (kg)	Power (W)	Thruput (Mbps)	J
Honeywell ASTIII	3	4921	5.2	30	2.5	-34.621
ASCM-CPM	1 to 5	5899	8.98	25.3	3	-32.179
Fairchild	1.75	10078	11.4	12	1.7	-30.028
ASCC-ATIM	2 to 6	5899	7.8	25	3.5	-29.199
IBM GVSC	3.9	1280	8.2	23	4.5	-24.08
Rockwell RI-1750A/B	3.906	2050	2.5	6.6	1.8	-5.444

The Rockwell computer has a trade study value of -5.444, which is the best of the six values, while the IBM GVSC is the next best choice with a trade study value of -24.08. The IBM computer has been chosen for the orbiter because a larger throughput rate is needed to transmit all of the stored data recorded during non-transmission times. In addition, Fairchild solid recorders will be used on the orbiter and landers to store data collected during non-transmission times. The Fairchild recorder has a total storage capacity of 1.664 Gbits with a

maximum record and playback rate of 10 Mbps. This rate is well above the throughput of the Rockwell and the IBM computers, therefore transmission rates will not be hindered by the playback rate of the recorder.

6.2.1 Lander Selection

The computer system selected for both landers is the Rockwell RI-1750A/B. The computer's throughput of 1.8 Mbps corresponds to the transfer rates of the landers' low-gain antennas. Each lander will also have one Fairchild solid state recorder for data storage. The Deimos lander will store a total of 1.664 Gbits of instrument data for the 1.85 hours of non-transmission time with the orbiter. Due to the large memory requirements of the panoramic cameras, the cameras will only operate for approximately 132 seconds during non-transmission times. This operation time will fill the memory of the recorder and require 15.41 minutes for transmission with other incoming data. The Phobos lander is limited to storing 1.664 Gbits of data for the 7.08 hours of non-transmission time. The Phobos lander's computer will also need 15.41 minutes to transmit stored data.

6.2.2 Orbiter Selections

The IBM GVSC has been chosen for the orbiter, because it has a high throughput rate of 4.5 Mbps. This rate is needed to transmit the stored data recorded during non-transmission times with Earth. In addition, the orbiter is equipped with two Fairchild solid state recorders, having 1.664 Gbits of storage capacity each. The two recorders have been placed in the orbiter to increase the storage capacity during the mapping phase of the mission. The increased storage will allow mapping to be completed more quickly and almost continuously.

During contact times, the data will be transferred to Earth via a high-gain antenna at a rate of 4.5 Mbps, which coincides with the maximum throughput rate of the IBM computer. Table 6.4 lists the scientific instruments which will be operating during the mapping of the moons. During non-communication times, the solid state recorder will only be able to store

44.9 minutes of continuous data, which corresponds to approximately 45 seconds of recording for every minute of non-communications time. When the orbiter is able to communicate with Earth, 3.27 Mbps of the orbiter's 4.5 Mbps transmission rate will be allocated to the stored data. With this allocation the orbiter can continuously receive data from the moons and partially empty the stored data. It will take 16.98 minutes to completely empty the stored data.

Once mapping is complete, the orbiter will transfer to a Mars parking orbit and begin the Mars observation experiments. At this time, the landers will require 3.6 Mbps (1.8 Mbps each) of the high-gain antenna transfer rate. This will leave a total of 0.9 Mbps for the lower priority Mars observation instruments listed in Table 6.6. During the non-communications time of 5 hours, a total of 95 minutes of data can be stored by the recorder. With the reduced data rates, it will take the remaining 10.45 hours of the orbit to transmit both the stored and incoming data.

Table 6.6. Mars Observation Instrument Data Rates

Instrument	BPS
Retarding Potential Analyzer	1500
Near-Infrared Spectrometer	800000
Gravity Gradiometer	1000
Magnetometer	3600
Housekeeping w/error correction	142.38
TOTAL	806100.0
w/error correction (bps)	2.54E+06

6.2.3 Penetrator Selection

The Rockwell computer has been selected for the penetrator, due to its small size, mass, and power requirement. The computer's throughput rate of 1.8 Mbps is well above the

XRFS recording data rate of 0.3 kbps and also has space available for the data collected by the XRFS, which eliminates the need for a data storage device.

6.3 Summary

The orbiter is equipped with an IBM GVSC computer and two Fairchild solid state recorders. The computer has a throughput of 4.5 Mbps and the recorders provide a total of 3.328 Gbits of data storage. The orbiter's communications are distinguished by two mission phases; mapping of the moons and surface analysis with long term experiments.

During the mapping phase of the mission, data will be transmitted to Earth for 4.5 hours and stored for 1 hour of the 5.5 hour mapping orbit. Throughout the 1 hour of non-communications time, 45 minutes of data can be stored, filling the memories of the two recorders. A transmission time of 16.98 minutes is required to fully empty the recorders.

Once the mapping phase of the mission is complete, the second phase, surface analysis and long term experiments, will begin. For this second phase data is sent for 10.45 hours and stored for 5 hours of the 15.45 hour parking orbit. Of the 4.5 Mbps transmission rate, 1.6 Mbps is allocated for lander data, leaving 2.9 Mbps for the orbiter's long term experiments. With the reduced data rate, the orbiter requires 10.45 hours to transmit 95 minutes of stored data. The 95 minutes of storage space is filled by taking measurements at three second intervals for the 5 hour period of non-transmission.

Both the Deimos and Phobos landers are equipped with a Rockwell R1-1750A/B computer and one Fairchild solid state recorder with a memory capacity of 1.664 Gbits. It will require 15.41 minutes to fully empty the recorder, during transmission times. The Deimos lander transmits data to the orbiter for 13.6 hours and stores data for 1.85 hours of each orbiter period of 15.45 hours. During non-transmission times, instrument readings will be recorded every 30 seconds and the panoramic cameras will operate for 132 seconds, filling the recorder's memory. The Phobos lander will transmit data to the orbiter for 8.37 hours and stores data for 7.08 hours of each orbiter period of 15.45 hours. During non-transmission

times, instrument readings will be recorded every 30 seconds, the panoramic cameras will operate for 112 seconds, and the wide angle camera will operate for 224 seconds, filling the recorder's memory.

The penetrator is equipped with a Rockwell RI-1750A/B computer, which contains a built-in memory of 3.9 Mbits and a throughput of 0.8 Mbps. Since the penetrator will operate for a total of less than two hours, information from the penetrator will be sent during a contact time so extra memory storage will not be necessary.

7.0 Communications

7.1 Communications Requirements

The communications subsystem is responsible for the exchange of information between Earth (telemetry and commands) and the spacecraft (experimental data and status information) during the course of the mission, from Mars transfer to end-of-life. The communications subsystem also interconnects the mission systems (lander, orbiter, and penetrator) so they can work together to complete the mission objective. Therefore, the communications subsystem must also connect the various mission systems to Earth to facilitate the exchange of information in a signal efficient and timely manner.

7.2 Communications Architecture Selection

For Project Arma's mission to the moons of Mars, Phobos and Deimos, several communication scenarios were investigated. The scenarios were based on the mission system breakdown of one (1) orbiter, two (2) landers (one per moon), and one (1) experimental Phobos penetrator. The scenarios considered for Project Arma's communications architecture were:

(1) Each lander would have a high-gain antenna (HGA) for communications with Earth. Each lander would also have a low-gain antenna (LGA) for communication with the orbiter LGA and penetrator LGA or even, in the case of an antenna failure, communication with the other lander.

(2) A lander would have a HGA for communication with Earth. The lander would also have a LGA for communications with the other mission system's LGAs, one on the other lander, one on the orbiter, and one on the penetrator.

(3) The orbiter would have a HGA for communications with Earth. The orbiter would also have two LGAs for communications with the other mission systems, landers and penetrator, which have one LGA each.

(4) The orbiter and one lander would each have a HGA for communications with Earth. The orbiter would have two LGAs and the lander one LGA for communications with the LGAs of the other mission systems.

Each of the aforementioned scenarios have their advantages and disadvantages. The best communications architecture was selected via a trade study.

The trade study rated each scenario from one, the highest, to four, the lowest, in five different categories. The scenarios were rated in cost, performance, scheduling merit, risk, and weight. The trade study values, J, of the scenarios were determined from the equation

$$J = k_c(cost)+k_p(performance)+k_{sm}(scheduling\ merit)+k_r(risk)+k_w(weight) \qquad (7.1)$$

where k_c is the cost coefficient, k_p is the performance coefficient, k_{sm} is the scheduling merit coefficient, k_r is the risk coefficient, and k_w is the weight coefficient. A minimum trade study value indicates the scenario which would best satisfy the communication subsystem requirements.

Table 7.1 shows the results of the trade study. With k_c equal to 0.25, k_p equal to 0.20, k_{sm} equal to 0.15, k_r equal to 0.20, and k_w equal to 0.20, the trade study equation indicates that scenario number three, with a value of 2.20, is most suited for Project Arma's communications architecture. Scenario number 4, with a value of 2.35, is the second option.

Table 7.1. Communications Architecture Trade Study for Project Arma.

Scenario	Cost	Performance	Scheduling Merit	Risk	Weight	Trade Study Value
1	3	3	3	2	3	2.80
2	1	4	4	4	1	2.65
3	2	2	2	3	2	2.20
4	4	1	1	1	4	2.35

7.3 High-Gain Antenna Design

With the selection of the communications architecture complete, the communications subsystem hardware was selected and sized. The orbiter's parabolic HGA must be capable of simultaneous transmission and reception with the Deep Space Network's (DSN) 34 m diameter antennas.

The 1.50 m diameter x 0.70 m gimbaled HGA will transmit on channel 18 of the DSN's X-band frequency range (f = 8.42 GHz). The HGA will be deployed following launch and communication with Earth will begin after approximately the first two months of the cruise phase. Once deployed, the antenna will be located at the end of a 2 m long boom to prevent spacecraft interference during communication efforts and to reduce sidelobe interference with the orbiter's experiments.

Table 7.2 contains the HGA characteristics. During simultaneous transmission and reception, the HGA will require 45 W of power. For periods of transmission only, approximately 35 W will be required to produce the 0.7 W of radio frequency (RF) output power needed for communication with Earth. The required power for receiving information is 10 W. A stay alive power of approximately 4.5 W is required when the HGA is inactive.

Table 7.2. Orbiter High Gain Antenna Characteristics.

Dimensions (m)	1.50 dia. x 0.70
Mass (kg)	9.5
Power required (W)	45
Power transmitted (W)	0.7
Power stand-by (W)	4.5
Gain (dB)	39
Frequency (GHz)	8.420432097
Antenna efficiency	0.499
Beamwidth (degrees)	1.4248
Signal-to-noise ratio (dB)	8.9431
Data transmission rate (Mbps)	4.5
Effective isentropic radiated power (dBw)	55.53

The transmitted power of the orbiter HGA was determined by using the maximum computer throughput and Shannon's formula [28]. With a maximum data rate of 4.5 Mbps and an X-band, channel 18 bandwidth of 1.36 MHz, the minimum signal-to-noise ratio, SNR, was calculated as 8.9431 dB. From this value, a minimum RF output power of 0.7 W was derived. Appendix B presents this calculation in a step-by-step manner.

The HGA communication subsystem bus controls how signals are transmitted and received, as well as modulated and demodulated. The bus consists of a waveguide, RF switches, filters, a diplexer, a transmitting transponder, and a receiving transponder. The mass, required operating power, and dimensions of these components are listed in Table 7.3.

Table 7.3. Communications Bus Characteristics (Modified from Wertz, J.R. and Larson, W.J., Spacecraft Mission Analysis and Design. 2nd Edition, 1993, p. 341.)

Component	Mass each (kg)	Mass total (kg)	Power (W)	Dimensions (cm)
Waveguide	3.70	3.70	0.0	3.174 x 1.5875 x 200
RF switches, filters, diplexer	1.5	1.5	0.0	10 x 22 x 4
Transponder				
Transmit	4.75	4.75	10.4	7 x 15 x 4.5
Receive	4.75	4.75	35.00	7 x 15 x 4.5

7.4 Low-Gain Antenna Design

The low-gain antennas for the various mission systems will share the same design. The antennas are designed for a large beamwidth so a wider coverage and increased communication time can be obtained. The low-gain antennas are responsible for the exchange of information between the mission systems at the Martian planetary system and between the spacecraft and Earth during the early stages of cruise.

Table 7.4 lists the parabolic LGA characteristics. The two driving factors in the LGA design were the attainment of a large beamwidth and the matching of the antennas' maximum data rate to the maximum computer throughput. To produce a large beamwidth of 173 degrees, the communication frequency was lowered to the L-band range, 1.21 GHz, and the diameter of the antennas were reduced to 0.10 m. The maximum data rate of 1.8 Mbps was used to find the SNR through Shannon's formula in the same manner used for the HGA. From the SNR, the required RF output power was determined to be approximately 0.33 W.

Table 7.4. Low-Gain Antenna Characteristics

Dimensions (m)	0.10 dia. x 0.06
Mass (kg)	0.50
Power required (W)	15
Power transmitted (W)	0.33
Power stand-by (W)	1.5
Gain (dB)	2.06
Frequency (GHz)	1.21
Beamwidth (degrees)	173
Signal-to-noise ratio (dB)	14.478
Data transmission rate (Mbps)	1.8
Effective isentropic radiated power (dBw)	13.821

The low-gain antennas require a communications bus to modify the signal characteristics. The bus consists of coaxial cables, RF switches, filters, a diplexer, a transmitting transponder, and a receiving transponder. Several characteristics for these components are tabulated in Table 7.5.

Table 7.5. Low-Gain Communications Bus Characteristics (Modified from Wertz, J.R. and Larson, W.J., Spacecraft Mission Analysis and Design. 2nd Edition, 1993, p. 341.)

Component	Mass each (kg)	Mass total (kg)	Power (W)	Dimensions (cm)
Coaxial cables	2.5	2.5	0.0	3 dia. x 100
RF switches, filters, diplexer	1.5	1.5	0.0	10 x 22 x 4
Transponder				
Transmit	4	4	11.5	5 x 12 x 4
Receive	4	4	3.5	5 x 12 x 4

7.5 Communications Design Summary

The primary communication link between the Martian system and Earth will be a high-gain antenna located on the orbiter. The reflector high-gain antenna will be 1.50 m in diameter and will transmit on the Deep Space Network's X-band, channel 18 frequency (8.42 GHz). The antenna will require 45 W of supplied power to transmit 0.70 W of power with a maximum data transmission rate of 4.5 Mbps. The antenna will be complimented by two transponders for redundancy and simultaneous transmission-reception capability, a waveguide for efficient radio frequency wave transmission, and switches, filters, and a diplexer for signal modulation-demodulation.

All of the low-gain antennas (two on the orbiter, one per lander, and one on the penetrator) share the same design. These antennas are designed for wide coverage, 173 degrees, and maximum throughput, 1.8 Mbps. Each of the low-gain antennas will be 0.10 m in diameter and will transmit on a 1.21 GHz frequency band. A required power of 15 W will produce 0.33 W of radio frequency output power. The low-gain communications bus will consist of two transponders for redundancy and simultaneous transmission-reception capability, as well as coaxial cables for signal transmission, and switches, filters, and a diplexer for signal modulation-demodulation.

8.0 Thermal Control Subsystem

8.1 Requirements

The Thermal Control Subsystem (TCS) fulfills the basic function of regulating the spacecraft temperatures. The TCS is responsible for maintaining temperatures within specific limits as required by individual spacecraft components. This regulation is accomplished by using a semi-passive thermal control system, including multi-layer insulation, thermal coatings, louvers, and heat pipes. The use of a semi-passive system is desired over an active control system because it will reduce the mass, size, cost, and level of complexity of the system. The mass and cost of the semi-passive TCS are estimated at 4% of the spacecraft's dry weight and 4% of the spacecraft's total cost [11].

Work on the Thermal Control Subsystem of Project Arma includes research of spacecraft component temperature limits, the determination of factors affecting the spacecraft temperatures, and thermal considerations of the aerobraking maneuver. These factors include solar and albedo fluxes, surface and profile view areas of the spacecraft, and waste heat generated by the power subsystem. A thermal balance equation is employed for the investigation of the spacecraft TCS design.

The thermal balance equation is used for the purposes of the current design investigation. A more evolved thermal control design requires work with a finite element code such as I-DEAS in order to determine the thermal loads acting on specific spacecraft components. This design could then be tested experimentally for validation. Results from the application of the thermal balance equation will suffice due to the scope and time restraints of the current design.

8.2 Temperature Ranges

For thermal control design it is important to know at what temperature ranges the selected hardware can operate without undergoing permanent damage. Efficient thermal

control design keeps these components within their designed temperature ranges. The design process for the maintenance of the temperature ranges starts with the collection of the selected subsystem components. Next, the operational and non-operational temperature range for these components are quantified. Also, the surface area of each component is obtained for the internal flux determination of that component.

Compiled in Table 8.1 is the component temperature ranges for each subsystem and its location on either the orbiter, penetrator, or landers. Also, listed in the table is the location of the particular spacecraft component. The last two columns are for the surface area and internal flux of each separate spacecraft component.

Table 8.1: Subsystem Component Temperature Ranges

Guidance, Navigation, and Control Subsystem

Component	Temperature (Kelvin)	Location	Power (Watt)	Surface Area (Sq.Meter)	Internal Flux (Watt/Sq.Meter)
Reaction Wheel		Orbiter	100.0	2.16	46.30
Operational	274 to 318	Orbiter			
Non-Operational	258 to 328	Orbiter			
Inertial Measurement Unit	274 to 318	Orbiter	100.0	0.06	1666.67
Horizon Sensor (2)		Orbiter	5.0	0.075	66.67
Operational	243 to 323	Orbiter			
Non-Operational	243 to 328	Orbiter			
Star Sensors (2)		Orbiter	20.0	0.25	80.00
Operational	243 to 323	Orbiter			
Non-Operational	243 to 328	Orbiter			
Sun Sensors (3)		Orbiter	6.0	0.57	10.53
Operational	243 to 323	Orbiter			
Non-Operational	243 to 328	Orbiter			

Table 8.1. (cont.)

Power Subsystem

Component	Temperature (Kelvin)	Location	Power (Watt)	Surface Area (Sq.Meter)	Internal Flux (Watt/Sq.Meter)
		Orbiter	3910	1.236	3163.43
RTG					
RTG (2)		Lander	925	0.52	1778.85
Battery		Penetrator	39		

Scientific Instruments Subsystem

Component	Temperature (Kelvin)	Location	Power (Watt)	Surface Area (Sq.Meter)	Internal Flux (Watt/Sq.Meter)
Mass Spectrometer		Orbiter	15.0	0.885	16.95
Sensor #1	253 to 293	Orbiter		0.245	0.00
Sensor #2	253 to 293	Orbiter		0.324	0.00
Electronics	253 to 303	Orbiter		0.316	0.00
Laser	253 to 293	Orbiter			
Radar Sounder		Orbiter			
Operational	243 to 313	Orbiter	50.0	0.207	241.55
Non-Operational	233 to 323	Orbiter		0.207	
Laser Altimeter		Orbiter			
Operational	243 to 313	Orbiter	30.0	0.0000317	946372.24
Non-Operational	243 to 313	Orbiter	5.0	0.0000317	157728.71
Infrared Mapper		Orbiter			
Operational	243 to 313	Orbiter	12.0	0.708	16.95
Non-Operational	233 to 323	Orbiter	6.0	0.708	8.47
Magnetometer	245 to 309	Orbiter	3.1	0.135	22.96
Potential Analyzer	245 to 309	Orbiter	4.5	0.54	8.33
Gravity Gradient	245 to 309	Orbiter	50.0	0.54	92.59
Gamma Ray Spectrometer	245 to 309	Orbiter	2.0	2.13	0.94
Visual Instrumentation	245 to 309	Orbiter	29.8	1.13	26.37
DION	253 to 293	Orbiter	20.0	0.54	37.04
Panoramic Camera (4)	> 253	Lander	1.0	0.0288	34.72
Temperature Probe (2)		Lander	1.0	0.06	16.67
Radiation Detector (2)	245 to 309	Lander	5.0	0.06	83.33
XRFS (2)	253 to 293	Lander	8.0	0.54	14.81
Wide Angle Camera		Lander	16.3	1.202	13.56
Thermal Logger (2)		Lander			
Operational	243 to 313	Lander			
Non-Operational	233 to 323	Lander			
Seismometer (2)	245 to 309	Lander	10.0	0.259	38.61
Mass Spectrometer		Penetrator	8.0	0.774	10.34
Sensor #1	253 to 293	Penetrator			
Sensor #2	253 to 293	Penetrator			
Electronics	253 to 303	Penetrator			
Laser	253 to 293	Penetrator			

Table 8.1. (cont.)

Communications Subsystem

Component	Temperature (Kelvin)	Location	Power (Watt)	Surface Area (Sq.Meter)	Internal Flux (Watt/Sq.Meter)
Omni Antenna (2)	103 to 363	Orbiter	30.0	0.327	91.74
High Gain Antenna	103 to 363	Orbiter	45.0	1.77	25.42
Omni Antenna (2)	103 to 363	Lander	15.0	0.621	24.15
Omni Antenna	103 to 363	Penetrator	15.0	0.229	65.50

Command and Data Handling Subsystem

Component	Temperature (Kelvin)	Location	Power (Watt)	Surface Area (Sq.Meter)	Internal Flux (Watt/Sq.Meter)
Computer	253 to 333	Orbiter	23.0	0.06	383.33
Data Storage Unit (2)	253 to 333	Orbiter	6.0	0.495	12.12
Computer (2)	253 to 333	Lander	6.6	2.77E-06	2382671.48
Data Storage Unit (2)	253 to 333	Lander	3.0	0.495	6.06
Computer	253 to 333	Penetrator	6.6		

Propulsion Subsystem

Component	Temperature (Kelvin)	Location	Power (Watt)	Surface Area (Sq.Meter)	Internal Flux (Watt/Sq.Meter)
Tanks (4)		Orbiter		0.657	
Hydrazine		Orbiter			
Freezing Point	274	Orbiter			
Boiling Point	387	Orbiter			
MMH		Orbiter			
Freezing Point	221	Orbiter			
Boiling Point	360	Orbiter			
Nitrogen-Tetroxide		Orbiter			
Freezing Point	262	Orbiter			
Boiling Point	294	Orbiter			
Main Thrusters (4)	283 to 393	Orbiter	60.0	0.465	129.03
Backup Thrusters (4)	283 to 393	Orbiter	40.0	0.116	344.83

From the table, certain components like the Laser Altimeter, Inertial Measurement Unit, Computers, and RTGs emit high internal fluxes. The small surface area and high power dissipation are the cause of the these high fluxes. Therefore, these components will need insulation to protect the other components from this potentially harmful heating. Heat pipes are needed to route the heat to some other part of the spacecraft.

These temperature ranges and internal fluxes are collected to develop a thermal control architecture. The architecture arranges the components to minimize the required thermal control. Insulation, coatings, and heat pipes are added to the design of Project Arma to maintain the specified temperature range for all of the components.

8.3 Thermal Factors

The thermal balance equation is used in an investigation of temperature regulation through the use of surface coatings. A desired equilibrium temperature of 283 K is established based on the temperature range data displayed in the previous section. Using this temperature of 283 K with the thermal balance equation, a required surface emissivity and absorptivity may be solved for. The thermal balance equation is represented by:

$$P_{in} + P_{internal} = P_{out} \tag{8.1}$$

where, P_{in} is the radiative power acting on the spacecraft, $P_{internal}$ is the waste heat generated within the spacecraft, and P_{out} is the power radiated by the spacecraft. Note that the use of this form of the energy balance neglects any effects of conductivity. This results in an equation that yields an equilibrium temperature.

The radiative power acting on the spacecraft, P_{in}, is a combination of solar, albedo, infrared, and thermal radiation. The current investigation neglects the affects of infrared and thermal radiation, as well as the albedo radiation from Deimos and Phobos. The driving flux term is the solar radiation. The solar and albedo fluxes acting on the spacecraft for a Martian

orbit of 9378 km are 595.6 W/m^2 and 6.01 W/m^2, respectively. The results may be used to find the external power acting on the spacecraft. The external power equation is given as:

$$P_{in} = S\, A_{ps}\, \alpha + a\, A_{pa}\, \alpha \qquad (8.2)$$

where; S is the solar flux, A_{ps} is the spacecraft profile area subject to the solar flux, a is the albedo flux, A_{pa} is the spacecraft profile area subject to the albedo flux, and α is the absorptivity of the surface. The profile areas are found from the spacecraft dimensions provided by the Structures Subsystem Team. Table 8.2 displays the spacecraft dimensions as well as the areas used in the calculations. The dimensions provided by the Structures Team are a simplification of the actual spacecraft geometry. These dimensions are used to determine the spacecraft surface and profile areas.

Table 8.2. Spacecraft Geometry

	Dimensions (m)	Surface Area (m^2)	Profile Area (m^2)
Orbiter	1.6 x 1.6 x 2.5	21.12	4.0
Landers	1.0 x 1.2 x 0.8	5.92	0.96

Internal power is dependent upon the power dissipated by spacecraft components and waste heat generated by the power sources. Table 8.3 displays the waste heat terms provided by the Power Subsystem Team. For the purposes of the thermal balance approximation, only the highest heating values are considered.

Table 8.3. Internally Generated Power

	Dissipated Power (W)	Waste Heat (W)	Total (W)
Orbiter	684	8280	8964
Phobos Lander	114	1380	1494
Deimos Lander	95	1150	1245

The power radiated by the spacecraft, P_{out}, is calculated by applying the Stefan-Boltzmann equation in a form given as:

$$P_{out} = \varepsilon \sigma A_S T^4 \tag{8.3}$$

where; ε is the emissivity, σ is the Stefan-Boltzmann constant, A_S is the surface area, and T is the equilibrium temperature. The developed thermal balance equation is used to solve for the equilibrium temperature. Varying spacecraft profile areas are neglected by this investigation because of the limits in the accuracy of the thermal balance approximation.

8.4 Thermal Control Design

The thermal balance equations provide an estimation of thermal control devices required to maintain an equilibrium temperature of 10° C. Results of the thermal balance equation indicate that the orbiter will maintain the desired equilibrium temperature with white enamel surface coating, louvers covering 6 m^2 of the orbiter's 21.12 m^2 surface, and varying the boom positions holding the RTGs.

Calculations for this thermal control system assume a maximum boom length of 2 m, and a wide-open louver capable of discharging a heat flux of 387.98 W/m^2. This assumption is based on the stated louver capability of 430 W/m^2 at a temperature of 304 K [11]. The

assumed maximum louver discharge flux is required during the aerobraking maneuver and orbiter transit maneuvers when the RTG booms are fully retracted and impinging on the orbiter's surface. Thermal control will then require thermostats, activation devices, and a temperature maintenance code to coordinate the RTG boom positioning and louver aperture in order to maintain an equilibrium temperature of 283 K. A more evolved thermal control design includes multi-layer insulation (MLI).

Application of the thermal balance equation indicates that the TCS of the lander may be accomplished through a combination of thermal coatings. The equilibrium temperature may be achieved through a combination of white enamel and OSR (Quartz over Silver) thermal coatings. A combination of thermal coatings takes advantage of individual coating characteristics to achieve an equilibrium temperature of 284 K.

White enamel's low absorptivity ($\alpha = 0.252$) may be taken advantage of by placing the coating over surfaces subject to a great deal of solar flux [11]. However, the high emissivity of this coating ($\varepsilon = 0.853$) results in an equilibrium temperature below the 284 K requirement [11]. A second coating such as OSR will be used in areas of the surface not subject to high solar flux. This will take advantage of a lower emissivity and achieve the equilibrium temperature of 284 K. The amount of area covered as well as coating material will differ between the Phobos lander and the Deimos lander due to differing internal fluxes. This TCS design neglects the effects of varying surface profile areas subject to solar radiation and shading of the landers from the sun. For these reasons a more evolved thermal control design requires such components as louvers, MLI, and heaters.

8.5 Aerobraking Maneuver

An aerobraking maneuver is selected for Project Arma's capture into a Martian orbit. The maneuver will save cost by reducing the amount of propellant necessary for Martian capture. The design of the aerobraking system has involved the Guidance, Navigation, and Control (GNC), Structure, and Thermal Control Subsystems. The Thermal Control

Subsystem work deals primarily with the heating that the spacecraft experiences during the aerobrake maneuver.

Cooper and Arnold pointed out that high ionization levels in the Martian atmosphere will heat the shield to high temperatures [29]. Because of these high temperatures, an ablative shield is selected for the aerobraking maneuver. The ablative shield will also be used because, Project Arma only requires the shield for one maneuver and then it is discarded. The disposable ablative shield will char and burn when in the Martian atmosphere, similar to the shield layer employed for the Apollo missions. The shield is also large enough to protect spacecraft components from the effects of turbulent heating.

To limit the heating effects, a shield with a low lift to drag ratio, 0.5, is selected for Project Arma. Other characteristics of the selected ablative heat shield are the ballistic coefficient, the nose radius, the velocity, the heating, and the altitude. These values are taken from Walberg, who conducted a study of Martian aerobraking maneuvers, assuming the nose radius of the shield to be 16.3 m and the values are listed in Table 8.4 [22]. These values are the worst case scenarios. The maximum velocity and heating values occur when the spacecraft reaches its lowest altitude in the Martian atmosphere. The GNC Subsystem estimates the minimum altitude to be between 40 and 50 km and the velocity between 6 and 7 km/sec. At these altitudes and speeds, the heating of the shield can be expected to be about 15 W/cm^2. Radiative and convective heating are the two types of heating experienced by the heat shield during an aerobraking maneuver. Convective heating will dominate the heating of this particular shield because of its geometry. The ballistic coefficient, another trait dependent on the velocity and altitude, is approximately 400 kg/m^2.

Table 8.4. Aerobrake Maneuver Characteristics

Characteristic	Value
Lift/Drag	0.5
Ballistic Coefficient	400 kg/sq. m
Nose Radius	16.3 m
Velocity	6 to 7 km/sec
Heating	14.95 W/sq. cm
Altitude	40 to 50 km

8.6 Summary of the Design

Project Arma will have a semi-passive thermal control system, including multi-layer insulation, thermal coatings, louvers, and heat pipes. The mass and cost of the semi-passive TCS are estimated at 4% of the spacecraft's dry weight and 4% of the spacecraft's total cost.

Temperature ranges and internal fluxes are collected to develop a thermal control architecture. The architecture arranges the components to minimize the required thermal control. Insulation, coatings, and heat pipes are added to the design of Project Arma to maintain the specified component temperature range for all of the components.

The TCS of the orbiter will consist of a white enamel thermal coating, louvers covering 6 m^2, multi-layer insulation, and heat pipes. The 6 m^2 louvers will be required for orbiter transit when the RTG booms are fully retracted. The landers will make use of a combination of white enamel and OSR thermal coatings, louvers, multi-layer insulation, and heaters. The heaters and multi-layer insulation are required during periods of shading.

The aerobraking shield is made out of ablative material and has a lift to drag ratio of 0.5. The shield sufficiently protects the spacecraft from convective, radiative, and turbulent heating.

9.0 Scientific Instruments Subsystem

9.1 Requirements

The primary goal of this subsystem is to perform regolith analysis on the moons of Mars, Phobos and Deimos. Until accurate data is obtained on the compositions of the moons, several important questions pertaining to both the feasibility of mining for propellant and the moons' true origins will remain unanswered. Due to this requirement, the instrumentation chosen to be used on the mission is heavily oriented toward accomplishing this goal with the largest amount of accuracy possible. All three of the probes to be utilized upon arrival to the Martian system, the orbiter, the lander, and the penetrator, include their own completely independent regolith analysis equipment.

The secondary goal of this mission is to obtain additional information on Mars and its moons in several key areas. These include gravity wave determinations, possible solar wind effects on the Martian atmosphere, temperature profiles, magnetic field properties, and both topographic and photographic mapping of the moons. Many of these requirements satisfy the objectives proposed by a study called NEAR (Near-Earth Asteroid Rendezvous) which was conducted by a committee of scientists called The Science Working Group [30]. This group created a list of experiments which were believed to provide the most valuable information from missions to asteroids. It is believed that these experiments are very applicable to the Arma mission to Phobos and Deimos due to the moons possible asteroid-like characteristics.

9.2 Orbiter Instrumentation

The characteristics of the instruments to be placed on the orbiter are listed in Table 9.1.

Table 9.1. Orbiter Instrument Masses, Powers, Data Rates, and Volumes

Instrument	Power (Watts)	Mass (kg)	Temp. (C)	Data Rate (kbps)
Radar Sounder (a)	50	6	-30/40 (op) -40/50(non-op)	1.6-352
Magnetometer (b)	3.1	3	-28/36*	3.6
Retarding Potential Analyzer (b)	4.5	3.4	-28/36*	1.5
Gravity Gradiometer (c)	50	25	-28/36*	1
Gamma Ray Spectrometer (c)	2	5.44	-28/36*	0.655*
Mars Observer Camera (d)	22.8-29.8	21	-28/36*	29.26
Mass Spectrometer (a)	15	15	-20/30	0.4-4
Near-Infrared Mapping Spectrometer (a)	12	5.2	-30/40 (op) -40/50(non-op)	0.035-8
Laser Altimeter (a)	30	13	-30/40	3.2
DION (e)	20	18	-28/36*	0.6*
Laser (f)	.01	7	-	-

Instrument	Volume
Radar Sounder (a)	1.4 m-boom, .01 x. 01 x 0.1 m^3 electronics*
Magnetometer (b)	0.15 x 0.15 x 0.15 m^3*
Retarding Potential Analyzer (b)	0.3 x 0.3 x 0.3 m^3*
Gravity Gradiometer (c)	0.3 x 0.3 x 0.3 m^3*
Gamma Ray Spectrometer (c)	77.5 x 43.5 x 60 cm^3
Mars Observer Camera (d)	70 (h) x 10 (dia) cm cylinder
Mass Spectrometer (a)	sens.1:12 x 25 x 25 cm^3, sens.2:12 x 30 x 30 cm^3 Electronics: 16 x 20 x 35 cm^3
Near Infrared Mapping Spectrometer (a)	Telesc.: 44.8 x 19.1 x 32.7 cm^3 Electronics: 15.7 x 13.3 x 13.3 cm^3
Laser Altimeter (a)	7000 cm^3
DION (e)	0.3 x 0.3 x 0.3 m^3*
Laser (f)	0.484 m(h) x 0.0442 m (dia) cylinder

*Estimated Values

Note:
a. Rosetta-CNSR-"A Comet-Nucleus Sample-Return Mission," Mission System Definitions Document, ESA SP-1125, June 1991.
b. "Report on ESA's Scientific Satellites," Science Department, ESA Publications Division, 1989.
c. "CRC Handbook of NASA Future Missions and Payloads, Vol.2," Michael R. Hord, CRC Press, Boca Raton, Florida, 1984.
d. Potts, D.L., "Mars Observer Description," J Spacecraft Vol.28 No.5.
e. Surkov, Yuri, "Exploration of Terrestrial Planets From Spacecraft," Ellis Horwood Limited, West Sussex, England, 1990.
f. "Lasers and Optronics," Gordon Publications Inc., Morris Plains, NJ., 1989.

It can be seen from the table that many of the instruments share an estimated temperature range of -28 ^{o}C to 36 ^{o}C. These estimated values were calculated by averaging the high and low values of the known temperature ranges. This had to be done due to a lack of information on these instruments.

The primary method of regolith analysis which is performed from the orbiter utilizes a technique similar to that of the Soviet Phobos II mission [37]. A 0.5 Joule laser is fired from the orbiter at the surface of the moons, vaporizing a small sliver of the moon's sub-surface material. This process releases ion particles into space which are then measured by the Mass Spectrometer at an atomic level. A second process is then employed using DION (secondary-ion mass-analyzer) which will determine the surface composition of the upper-most layer of the moon [37]. This requires the firing of a beam of highly energetic krypton ions at the surface, releasing low energy ions from the moon's crust which are then measured by the Mass Spectrometer. The analysis performed by this experiment determines the composition of the moons' regolith which is most affected by the space environment. The data obtained may then be compared to the compositions of the sub-surface material, which is less affected by the moons' environment. This comparison will provide a unique insight into the history of the moons since their creation.

Regolith analysis will also be accomplished on an atomic level from the orbiter through the use of the Gamma Ray Spectrometer. This instrument measures gamma rays released from the surface of the moon by the regolith's natural decay when exposed to sunlight. Even though it is a less accurate measurement, it is more reliable than the fairly complex operation involving the laser discussed previously.

Many other measurements will also be made from the orbiter. The Radar Sounder will determine the internal structures of the moons as well as taking surface roughness measurements. The Magnetometer maps the properties of the Martian magnetic field. The Retarding Potential Analyzer will measure the extent of the degradation of the Martian atmosphere by solar wind. The Gravity Gradiometer makes gravity wave determinations

around both Mars and its moons. The Mars Observer Camera [34] will visually map the surfaces of Phobos and Deimos while the Near-Infrared Mapping Spectrometer produces detailed thermal maps. Finally, the Laser Altimeter takes orbit to surface distance measurements, aiding in the production of topographical maps of the moons.

9.3 Lander Instrumentation

Listed in Table 9.2 are the characteristics of the instruments placed on the lander.

Table 9.2. Lander Instrument Masses, Powers, Data Rates, and Volumes

Instrument	Power (Watts)	Mass (kg)	Temp. (C)	Data Rate (kbps)
X-Ray Fluorescence Spect. (a)	10	11	-28/36*	0.3
Seismometer (b)	10*	5*	-28/36*	0.128*
Panoramic Camera (b)	1	0.225	T > -20	2000
Temperature Probe (b)	1	0.2	10	0.01*
Radiation Detector	5*	5*	-28/36*	-
Wide Angle Camera (b)	16.3/7	21.3	-20/0	6.2-350

Instrument	Volume
Seismometer (b)	0.1016 m (r) x 0.3084 m (h) cylinder*
Panoramic Camera (a)	12 x 6 x 4 cm^3
Temperature Probe (a)	-
Radiation Detector	-
X-Ray Fluorescence Spectrometer (b)	0.3 x 0.3 x 0.3 m^3*
Wide Angle Camera (a)	Camera: 28 x 32 x 60 cm^3 Electronics: 32 x 22 x 15 cm^3

*Estimated Values

Note: a. Rosetta-CNSR-"A Comet-Nucleus Sample-Return Mission," Mission and System Definitions Document, ESA, SP-1125, June 1991.
b. "CRC Handbook of NASA future Missions and Payloads, Vol. 2," Michael R. Hord, CRC Press, Boca Raton, Florida, 1984.

The regolith analysis performed by the lander employs the use of an X-ray Fluorescence Spectrometer (XRFS). This instrument is chosen to be used on the lander due to its ability to take accurate measurements when at a close proximity to the regolith sample. Its position within the lander is at the bottom so that it can be easily exposed to the surface. This placement also eliminates the need for a mechanical arm which would have been required to place a regolith sample in the XRFS.

A long-term instrument used on the lander is the Wide Angle Camera. It is positioned at the top of the lander exploring Phobos. This location on the Phobos lander is chosen so that the camera will be within close proximity to Mars thus making it an ideal Martian observing post. From the surface of Phobos it will be able to make long term observations of Martian weather and dust storms which are of extreme importance to future manned missions to Mars.

Another instrument utilized on the lander is the Seismometer. It will measure and record any seismic activities on the surface of the moons. It is also hoped that the solar cycle of the moon will produce measurable surface waves which will possibly give greater insight into the internal structure of the moon and its compactness.

Additional lander instrumentation includes the Panoramic Camera, the Temperature Probe, and the Radiation Detector. The Panoramic Camera will provide surface photographs giving insight into the granular size of the surface regolith and other features. The Temperature Probe will provide temperature readings from the surface of the moon throughout its solar cycle while the Radiation Detector will measure the amount of radiation the regolith is exposed to.

9.4 Penetrator Instrumentation

The goal of the penetrator is to perform a composition analysis on the moon's sub-surface material. Figure 9.1 illustrates the preliminary design for the penetrator. This design consists of two major components. The first of these is the upper communications pod which

remains at the surface when the penetrator strikes the moon. The second is the deep probe which continues into the moon's crust as deep as 5 meters. This portion, which is connected to the communication pod by an umbilical cord, houses the XRFS. The characteristics of the XRFS are listed in Table 9.3. Once its descent is complete the XRFS will be exposed to the sub-surface regolith by a port on the side of the penetrator. The XRFS will then analyze the composition of this material and send its data to the communications pod. The major assumption concerning this design is that the XRFS can be manufactured to withstand the 1000 g impact it will encounter when it arrives at Phobos [30]. According to several sources it is possible to accomplish this since the Russians and NASA-Ames have designed instruments with high impact resistance which are similar to the XRFS for possible future use on penetrators [37]. One of the these missions, the Vesta project proposed by ESA (European Space Agency) and CNES (Centre National d'Etudes Spatiales), is similar to Arma in that it supports plans to visit multiple sites including two large asteroids where it will probe chemical and physical properties by utilizing the penetrator concept [30].

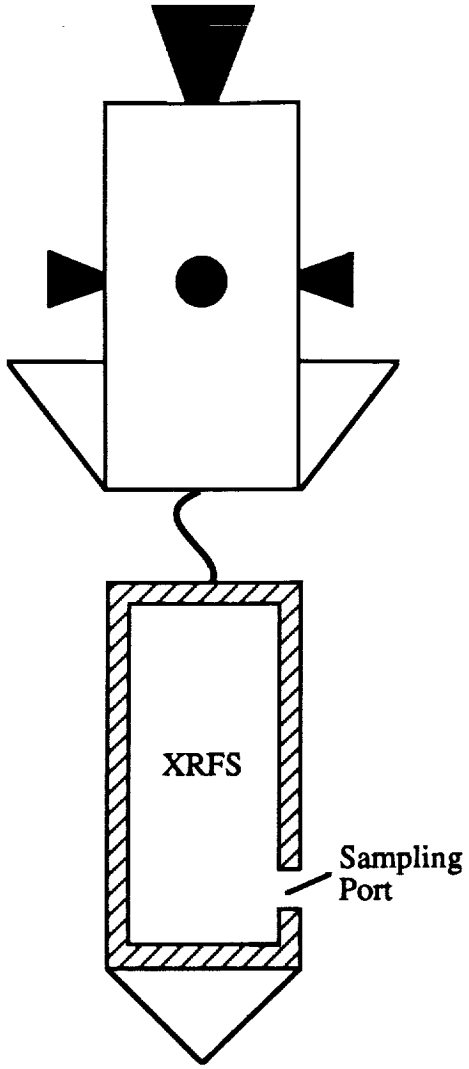

Figure 9.1. Penetrator Design [Based on design from Burgess, E., Return to the Red Planet, New York, Columbia Press, 1990.]

Table 9.3. Penetrator XRFS Instrument (Rosetta-CNSR-"A Comet-Nucleus Sample-Return Mission", Mission and System Definitions Document, ESA SP-1125, June 1991)

Power (W)	8
Mass (kg)	20
Data Rate (kbps)	0.3*
Volume	0.3 m (r) x 0.6 (h) cylinder

*Estimated Value

It is believed that the penetrator is feasible on the moons due to the belief that their compositions are quite fragile, similar to that of a class-C carbonaceous chondrite, a stony asteroid rich in organic compounds and rather metal poor [30]. In fact, its structure is so fragile that meteorites from these asteroids rarely make it to Earth [38]. Even though it looks as though penetrating the moon's crust is possible, due to the new technologies employed in the penetrator design and the fact that it has never been used before on an actual mission, it has been decided that for this mission it will only be utilized on Phobos.

9.5 Summary of the Design

A mission to the moons of Mars is an ambitious and scientifically demanding project. It is believed that the instruments chosen to be part of Project Arma satisfy the mission goals of regolith analysis and the collection of data which will be useful to future missions to Mars to a high degree.

By utilizing several different regolith analysis instruments and techniques, Project Arma will also be capable of successfully determining the moons compositions at several depths. One of these methods, using the XRFS from the penetrator to obtain a sub-surface composition analysis, is to date an unproven concept and is considered as an experiment in itself. However, it is believed that if successful, it will not only prove to be valuable as a tool for providing information for project Arma but future missions as well.

Of the instruments placed on the lander, the Wide Angle Camera, which is utilized to establish a long term observing post on Phobos, may prove to be the most valuable for future manned Mars missions. It could provide details of Martian weather patterns, including its massive dust storms, which have not been available using earth-based telescopes.

10.0 Launch Vehicles

Table 10.1 shows the three launch vehicles presently being considered for Project Arma.

Table 10.1. Launch vehicles considered for Project Arma (Isakowitz, Steven J., *International Reference Guide to Space Launch Systems*, American Institute of Aeronautics and Astronautics, 1991 Edition.)

Rocket	Payload Dimensions Length (m): Dia.(m)	Lift to LEO (kg)	Launch Cost	$ / kg (avg.)
Proton (Russia)	7.50 : 3.67	6,200[a]	$35 - 70M	$8,467
Shuttle	18.6 : 4.7	24,400	$245M	$10,409
Titan III	11.15 : 3.65	14,515	$130-150M [b]	$9,645

a Launch to Mars transfer orbit from Earth based launch pad
b Costs do not include compatible upper stages

A trade study was performed on the vehicles using the following formula:

$$J = K_1(\textit{launch cost}) + K_2(\textit{lift capacity}) + K_3(\textit{payload dimensions}) \qquad (10.1)$$

where K_1=-5, K_2=3, and K_3=4. A value of 1 was considered the worst and 5 the best. Table 10.2 shows the values assigned to the components of the trade study.

Table 10.2. Trade Study Results

Rocket	Launch Cost	Lift Capability	Payload Dimensions	Trade Value
Proton	5	3	3	-4
Titan III	3	4	4	13
Shuttle	1	5	5	30

Based on the trade study, the Proton rocket was chosen as the launch vehicle for Project Arma. The final estimate for the dry and wet masses of the spacecraft are approximately 1800 kg and 5113 kg, respectively. Therefore, the Proton was also chosen due to its lower lift capability, thus providing better parity with the size of the Project Arma spacecraft.

Due to the continuing political and social unrest in the former Soviet Union, the Proton rocket may not be available at the specified launch date. Thus, the Titan III has been chosen as a backup launch system if the Proton is unavailable. However, the total spacecraft weight may have to be trimmed slightly to accommodate an upper stage to boost the spacecraft from LEO into a Mars transfer trajectory.

11.0 References

[1] Mulqueen, Jack, "Manned Mission Transfer from Mars Parking Orbit to Phobos and Deimos," Manned Mars Mission Working Group Papers, Vol. 1, Sections 1-4, NASA Marshall Spaceflight Center, Huntsville, AL, May 1986, pp. 37-52.

[2] Blume, William H., Suzanne R. Dodd, and Charles W. Whetsel, "Mars Observer Mission Plan," *Journal of Spacecraft and Rockets*, Vol. 28, No. 5, September/October 1991, p. 506.

[3] Glasstone, S., *The Book of Mars*, NASA Office of Technology Utilization, 1986, p. 72.

[4] Zaitsev, Y., "The Success of Phobos-2," *Spaceflight*, November 1989, pp. 375-777.

[5] Agrawal, Brij N., Design of Geosynchronous Spacecraft, Prentice-Hall, Inc., Englewood Cliffs, NJ, 1986.

[6] Weast, Robert C., Melvin J. Astle, and William H. Beyer, CRC Handbook of Chemistry and Physics, CRC Press, Inc., Boca Raton, FL, 1989.

[7] Phone correspondence with Roger Boe, Hercules Aerospace, Inc., Magna, UT, October 6, 1992.

[8] Cooper, David M. and James O. Arnold, "Technologies for Aerobraking," NASA-TM-102854, March 1991.

[9] Strong, A.B., Fundamentals of composites Manufacturing: Materials, Methods, and Applications, Society of Manufacturing Engineers, Dearborn, MI, 1989.

[10] Metals Handbook, American Society for Metals, Columbus, OH, 1990, pp. 20, 35.

[11] Wertz, J.R. and W.J. Larson, Space Mission Analysis and Design, Kluwer Academic Publishers, Boston, MA, 1991.

[12] Hartman, Robert F., "Modular RTG Technology Status," General Electric Company, Philadelphia, PA, 1990.

[13] TRW Variable Thrust Engine Technical Specifications.

[14] Palocz, S., "Mars Observer Mission and Systems Overview," *Journal of Spacecraft and Rockets*, September/October 1991.

[15] TRW MRE-1 Monopropellant Thruster Technical Specifications.

[16] Wiesel, W.E., Spaceflight Dynamics, McGraw-Hill, Inc., 1989.

[17] Fowler, W., Spacecraft Subsystems, Department of Aerospace Engineering and Engineering Mechanics, The University of Texas at Austin, January 1992.

[18] Goetzel, C., J.B. Rittenhouse, and J.B. Singletary, Space Materials Handbook, Lockheed Missiles and Space Company, 1965.

[19] Halsell, C.A. and W.E. Bollman, "Mars Observer Trajectory and Orbit Control," *Journal of Spacecraft and Rockets*, Vol. 28, No. 5, September/October 1991.

[20] Corliss, William R., "Viking Mission to Mars," NASA-SP-334, 1974.

[21] Rabb, Gus and William Stump,. "Comparison of Mars Mission Design," Manned Mars Mission Working Group Papers, Vol. 1, Sections 1-4, NASA Marshall Spaceflight Center, Huntsville, AL, May 1986, pp. 154-161.

[22] Walberg, Gerald D., "A Review of Aerobraking fro Mars Missions," International Astronautical Congress, IAF-88-196, 1988.

[23] Braun, Robert D., Richard W. Powell, and Lin C. Hartung, "Effect of Interplanetary Trajectory Options on a Manned Mars Aerobrake Configuration," NASA-TP-3019, August 1990.

[24] Ward, Donald T., "Control Algorithms for Aerobraking in the Martian Atmosphere," NASA-CR-185665, September 1991.

[25] Luria, F., "Analysis of Periodic Orbits About the Martian Moons by Continuation Techniques," M.S. Thesis, AFIT/GA/ENY/90D, School of Engineering, Air Force Institute of Technology, Wright-Patterson AFB, OH, December 1990.

[26] Bryant, S.R., "Realistic Orbits About the Martian Moons," M.S. Thesis, AFIT/GA/ENY/90D-1, School of Engineering, Air Force Institute of Technology, Wright-Patterson AFB, OH, December 1990.

[27] Wertz, p. 341.

[28] Seifert, Howard S., Introduction to Space Communication Systems, 1964, pp. 121-124.

[29] Arnold, J.O. and D.M. Cooper, "Techniques for Aerobraking," NASA Ames Research Center.

[30] Binzel, R.P., T. Gehrels, and M.S. Matthews, Asteroids II, University of Arizona Press, Tucson, AZ, 1989.

[31] Rosetta/CNSR "A Comet Nucleus Sample Return Mission," Mission Systems Definition Document, ESA SP-1125, June 1991.

[32] "Report on ESA's Scientific Satellites," Science Department, ESA Publications Division, 1989.

[33] Hord, Michael R., CRC Handbook of NASA Future Missions and Payloads, Vol. 2, CRC Press, Boca Raton, FL, 1984.

[34] Potts, D.L., "Mars Space Observer Description," *Journal of Spacecraft and Rockets*, Vol. 28, No. 5.

[35] Surkov, Yuri, Exploration of Terrestrial Planets from Spacecraft, Ellis Horwood Limited, West Sussex, England, 1990.

[36] Lasers and Optronics, Gordon Publications, Inc., Morris Plains, NJ, 1989.

[37] Burgess, E., Return to the Red Planet, Columbia Press, New York, NY, 1990.

[38] Robertson, D., "Soviet Phobos Mission to Probe the Moons of Mars," *Astronomy*, Vol. 15, No. 11, November 1987.

[39] Yeun, Joseph H., Deep Space Telecommunications System Engineering, 1983, pp. 422-25.

Appendix A: Phobos Penetrator

The volume of the penetrator tip was calculated using the equation below (h_1, h_2, and r dimensions are shown in Figure 2.1)

$$V = \pi r^2 h_1 + \int \pi r^2 h_2 dr \tag{A.1}$$

h_1 = height of cylinder section of tip = 3.13×10^{-3} m
h_2 = height of conical section of tip = 3.13×10^{-3} m
r = radius of the tip = 0.125 m
V = volume of the penetrator tip

From Equation A.1 the volume was found to be 1.602 x 10-4 m^3. The mass of the penetrator tip was then found with the following equation:

$$m = V\rho \tag{A.2}$$

ρ = density of depleted uranium = 19000 kg/m^3
V = volume of the penetrator tip = 1.602×10^{-4} m^3
m = mass of the penetrator tip

From this equation the mass of the penetrator tip was found to be 3.044 kg. The Herrman Jones Logarithmic Penetration Law [18] was used to determine the velocity required to penetrate the surface of Phobos a distance of 3 m:

$$p = K_1 \left(\frac{6}{\pi}\right)^{\frac{1}{3}} \frac{\rho^{\frac{1}{3}}}{\rho_t^{\frac{1}{3}}} \ln\left\{\frac{1+\left(\frac{\rho}{\rho_t}\right)^{\frac{2}{3}} \rho_t V^2}{K_2 H_t}\right\} m^{\frac{1}{3}} \tag{A.3}$$

The following assumptions were made:

p = surface penetration depth = 300 cm
K_1, K_2 = material constants = 1 for semi-infinite targets
m = projectile mass (penetrator tip mass) = 3044 g
ρ = projectile density (deplete uranium tip) = 19 g/cm^2
ρ_t = target density (Phobos) = 2.0 g/cm^2 [38]
H_t = target Brinell Hardness (Phobos)
V = velocity at impact (cm/s)

The surface of Phobos is considered to be quite fragile, containing primarily organic compounds and relatively metal poor [38]. From this assumption the Brinell Hardness of the surface of Phobos was estimated to be approximately 2 x 10^6 dynes/cm^2. From the Herrman Jones Logarithmic Penetration Law the velocity needed to penetrate the surface of Phobos 3 m was calculated to be V = 67520 cm/s = 675 m/s.

Appendix B: Communications Subsystem

The orbiter High-Gain Antenna (HGA) was allocated 0.7 W of transmitted power on the X-Band frequency range. The parabolic antenna diameter was estimated to be 1.5 meters. From these values, many antenna characteristics could be determined.

The signal beamwidth, θ, is determined from

$$\theta = \frac{60\lambda}{D} \tag{B.1}$$

where λ is the signal wavelength (0.035603 m), and D is the distance between antennae (3.75E8 km). The beamwidth was calculated to be 1.425 degrees.

From [39], an antenna efficiency, μ, can be determined from

$$\eta_{ap} = e\eta_t\eta_1\eta_2\eta_3\eta_4\eta_5\eta_6\eta_7\eta_8 \tag{B.2}$$

where e = radiation efficiency
η_t = aperture taper efficiency
η_1 = spillover efficiency
η_2 = random surface error efficiency
η_3 = aperture blockage efficiency
η_4 = strut blockage efficiency
η_5 = squint efficiency
η_6 = astigmatism efficiency
η_7 = surface leakage efficiency
η_8 = depolarization efficiency

The radiation efficiency, e, is estimated to be 0.95. The product of the spillover efficiency, η_1, and the aperture taper efficiency, η_t, can be estimated to be 0.78 from Figure 8-5 on page 422 of [39]. The random surface efficiency, which is dependent on the ratio of the focal length (0.7 m) to the antenna diameter (1.5 m), was found to be 0.94 from Figure 8-

6 on page 423 of [39]. The aperture blockage efficiency was estimated to be 0.944 from Figure 8-7 on page 424 of [39] for a blockage of 0.15 m. The strut blockage efficiency was estimated to be 0.96 from Table 8-1 on page 425 of [39]. A squint efficiency value of 0.98, astigmatism efficiency of 0.93, surface leakage efficiency of 0.99, and depolarization efficiency of 0.98 were cited by [39] as typical values. These values result in an antenna efficiency of 0.499.

The antenna efficiency was used to determine the effective antenna radiating area. The effective radiating area, A_T, was found to equal 0.989 m^2 from

$$A_T = \eta_{ap} A_t \tag{B.3}$$

where A_t is the actual antenna area, 1.767 m^2.

The equation governing the parabolic antenna gain is

$$G_T = \frac{4\pi A_T}{\lambda^2} \tag{B.4}$$

Using the values calculated above, the HGA gain was determined to be 9802.96. In decibels, the gain is 39.91 dB.

Using Shannon's formula and the maximum throughput of the systems computer, the signal-to-noise ratio (SNR) could be determined. From the SNR, the required transmitted power could be determined. Shannon's formula is given by Seifert [28] to be

$$R = B\log_2(SNR + 1) \tag{B.5}$$

With the X-band bandwidth, B, of 1.358 MHz and maximum computer throughput of 4.5 Mbps, the SNR was calculated to be 8.9431 dB. According to [28], the SNR is related to the carrier-to-noise ratio (CNR) by

$$SNR = 2.2CNR \text{ (in dB)} \qquad \text{(B.6)}$$

for binary encoded pulse sequences (PCM).

The CNR is related to the antenna characteristics and link parameters by

$$CNR = 228.6 + 10 \log P_t + G_t + G_R - L_p - L_x - 10 \log B - 10 \log T \qquad \text{(B.7)}$$

where P_t is the power transmitted , G_t is the gain of the transmitting antenna (39.9 dB), GR is the gain of the receiving antenna (63 dB), L_p are the space losses (222.45 dB), L are the system losses (5 dB), B is the bandwidth (1.358 MHz), and T is the temperature at the receiving antenna (290 K). The power transmitted was calculated to be 0.7 W.